Regulation of Human Telomerase Assembly and Recruitment to Telomeres

By

Jacob Michael Vogan

A dissertation submitted in partial satisfaction of the

requirements for the degree of

Doctor of Philosophy

in

Molecular and Cell Biology

in the

Graduate Division

of the

University of California, Berkeley

Committee in charge:

Professor Kathleen Collins, Chair
Assistant Professor Dirk Hockemeyer
Professor Michael Rape
Associate Professor Jen-Chywan Wang

FALL 2016

ABSTRACT

Regulation of Human Telomerase Assembly and Recruitment to Telomeres

By

Jacob Michael Vogan

Doctor of Philosophy in Molecular and Cell Biology

University of California, Berkeley

Professor Kathleen Collins, Chair

Telomerase is the ribonucleoprotein complex that synthesizes telomeric repeats and maintains telomere length in cells where it is expressed. The telomerase holoenzyme is composed of many regulatory factors which instruct telomerase biogenesis and engagement with telomeres. Common themes of telomerase regulation in divergent organisms emerge in the form of telomerase RNA accumulation, trafficking among cellular compartments, and cell cycle dependent access to telomeres. My investigations have focused on human telomerase regulation.

I found that a key chaperone which localizes telomerase to Cajal bodies binds and releases telomerase in a cell cycle dependent fashion in coordination with the increased accessibility of telomeres during the replication phase (Chapter two). I also investigated the role of the canonical H/ACA small nucleolar RNA pathway in human telomerase maintenance of telomeres. I found that the H/ACA pathway was required for endogenous telomerase to assemble into active enzyme and that chaperone trafficking of telomerase to Cajal bodies regulated telomere length homeostasis, but was not a requirement for telomere maintenance (Chapter Three)

ACKNOWLEDGEMENTS

I would like to thank my mentor, Kathy Collins, for her constant support, for widening my scientific vision, and for cultivating a wonderful laboratory environment. Kathy has always provided encouragement and her excitement for scientific discovery is contagious. I am very grateful to have joined her lab and to have worked on interesting questions involving human telomerase biology.

The Collins' lab has been full of great people. In particular, a big thank you to my awesome baymate, Heather Upton, for her phenomenal kindness, interesting scientific discussions, and putting up with me as a baymate for so long. Thank you to Xiaozhu Zhang for her brilliant work and warmheartedness. Thank you to Emily Egan for mentoring me on my first telomerase experiments. Alex Wu, Alec Sexton, Dan Youmans, Kelly Nguyen, and Jane Tam have all been thoughtful and brilliant labmates. Thank you to my graduate student mentor George Katibah. We shared fantastic scientific discussions and discoveries. Meeting George also precipitated my joining of the Collins lab and he was part of a great first impression during my lab rotation where we worked on characterizing IFIT5.

Thank you to Ming Hammond for a fantastic lab rotation which built my expertise in working with RNA and for her scientific input during my qualifying exam. Thank you to Jamie Cate for chairing my qualifying committee and providing me with insightful feedback. Thank you to Eva Nogales, who not only provided a great lab rotation experience, but also shared great scientific discussions with me during my initial graduate school interview and afterwards.

Thank you to my thesis committee members Dirk Hockemeyer, Michael Rape, and Wally Wang for the insightful scientific questions and advice. An extra thank you to Dirk for the always insightful comments during our lab meetings and for the wonderful collaborations. From Dirk's lab, thank you to Chiba, Sam, John, and Josh for being smart, fun, and positive colleagues.

I am eternally grateful to my previous mentors, Robin Shaw and James Smyth, for their patience, sharing of knowledge, and friendship. I would not have made it to graduate school without their extraordinary mentorship and support.

Thank you to my supportive friends. In particular, Paul, Ali, Tony, Damoon, Ty, Jason, Gagan, and the Thao family. Thank you to Siying. And thank you to my parents, Robert and Mary, as well as my grandparents, Bob and Odette, for their wonderful support over the years.

TABLE OF CONTENTS

ABSTRACT 1

ACKNOWLEDGEMENTS i

CHAPTER ONE: The telomerase holoenzyme 1

CHAPTER TWO: Cell cycle dynamics of human telomerase holoenzyme assembly 5

- Abstract 5
- Introduction 6
- Materials and Methods 8
- Results 12
- Discussion 18

CHAPTER THREE: Minimized human telomerase maintains telomeres and resolves endogenous roles of H/ACA proteins, TCAB1, and Cajal bodies 36

- Abstract 36
- Introduction 37
- Materials and methods 39
- Results 44
- Discussion 50

REFERENCES 75

CHAPTER ONE

The telomerase holoenzyme

Introduction

The loss of nucleotide sequence at the ends of chromosomes is inherent to each round of genome replication by DNA-dependent DNA polymerases. A solution to counteract this erosion was the emergence of telomerase. Telomerase is the essential enzyme for synthesizing telomeric repeats at the ends of chromosomes. The core of telomerase is a ribonucleoprotein (RNP) complex composed of a reverse transcriptase and an integral RNA subunit which contains the template for telomeric repeat synthesis (Greider and Blackburn 1989). The telomerase RNA component also contains motifs which allow for additional telomerase holoenzyme proteins to assist in assembling the active ribonucleoprotein and promote telomerase engagement at telomeres.

The first detection of telomerase activity was in cell extract from the ciliate, *T. thermophila* (Greider and Blackburn 1985). Later, telomerase activity was found in various human immortalized cell lines and cancers (Morin 1989; Kim et al. 1994). Most human tissues lack telomerase activity. Its expression is limited to early human development (Aubert 2014), with robust expression in human embryonic stem cells (Hiyama and Hiyama 2007). Devastating diseases arise from insufficient telomerase activity, including bone marrow failure and pulmonary fibrosis (Holohan, Wright, and Shay 2014). Most cancers also express telomerase, where aberrant reactivation of telomerase can embolden tumorigenesis through immortalization (Shay 2016). Studying the cellular regulation of telomerase provides insights into tissue renewal, ageing, and diseases which perturb telomerase action at telomeres.

Divergent interactions and common themes of telomerase biogenesis

In cell extract, two telomerase subunits are sufficient to assemble an active telomerase "minimal RNP" (Weinrich et al. 1997): the telomerase RNA (TER) and telomerase reverse transcriptase (TERT). However, many interactions and factors beyond TERT and TER are required for telomerase assembly and action at telomeres in cells. This includes telomerase holoenzyme proteins that stably associate with TER to protect TER's 3' end from exonucleases, as well as interactions with chaperones for folding and trafficking (Figure 1). While there is broad conservation of essential TERT and TER domains for folding into active RNP, entirely different pathways of telomerase biogenesis and regulation have evolved in ciliates, fungi, and vertebrates

TER folding and telomerase assembly follows a multistep pathway in cells (Londono-Vallejo and Wellinger 2012). The ciliate, *T. thermophila* telomerase RNP is composed of TERT, TER, and the La- and RRM-domain RNA-binding protein p65 (Figure 4a)(Witkin and Collins 2004). Roles of the p65 La-family protein include protection of the RNA Polymerase III TER transcript ends from exonucleases and folding TER to promote TERT interaction (Stone et al. 2007). Other TERs are transcribed by RNA Polymerase II and are typically modified to bear a 5' trimethylguanosine (TMG) cap which stabilizes nuclear RNAs. In *S. cerevisiae,* the TER precursor 3' end is demarcated by the Nrd1/Nab3/Sen1-pathway (Noël et al. 2012). In other

fungi, the 3’ end is determined by aborted splicing (Box et al. 2008). In human cells, the 3’ end of TER is terminated by transcription-coupled polyadenylation (Nguyen et al. 2015). Protein complexes protect the 3’ end of TERs from exonucleases. In most fungi, the Sm protein ring assembles on the TER 3’ end (Podlevsky and Chen 2016).

In vertebrates, the 3’ end of TER is determined by assembly of a H/ACA RNP composed of two subunits each of dyskerin, NHP2, NOP10, and GAR1 (which is exchanged with the NAF1 protein) on a two-hairpin H/ACA motif (Mitchell, Cheng, and Collins 1999). Human disease-associated mutations have been found in the H/ACA proteins (Kiss, Fayet-Lebaron, and Jády 2010) which reduce levels of human TER (hTR). These mutations have a disproportionate effect on hTR compared to other H/ACA small nucleolar and small Cajal body RNAs (Stanley et al. 2016). The strong, selective impact of these mutations may arise from vulnerability of the hTR precursor transcript to rapid degradation, which is balanced against by H/ACA RNP assembly and hTR 3’ end processing by the polyadenosine-specific ribonuclease PARN (Egan and Collins 2012a; Stuart et al. 2015; Nguyen et al. 2015; Tseng et al. 2015).

Telomerase maturation and trafficking

Proteins that traffic telomerase subunits and RNPs within a cell play vital roles in active RNP biogenesis and action at telomeres. Step-wise trafficking and RNP assembly of human telomerase RNP involves trafficking between Cajal bodies, nucleoli, and nucleoplasm (Figure 2). The nascent hTR transcript binds two sets of core H/ACA proteins (dyskerin, NOP10, and NHP2), scaffolded together by NAF1 (Egan and Collins 2012a). Nascent hTR H/ACA RNP is thought to rapidly acquire a 5’ TMG cap, possibly by transiting through Cajal bodies (Fu and Collins 2006). The 5’ leader of hTR is also acted on by the RNA helicase DHX36 to resolve guanosine quaduplex structures (Sexton and Collins 2011). During hTR RNP maturation, NAF1 is exchanged for the H/ACA RNP subunit GAR1. In addition, the Cajal body localization chaperone TCAB1 binds the CAB-box motif in the hTR 3’ stem loop (Figure 2c; TCAB1 is described in more detail below). A fraction of hTR binds TERT to form active RNP. While the exact location of TERT assembly with hTR is not fully resolved, evidence for assembly in nucleoli is supported by several lines of evidence. In studies of nucleoplasmic hTR without H/ACA proteins, endogenous TERT was unable to assemble into active RNP. The loss of TCAB1 interaction with hTR leads to hTR localization in nucleoli without impeding active RNP assembly (Vogan et al. 2016).

TCAB1 shifts telomerase from nucleoli to Cajal bodies and nucleoplasm (Venteicher et al. 2009). TCAB1 gene disruption decreases the length at which telomeres are maintained, but it does not compromise long-term telomere length homeostasis (Vogan et al. 2016). Decreased telomere length in stem cells, and thus reduced proliferative capacity of cell lineages differentiated from them, offers an explanation as to why mutations in TCAB1 cause diseases of premature telomere shortening (Zhong et al. 2011). Since genetic disruption of Coilin protein, and thus Cajal bodies, does not affect telomerase assembly or telomere length in human cancer cells or embryonic stem cells (Chen et al. 2015), telomere access by telomerase can occur from the nucleoplasm. This conclusion is consistent with the biological function of active RNPs containing hTR without an H/ACA motif, which is exclusively nucleoplasmic (Vogan et al. 2016).

Figure 1. Evolutionary divergence of telomerase RNA binding partners

Telomerase RNAs (TERs) have acquired divergent binding partners to account for specific cellular contexts. In ciliates, TER is a La ribonucleoprotein (RNP), similar to pre-tRNA. In budding yeast, TER forms a Sm RNP, similar to small nuclear RNPS. In vertebrates, TER assembles into a small Cajal body H/ACA RNP, a class of RNP which canonically pseudouridylates other RNAs. The acquisition of these binding partners, while maintaining the telomerase reverse transcriptase (TERT) interaction, provides telomerase RNAs with 3' end protection for accumulation, assistance for folding into active enzyme, and instructions for telomere engagement.

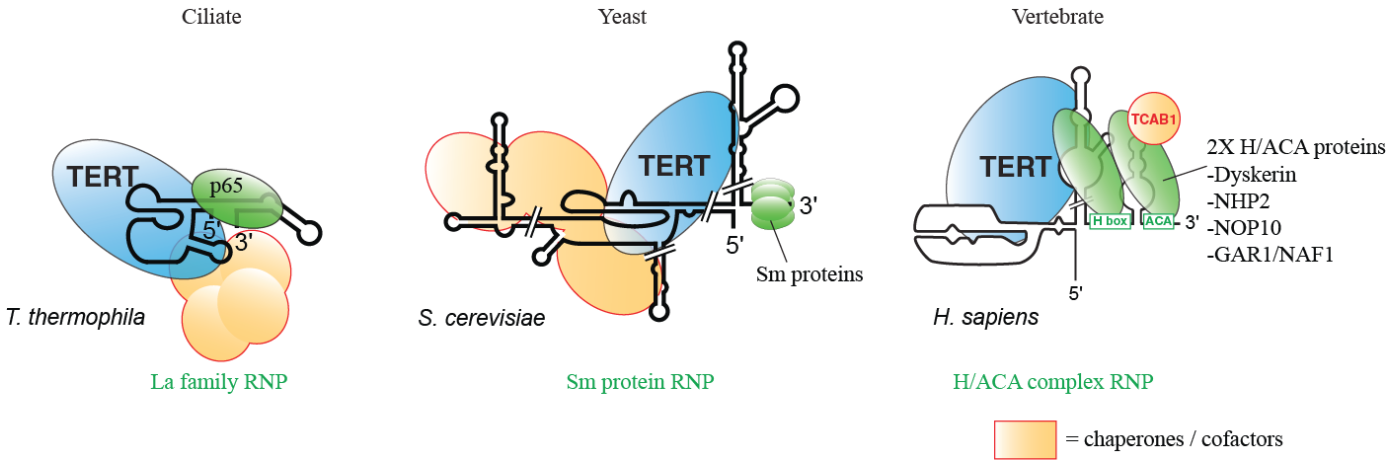

Figure 2. Model of human telomerase assembly and trafficking to telomeres

In this biogenesis model, human telomerase RNA (hTR) co-transcriptionally assembles with the H/ACA proteins, dyskerin, NHP2, NOP10, and NAF1. NAF1 is then exchanged for the GAR1 H/ACA protein in the nucleoplasm and the hTR H/ACA ribonucleoprotein (RNP) localizes to nucleoli. TERT then assembles with hTR to form telomerase. The Cajal body chaperone, TCAB1, then trafficks telomerase to Cajal bodies. Cajal body and nucleoplasmic localized telomerase is then able to effectively engage with telomeres during the replicative phase of the cell cycle.

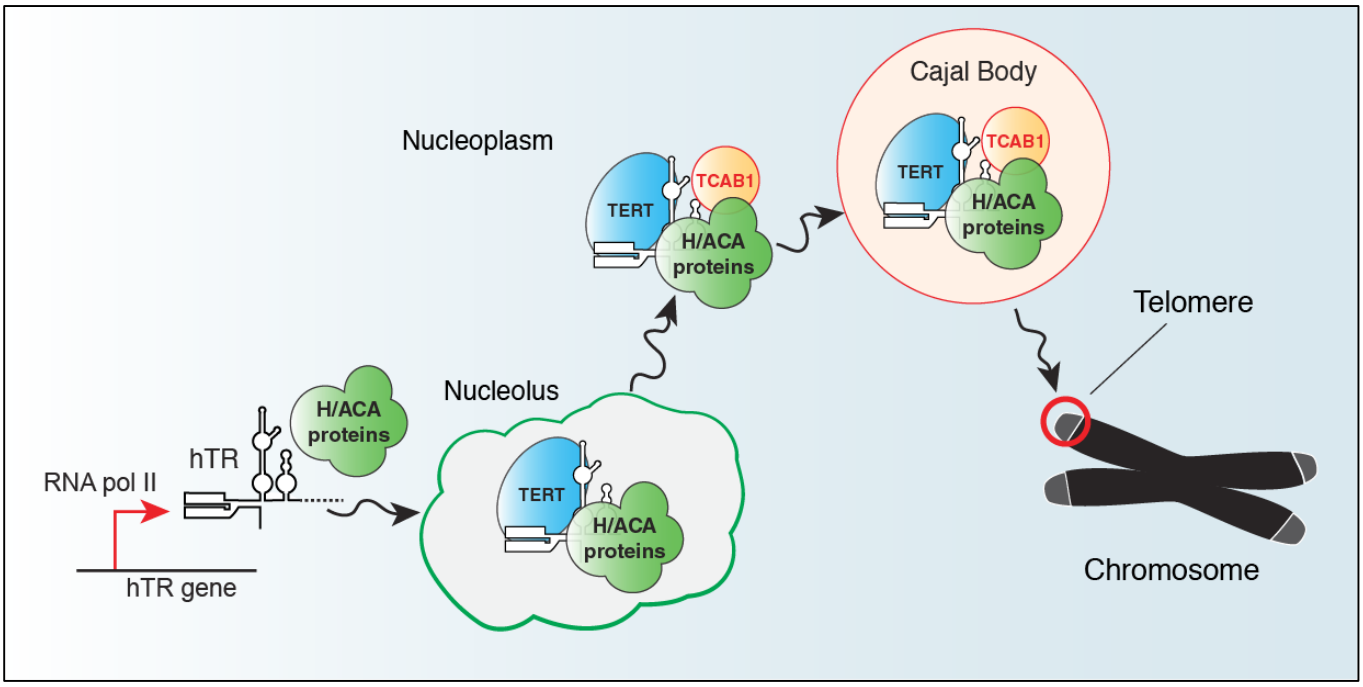

CHAPTER TWO

Cell cycle dynamics of human telomerase holoenzyme assembly

Abstract

Human telomerase acts on telomeres during the genome synthesis phase of the cell cycle, accompanied by its concentration in Cajal bodies and transient colocalization with telomeres. Whether regulation of human telomerase holoenzyme assembly contributes to the cell cycle restriction of telomerase function is unknown. We investigated the steady-state levels, assembly, and exchange dynamics of human telomerase subunits with quantitative *in vivo* crosslinking and other methods. We determined the physical association of telomerase subunits in cells blocked or progressing through the cell cycle synchronized by multiple protocols. The total level of human telomerase RNA (hTR) was invariant across the cell cycle. *In vivo* snapshots of telomerase holoenzyme composition established that hTR remains bound to human telomerase reverse transcriptase (hTERT) throughout all phases of the cell cycle, and subunit competition assays suggest that hTERT-hTR interaction is not readily exchangeable. In contrast, the telomerase holoenzyme Cajal body associated protein, TCAB1, was released from hTR in mitotic cells coincident with TCAB1 delocalization from Cajal bodies. This telomerase holoenzyme disassembly was reversible with cell cycle progression, without change in total TCAB1 protein level. Consistent with differential cell cycle regulation of hTERT-hTR and TCAB1-hTR protein-RNA interactions, overexpression of hTERT or TCAB1 had limited if any influence on hTR assembly of the other subunit. Overall these findings reveal a cell cycle regulation that disables human telomerase association with telomeres while preserving the co-folded hTERT-hTR RNP catalytic core. Studies here, integrated with previous work, lead to a unifying model for telomerase subunit assembly and trafficking in human cells.

Introduction

Safeguarding genomic stability requires a mechanism to maintain telomeres at the ends of chromosomes. The general eukaryotic solution to this obligation is the activity of telomerase, a reverse transcriptase specialized for the synthesis of telomeric repeats (Blackburn, Greider, and Szostak 2006). By copying an RNA template within the active RNP, telomerase extends a 3' overhang at the chromosome end. Telomerase is active in early human embryo cells but is repressed upon tissue differentiation (Forsyth, Wright, and Shay 2002). Without telomerase activity, human somatic cells count down cell divisions toward a proliferative limit due to progressive telomere shortening (Aubert 2014). To bypass this growth barrier, the majority of human cancers reactivate telomerase and balance the telomere attrition coupled to genome replication with new telomeric repeat synthesis (Shay and Wright 2011). Knowledge about the regulation of human telomerase is therefore essential for understanding changes in genome maintenance with human development and tumorigenesis.

Telomerase catalytic activity can be reconstituted by the combination of hTR and hTERT in a eukaryotic cell or cell extract (Weinrich et al. 1997; Podlevsky and Chen 2012). In addition to these two RNP catalytic core subunits, many additional proteins are necessary for the *in vivo* assembly, subcellular trafficking, and telomere association of a functional telomerase holoenzyme (Egan and Collins 2012b; Nandakumar and Cech 2013). Mature hTR biological stability requires precursor co-transcriptional assembly as an H/ACA small nucleolar RNP with dyskerin, NOP10, NHP2, and the chaperone NAF1, which is later replaced by GAR1. The crucial importance of this RNP biogenesis process is established by human gene mutations that cause telomerase deficiency diseases such as dyskeratosis congenita (Armanios and Blackburn 2012). After initial hTR H/ACA RNP biogenesis, a fraction of the biologically stable hTR RNP associates with hTERT through multiple direct protein-RNA interactions (Mitchell and Collins 2000; Blackburn and Collins 2011; Huang et al. 2014). Some or all of the hTR RNPs bind the telomerase Cajal body protein, TCAB1, via the Cajal body localization motif (CAB box) in the hTR 3' stem loop (Tycowski et al. 2009; Venteicher et al. 2009). TCAB1 increases the steady-state Cajal body association of hTR and a subset of other H/ACA RNAs that also contain CAB boxes (Jády, Bertrand, and Kiss 2004; Zhong et al. 2011). TCAB1 does not contribute to telomerase catalytic activation, but it is necessary for hTERT-hTR RNP recruitment to and extension of telomeres (Zhong et al. 2011; Batista et al. 2011; Stern et al. 2012).

Cell cycle regulation imparts coordination to cellular processes such as chromosome replication and segregation that occur in ordered progression through a first gap phase (G1), DNA synthesis (S), a second gap phase (G2), and mitosis (M). As for many other DNA replication enzymes, telomerase action is under cell cycle control. Physical assays of 3' overhang synthesis and processing in many organisms, including human cells (Zhao et al. 2009; Chow et al. 2012), support S/G2 as the interval for changes in telomeric DNA structure. Studies in budding and fission yeasts demonstrate that telomerase holoenzyme engagement of telomeres occurs only in S phase (Moser and Nakamura 2009; Gallardo et al. 2012; Ribeyre and Shore 2013; Nandakumar and Cech 2013). The telomere association of hTR detectable by *in situ* hybridization also occurs only in S phase (Jády et al. 2006; Tomlinson et al. 2006). Even in the ciliate *Tetrahymena*, which has thousands of chromosome ends per macronucleus, chromatin immunopurification (IP) assays showed cell cycle restriction of telomerase-telomere engagement (Upton, Hong, and Collins 2014).

Cell cycle regulation of telomerase action at telomeres could derive in part from regulation of telomerase holoenzyme. Yeast telomerase holoenzyme subunit interactions have cell cycle regulation, including exchange of a shared DNA binding subunit of mutually exclusive telomerase and telomere capping complexes (Li et al. 2009). In comparison there has been relatively little investigation of human telomerase cell cycle regulation. Several studies used lysates of cells harvested across synchronized cell cycle progression to survey for telomerase catalytic activity, with conclusions ranging from lack of regulation to S-phase maximal or S-phase specific activity (Holt et al. 1997; Zhu et al. 1996; Lee et al. 2014). Subcellular localization studies suggest differential intranuclear distributions of hTERT and hTR until they coassemble in S phase in Cajal bodies or nucleoli (Tomlinson et al. 2006; Lee et al. 2014). Enrichment of hTR in Cajal bodies is regulated by the cell cycle, peaking in S phase when hTR foci colocalize with telomeres (Jády, Bertrand, and Kiss 2004; Jády et al. 2006; Tomlinson et al. 2006). However, conclusions differ about whether telomerase requires Cajal bodies for association with telomeres: coilin gene disruption did not affect telomerase function in telomere maintenance (Chen et al. 2015) whereas coilin depletion reduced endogenous hTR and hTERT recruitment to telomeres (Stern et al. 2012) or even recruitment of overexpressed hTR and hTERT (Zhong et al. 2012). Curiously, no Cajal body localization was detected for mouse telomerase RNA, which, like hTR, becomes colocalized specifically in S phase with a few telomeres at a time (Tomlinson et al. 2010b), and overexpression of a CAB-box-mutant hTR lacking Cajal body association still elongates telomeres at least half as well as wild-type (Fu and Collins 2007; Cristofari et al. 2007). These findings leave open many possible hypotheses for cell cycle regulation of human telomerase holoenzyme.

In this study, we investigated cell cycle regulation of the levels of hTR, hTERT, TCAB1, and their protein-RNA interactions. We also tested whether increasing the level of an individual telomerase holoenzyme or RNP biogenesis protein affected hTERT-hTR or TCAB1-hTR interaction. We present a model in which hTERT and hTR assemble irreversibly, with synthesis of new hTR and active RNP maximal in G1. On the other hand, TCAB1 association with hTR undergoes cell cycle regulation. We observed coordinate M-phase TCAB1 loss from hTR and from Cajal bodies, which was reversible with cell cycle progression. These and additional findings provide new understanding of human telomerase holoenzyme regulation.

Materials and Methods

Cell culture

Cell lines were maintained in DMEM (Invitrogen) supplemented with 10% FBS (Invitrogen) and 100 μg/ml Primocin (Invivogen). Cells were maintained in a humidified atmosphere of 5% CO_2 at 37°C. Lipofectamine 2000 (Invitrogen) was used for transfection experiments.

Generation of retrovirus

Retrovirus was produced by transfecting the 293 Phoenix packaging cell line with the pBABE-HYGRO-ZZF-hTERT and pBABE-PURO-F-TCAB1, as well as empty vector, using established protocol (Wong, Kusdra, and Collins 2002). HeLa S3 cells were plated on 10 cm dishes and infected in the presence of 5 μg/ml Polybrene (Sigma-Aldrich) the next day. Media was replaced the following morning. Polyclonal stable cell lines were selected with either 300 μg/ml hygromycin B or 2 μg/ml puromycin.

Immunofluorescence

Cells were fixed with 4% paraformaldehyde in PBS for 15 min at room temperature. Cells were then washed with PBS 3 times and permeabilized with 0.1% TX-100 in PBS for 5 min. Cells were then washed and blocked with 4% BSA in PBS for 1 hour at room temperature before addition of primary antibodies. Primary antibodies used were rabbit anti-TCAB1 (1:300, NB100-68252, Novus Biologicals), mouse anti-Coilin (1:250, IH10, Abcam), and mouse anti-FLAG (1:2,000, F1804, Sigma-Aldrich). Following several PBS washes, cells were incubated for an additional hour with goat secondary antibodies conjugated to Alexa Fluor 488 or Alexa Fluor 568 (Invitrogen) and DAPI nuclear counterstain. Cells were then extensively washed with PBS and mounted using ProLong Gold (Invitrogen). Slides were dried overnight and imaged using a Zeiss LSM510 Meta confocal microscope with a ×100/1.49 Apo objective, with 364-, 488-, 543-, and 647-nm laser excitation. Image processing was performed using ImageJ (N.I.H.). Collection of cells held in mitotic block was performed as above, except without TX-100 permeabilization.

Immunoblotting

After heating at 80°C for 5 min, protein samples were cooled to room temperature and resolved by Bis-Tris SDS-PAGE in MOPS buffer (250 mM MOPS, 250 mM Tris, 5 mM EDTA, 0.5% SDS; pH 7.0). Protein was then transferred to nitrocellulose membrane and subsequently blocked using 4% nonfat milk (Carnation) in TBS buffer (150 mM NaCl, 50 mM Tris pH 7.5) for 1 hour at room temperature. Membranes were then incubated with primary antibodies overnight at 4°C. Primary antibodies used were mouse anti-tubulin (1:500, DM1A, Calbiochem), mouse anti-phosphoserine 10 Histone H3 (1:2,000, sc-8656-R, Santa Cruz Biotechnology), mouse anti-FLAG (1:4,000, F1804, Sigma-Aldrich), rabbit anti-cyclin A (1:2,000, H-432, Santa Cruz Biotechnology), rabbit anti-TCAB1 (1:2,000, NB100-68252, Novus Biologicals), rabbit anti-Cdc2 pTyr15 (1:1,000, 9111, Cell Signaling Technology), and rabbit IgG (1:10,000, Sigma-Aldrich). Membrane was washed in TBS and incubated with goat anti-mouse Alexa Fluor 680 (1:2,000, Life Technologies) and goat anti-rabbit IR Dye 800 (1:10,000, Rockland Immunochemicals) in 4% nonfat milk in TBS for 1 hour at room temperature. After extensive washing with TBS, the membrane was visualized on a LI-COR Odyssey imager.

Cell cycle synchronization

Cells were plated at 30-40% confluency. For G1/S synchronization, cells were incubated with 2 mM thymidine for 24 hours. Cells were then washed 3 times with PBS and fresh media was added. 8 hours later, cells were re-incubated with 2 mM thymidine for a second round of thymidine block. 16-18 hours later, cells were washed with PBS 3 times and fresh media was added to continue synchronized cell cycle progression. For mitotic synchronization, cells underwent a single round of thymidine block as above, and, 3 hours after cells were washed of thymidine, 100 ng/ml nocodazole (Sigma-Aldrich) was added. Cells were held in nocodazole for 12 hours. Cells were then collected, washed 3 times with PBS, and re-plated in fresh media to continue cell cycle progression. For synchronized progression into mitosis, cells were double thymidine block synchronized as above, released, and allowed to progress for 8 hours before addition of 9 nM S-Trityl-L-cysteine (STLC) (Sigma-Aldrich). For fluorescence microscopy of mitotic cells, asynchronous cells were held in 9 nM STLC for 4 hours to enrich the mitotic population before fixation. Synchronization was verified by cyclin A levels and the presence of Histone H3 phosphoserine 10.

Cellular crosslinking

Media was aspirated and cells were crosslinked on dishes in PBS containing 0.25% formaldehyde at 37°C for 10 min. Formaldehyde was then quenched with 300 mM Tris pH 8.0 for 10 min at room temperature. Cells were then washed 3 times with PBS, scraped into PBS, pelleted at 17,000 RCF for 5 min in Eppendorf tubes, and resuspended in RIPA buffer (150 mM NaCl, 50 mM Tris pH 7.5, 1 mM EDTA, 1% TX-100, 0.5% Na Deoxycholate, 0.1% SDS, 1 mM DTT) before sonication. For cells held in mitotic block and for collection of time points that included a mitotic synchronization step, cells were first scraped into suspension, centrifuged at 1,000 RCF for 5 min in 15 ml conical tubes, and resuspended in PBS with 0.25% formaldehyde, followed by incubation and quenching steps as above. Sonication was performed on ice with a Branson Sonifier 250 at 30% power, 50% duty cycle, and duration of 15 sec for 3 cycles. Samples were then centrifuged at 17,000 RCF for 5 min at 4°C and the supernatants were transferred to new tubes for processing.

RNP purification

For non-denaturing IP, whole cell extract was generated via hypotonic cell lysis as before (Mitchell, Wood, and Collins 1999), except that the salt concentration never exceeded 200 mM NaCl. Whole cell extract was rotated with magnetic anti-FLAG M2 beads (Sigma-Aldrich) for 2 hours at room temperature. Beads were then washed with HL150 buffer (20 mM HEPES pH 8.0, 2.5 mM $MgCl_2$, 0.25 EGTA, 10% glycerol, 1 mM DTT, 1 mM PMSF, and 150 mM NaCl) several times. After the final wash, a portion of the samples were eluted with 3xFLAG peptide (Sigma-Aldrich) for protein SDS-PAGE and the remainder was mixed with TRIzol (Life Technologies) for RNA purification. For denaturing IP of crosslinked whole cell extract, samples were rotated with magnetic anti-FLAG M2 beads, Rabbit IgG agarose resin (Sigma-Aldrich), or EZview Red anti-c-Myc affinity gel (Sigma-Aldrich) for 4 hours at 4°C. Samples were then washed with RIPA buffer 5 times. After the final wash, beads were resuspended in 50 µl RIPA buffer containing 100 µg/ml proteinase K. Samples were then incubated at 50°C for 1 hour, followed by 70°C for 1 hour for crosslinking reversal. TRIzol was then added directly to samples.

Reverse transcription and quantitative PCR (RT-qPCR)

RNA was purified via TRIzol according to manufacturer instructions (Life Technologies) using linear polyacrylamide as carrier. RNA was resuspended in H_2O and then treated with RQ1 DNase (Promega) in the presence of RNasin (Promega) for 30 min at 37°C. DNase was then inhibited by the addition of RQ1 stop buffer and incubation at 65°C for 10 min. cDNA generation from DNase-treated RNA samples was performed with target-specific oligonucleotides and Superscript III according to manufacturer instructions (Invitrogen) with slight modifications. Initial reverse transcription primer annealing was carried out with a 20 sec incubation at 80°C, followed by 2 min at 65°C, then 1 min at 50°C, before being cooled to 4°C. Superscript III reverse transcriptase was added to samples on ice, and then samples were incubated on a pre-warmed 55°C block for 30 min. Reverse transcription was halted by an 85°C incubation for 5 min. qPCR was performed on a CFX96 Touch Real-Time PCR Detection System (Bio-Rad). 2 µl of cDNA was used per 20 µl qPCR reaction with iTaq Universal SYBR Green Supermix and 300 µM each of the forward and reverse primers. qPCR was carried out for 35 cycles at 95°C for 15 sec and 60°C for 45 sec, after an initial 2 min 95°C hot start. RT-qPCR data was quantified using the delta-delta Ct method. Statistical analysis was performed in GraphPad Prism 6 (GraphPad Software) using ANOVA with Tukey's multiple comparison test, unless otherwise noted. Error bars represent standard error of the mean. PCR amplification efficiencies were calculated using the LinRegPCR program (Ramakers et al. 2003). Reference gene quality was assessed by the NormFinder Excel add-in (Andersen, Jensen, and Orntoft 2004). The following oligonucleotides were used, where the reverse transcription and the reverse primer for PCR are the same: hTR FWD (5'-CCCTAACTGAGAAGGGCGTA-3'), hTR REV (5'-AGAATGAACGGTGGAAGGCG-3'), RNA POL II FWD (5'-ACGAGTTGGAGCGGGAATTT-3'), RNA POL II REV (5'-TTCCTTGACTCCCTCCACCA-3'), U1 FWD (5'-TTTCCCAGGGCGAGGCTTAT-3'), U1 REV (5'CCCCACTACCACAAATTATGCA-3'), precursor hTR FWD (5'-CTCGGCTCACACATGCAGTT-3'), precursor hTR REV (5'-GCCCAGTCAGTCAGGTTTGG-3'), GAPDH FWD (5'-TGCACCACCAACTGCTTAGC-3'), GAPDH REV (5'-GGCATGGACTGTGGTCATGAG-3', actin FWD (5'-CTGGAACGGTGAAGGTGACA-3'), actin REV (5'-AAGGGACTTCCTGTAACAATGCA-3').

Quantitative telomeric repeat amplification protocol (QTRAP)

QTRAP was performed on whole cell extract generated from hypotonic lysis similar to previously published protocol (Wege et al. 2003). Protein concentration was determined by the BCA protein assay (Pierce). 2 µl of diluted whole cell extract was used per 20 µl QTRAP reaction constituted of iTaq Universal SYBR Green Supermix (Bio-Rad) and 0.1 µg TS and 0.02 µg ACX primers. Samples were incubated at 30°C for 30 min before a 2 min 95°C hot-start and 35 cycles of 95°C for 15 sec and 61°C for 90 sec. Relative telomerase activity was calculated by delta Ct to the reference sample. For RNase treatment, 20 µg/ml RNase A was added to whole cell extract.

Northern blot

RNA was purified using TRIzol. Northern blot detection of hTR and the recombinant RNA recovery control for RNA precipitation was performed as described (Fu and Collins 2003). U6 small nuclear (sn) RNA was detected using ^{32}P end-labeled probe (5'AGTATATGTGCTGCCGAAGCG-3') under similar conditions as hTR hybridization, except at 37°C.

Results

Quantitative assays detect human telomerase subunit assembly

We sought to evaluate cell cycle dependent changes in hTR association with hTERT and TCAB1. Subunit interactions can be assayed in non-denaturing conditions after gentle cell lysis or in denaturing conditions after *in vivo* crosslinking and harsh cell lysis. The latter method is more discriminating for physical proximity but less sensitive, due to low crosslinking efficiency. However, non-denaturing cell extract can allow interactions to occur that differ from interactions *in vivo*. Previous studies have used eukaryotic cell extracts to assemble recombinant hTERT and hTR as a minimal active RNP, but on the other hand, mixing of human 293T cell extracts containing overexpressed hTERT or overexpressed hTR showed little if any increase in active RNP (Wenz et al. 2001; Cristofari et al. 2007). Therefore we first evaluated whether the production of cell extracts affects the determination of *in vivo* protein-RNA interactions.

To test if telomerase subunit associations occurred *de novo* in extract, we transfected a telomerase-null immortalized human cell line, VA-13, to express tandem Protein A domain (ZZ) and 3x-FLAG (F)-tagged hTERT and hTR individually and combined the subunits after expression (Fig. 1A, left and middle). We used a SYBR Green quantitative PCR version of the telomeric repeat amplification protocol, QTRAP, to assay the amount of hTERT-hTR RNP product synthesis (Wege et al. 2003). Cell extracts were assayed using 200 ng total protein, which gives a robust and specific signal well within in the quantifiable linear range and discriminating for small changes in activity level (Fig. 2A-C). Due to the use of VA-13 cells, there was no background of active RNP in untransfected cell extract (Fig. 1A, Mock). As expected, robust assembly of active RNP was accomplished by coexpression of hTERT and hTR (Fig. 1A, set 1). In contrast, across a broad range of cell and extract mixing conditions including different times and temperatures, no active telomerase was assembled by mixing hTERT and hTR cell extracts after subunit synthesis (Fig. 1A, sets 2-4).

We next evaluated native extract assembly of hTR and TCAB1. We transfected VA-13 (data not shown) or 293T (Fig. 1B) cells to express hTR and/or F-TCAB1, separately or together. We assayed protein-RNA interaction by FLAG antibody IP of F-TCAB1 followed by northern blot for hTR. Maximal interaction was observed when the two subunits were coexpressed. TCAB1 IP of co-overexpressed hTR was much greater than TCAB1 IP of endogenous hTR (Fig. 1B, sets 2 and4). Importantly, TCAB1 IP of hTR increased if extracts from cells overexpressing TCAB1 or hTR alone were mixed after cell lysis (Fig. 1B, sets 2-3). Therefore, unlike the hTERT-hTR interaction, the TCAB1-hTR interaction can occur in cell extract as well as in intact cells.

The binding of TCAB1 to hTR in lysed cell extract obscures determination of RNP assembled *in vivo*. We therefore developed an *in vivo* crosslinking approach for detecting biologically assembled RNP. We combined formaldehyde crosslinking, to capture snapshots of the cellular milieu, with hTR quantification by RT-qPCR, because crosslinked RNA detection required more sensitivity than provided by northern blot hybridization. We designed RT-qPCR primers for hTR at the template/pseudoknot region and established their specificity for detecting hTR (Fig. 3A, B). With the goal of reliably quantifying hTR-bound proteins across the cell cycle, we determined the best reference gene for relative quantification (Fig. 3C) based on expression constancy throughout the cell cycle (Andersen, Jensen, and Orntoft 2004). Using transient transfection of 293T cells to overexpress the subunits, we verified that formaldehyde crosslinking detected hTR interaction with proteins known to bind hTR directly such as hTERT

and TCAB1 (see below). We also detected hTR crosslinking to dyskerin but not to the shelterin proteins TPP1 or TIN2 (data not shown).

We repeated the cell extract mixing experiments using *in vivo* crosslinking and denaturing rather than native binding conditions. TCAB1 interaction with hTR was quantified using RT-qPCR, normalizing bound to input hTR level in each sample. TCAB1-hTR association was detected when the subunits were coexpressed by transfection of VA-13 cells, with or without coexpression of hTERT (Fig. 1C, sets 1-3). Unlike the case for native cell extracts, mixing of extracts from crosslinked cells transfected to express only TCAB1 or hTR gave no detectable TCAB1-hTR interaction (Fig. 1C, set 4). The specificity of crosslinking and IP was confirmed by RT-qPCR for GAPDH mRNA and U1 snRNA, neither of which was detectable in association with F-TCAB1. These assays establish *in vivo* crosslinking as a method to quantify biological assembly of hTR with TCAB1. Furthermore, the findings demonstrate that hTERT is not required for TCAB1-hTR interaction *in vivo*.

Endogenous telomerase subunit and enzyme catalytic activity levels are unchanged across the cell cycle

To begin a coordinated study of telomerase holoenzyme assembly dynamics, we first established total hTR level and hTERT-hTR RNP catalytic activity across a synchronized HeLa cell cycle. Although some findings differ (Zhu et al. 1996; Lee et al. 2014), several previous reports describe no substantial change across the cell cycle of hTR level (Jády, Bertrand, and Kiss 2004; Xi and Cech 2014) or telomerase activity in cell extracts (Holt et al. 1997; Wong, Kusdra, and Collins 2002). Endogenous hTERT protein level has not been possible to assay for cell cycle regulation, due to low abundance. HeLa cells were synchronized at G1/S by double thymidine block, released to growth, and sampled with high temporal resolution of cell cycle progression. Cell cycle progression was followed by immunoblot for cyclin A (Fig. 4A, top). Cyclin A is an ideal marker for cell cycle progression because its expression steadily increases through S, peaks in G2, decreases as cells complete M, and remains low in G1 (Donjerkovic and Scott 2000). For HeLa cells synchronized at the G1/S border, cyclin A level peaked around 8 hours post-release, marking G2 (Fig. 4A, top). A dramatic decrease in cyclin A level occurred around 12 hours post-release from G1/S as cells completed M and entered G1. To verify that most cells recovered from the block to cell cycle progression and continued through S, we confirmed the loss of Cdc2 phosphorylation on tyrosine 15 (Fig. 4A).

We used QTRAP to assay telomerase activity and RT-qPCR to assay total hTR. Consistent with previous studies, here assayed by time points taken every 1.5 or 2 hours, telomerase catalytic activity in extract and total hTR level were unchanged throughout the cell cycle (Fig. 4A). Total TCAB1 protein level also did not fluctuate with cell cycle progression (Fig. 4B). In case HeLa cells represent a unique case of telomerase cell cycle regulation, we measured telomerase activity across a synchronized cell cycle of the spontaneously immortalized HaCaT human keratinocyte cell line. As found for HeLa cells, telomerase activity in HaCaT cell extracts remained at a stagnant level over the course of the cell cycle (Fig. 4C).

Increased hTERT or TCAB1 level does not stimulate assembly of the other subunit with hTR

To investigate the cell cycle regulation of hTR physical interaction with hTERT and TCAB1, we generated HeLa cell lines stably expressing F-tagged versions of the proteins. We verified the intended protein expression in HeLa ZZF-hTERT and HeLa F-TCAB1 cell lines by

immunoblots (Fig. 5A). F-TCAB1 accumulated to a much higher level than ZZF-hTERT, as F-TCAB1 but not ZZF-hTERT was readily detected by FLAG antibody immunoblot of whole cell extract. Telomerase activity assayed by QTRAP in the cell lines was similar to that of the parental HeLa cell line (Fig. 5A, right). In all cell lines, immunofluorescence (IF) localization of total TCAB1 showed protein concentration in discrete Cajal body foci, colocalized with coilin (Fig. 5B, additional data not shown). In the F-TCAB1 HeLa cells, FLAG antibody IF strongly stained Cajal bodies as expected (Fig. 5B). A few cells expressing ZZF-hTERT also had FLAG antibody staining of a few Cajal body foci (Fig. 5B), but most cells in the population lacked FLAG antibody staining, consistent with the low expression level of ZZF-hTERT and heterogeneous hTERT localization dependent on factors including the cell cycle. None of the negative-control parental HeLa cells stained with FLAG antibody (Fig. 5B).

We first used these cell lines to assay whether hTERT or TCAB1 reciprocally stimulated RNP assembly of the other subunit. Individual proteins were overexpressed in the ZZF-hTERT and F-TCAB1 cell lines by transient transfection, and impact of subunit overexpression on hTERT-hTR or TCAB1-hTR interaction was determined by QTRAP of native cell extract for the hTERT-hTR interaction and *in vivo* crosslinking and RT-qPCR for the TCAB1-hTR interaction. In HeLa ZZF-hTERT cells, overexpression of TCAB1 did not stimulate an increase in assembly of the active hTERT-hTR RNP (Fig. 5C). There was also marginal, if any, change in hTERT-hTR RNP upon overexpression of the shelterin protein TPP1 or the TPP1 oligonucleotide/oligosaccharide (OB) fold, which binds hTERT to assemble and activate telomerase at telomeres. Furthermore, none of several overexpressed H/ACA RNP biogenesis factors had an impact on telomerase activity level, including overexpression of the H/ACA RNP assembly chaperone NAF1 (Fig. 5C, additional data not shown).

We next assayed for factors affecting the level of hTR association with TCAB1. In HeLa F-TCAB1 cells, overexpression of hTERT did not substantially increase the amount of TCAB1-hTR RNP *in vivo* (Fig. 5D), paralleling the comparable TCAB1-hTR interaction in transfected VA-13 cells with or without co-expressed hTERT (Fig. 1C). Also, despite sharing a role with TCAB1 in telomerase recruitment to telomeres, neither TPP1 nor the TPP1 OB fold stimulated TCAB1-hTR interaction (Fig. 5D). Furthermore, overexpression of many H/ACA RNP biogenesis factors did not affect TCAB1-hTR interaction (data not shown). In contrast, overexpression of NAF1 increased TCAB1-hTR association by approximately 3.5-fold (Fig. 5D). This could reflect a role for NAF1 in targeting immature H/ACA RNPs to Cajal bodies for initial steps of RNA modification and RNP subunit exchange. Alternately, NAF1 overexpression could increase TCAB1 availability for hTR interaction indirectly.

The amount of hTERT-hTR interaction is independent of cell cycle progression

To capture the assembly states of hTR across the cell cycle, we assayed hTERT-hTR and TCAB1-hTR interactions by crosslinking. The ZZF-hTERT HeLa cell line was synchronized at G1/S by double thymidine block before release to cell cycle progression, monitored by cyclin A level (Fig. 6A, top). Post-release time points extensively covered S and G2 (0-10.5 hours post-release) and also M/G1 and G1 (12 and 18 hours post-release). We measured input hTR levels, GAPDH mRNA for normalization, and hTR bound to hTERT. The association of hTERT and hTR remained constant over the sampled 18 hours of the cell cycle (Fig. 6A, middle). This result is consistent with the lack of change in RNP catalytic activity monitored by QTRAP of native

ZZF-hTERT cell extracts (Fig. 6A, bottom), recapitulating the results for the HeLa parental cell line (Fig. 4A).

To complement cell cycle synchronization by release from G1/S block, we synchronized ZZF-hTERT cells at prometaphase by a single round of thymidine block followed by addition of the spindle checkpoint activator nocodazole. Mitotic block was confirmed by immunoblot for phosphorylation of Histone H3 serine 10 (Fig. 6B, top) and the ability of adherent cell cultures to easily lift from the dish bottom. Release from mitotic block into G1 and then S was evidenced by the loss of Histone H3 serine 10 phosphorylation (Fig. 6B, top). Cyclin A level was minimal in post-release cells completing M and began increasing after 12-14 hours, as cells entered S (Fig. 6B, top). Cell cycle progression occurred without change in hTERT-hTR interaction assayed by crosslinking and RT-qPCR (Fig. 6B, middle) or QTRAP (Fig. 6B, bottom), corroborating the results using synchronization by double thymidine block (Fig. 6A). Of relevance to the TCAB1 results described below, prolonged mitotic block had no impact on the amount hTERT-hTR RNP (Fig. 6B, compare t=0 of release from mitotic block to asynchronous cell culture).

The amount of TCAB1-hTR interaction varies with cell cycle progression

We next interrogated cell cycle progression changes in TCAB1-hTR interaction using in vivo crosslinking and quantification by RT-qPCR. No change was observed in the amount of hTR bound to TCAB1 in F-TCAB1 cells held at G1/S or released from G1/S block (Fig. 7A). However, in stark contrast to hTERT-hTR interaction, cells in nocodazole-induced mitotic block showed hTR loss of interaction with TCAB1 (Fig. 7B). TCAB1-hTR interaction was regained with 4-10 hours of cell cycle progression post-release (Fig. 7B). Importantly, TCAB1 level was not affected by the mitotic block (Fig. 7B, top). Therefore, TCAB1-hTR association was lost while TCAB1 and hTR subunit levels and hTERT-hTR RNP level all remained unaffected.

To investigate the M-phase dynamics of telomerase holoenzyme composition, we released G1/S-synchronized cells into mitosis. Cells were synchronized at G1/S using a double thymidine block, released to progress toward S, and then, at 8 hours post-release from double thymidine block, we added the mitotic kinesin inhibitor, STLC (Fig. 8A, B, top). The cell population became enriched in M-phase cells, as evidenced by phosphorylation of Histone H3 serine 10 and morphological changes, at 11-13 hours post-release from the initial G1/S block (Fig. 8A, B, top). The amount of hTERT associated with hTR did not decrease as cells approached and entered mitotic block (Fig. 8A). In contrast, TCAB1 association with hTR decreased approximately 5-fold in the M-phase enriched cell population (Fig. 8B).

The decrease in TCAB1-hTR interaction prompted the question of whether Cajal bodies were still present in cells experiencing STLC-induced mitotic block. IF for coilin revealed that Cajal bodies remained present during mitotic block (Fig. 8C), consistent with many previous visualizations of Cajal bodies in cells throughout the cell cycle. However, during mitotic block, TCAB1 lost colocalization with coilin. Instead of concentrating in Cajal bodies, TCAB1 was diffuse throughout the nucleus (Fig. 8C). This diffuse localization was reversed with restored prominent foci of TCAB1 by 8 hours post-release (Fig. 8D). This timing coincides with the restoration of TCAB1-hTR interaction following release from nocodazole-induced mitotic block (Fig. 7B). We conclude that an M-phase regulation of TCAB1 affects its association with both RNA and protein partners.

Holoenzyme exchanges TCAB1 but not hTERT

We next investigated holoenzyme subunit exchange. We synchronized the ZZF-hTERT HeLa line at the G1/S border, using a double thymidine block, or at prometaphase, using STLC after a single round of thymidine block. Cells were then released into cell cycle progression for 1 hour before being transfected to express a competitor Myc-tagged hTERT, followed by continued growth for a total of 10 or 18 hours post-release (Fig. 9 A, B, left). Expression of ZZF-hTERT remained constant, and expression of the competitor Myc-hTERT was detected only in cells transfected with this construct versus empty vector (Fig. 9A, B). We could not estimate a specific fold overexpression of the competitor Myc-hTERT relative to ZZF-hTERT, because only the overexpressed competitor was detectable by immunoblot with hTERT antibody (data not shown). Cyclin A levels indicate progression through the cell cycle following the release from synchronization and transfection. For the G1/S-synchronized cells, cyclin A levels were elevated at 10 hours post-release, indicating S/G2, and subsequently decreased 18 hours post-release, when cells completed M and entered G1 (Fig. 9A). Conversely, in M-phase synchronized cells, cyclin A levels were low 10 hours post-release, indicating cells still in G1, and were heightened 18 hours post-release as cells were passing through S/G2 (Fig. 9B).

We quantified the amount of hTR bound to ZZF-hTERT and the transiently overexpressed competitor Myc-hTERT using *in vivo* crosslinking, IP, and RT-qPCR. Bound hTR was normalized to input hTR and set relative to control samples transfected with empty vector. The amount of hTR bound to stably expressed ZZF-hTERT remained unchanged at 10 hours or 18 hours post-release from G1/S (Fig. 9A) or prometaphase (Fig. 9B). This suggests little or no exchange of previously assembled ZZF-hTERT with competitor Myc-hTERT. We detected the assembly of competitor Myc-hTERT RNP at all time points post-release, but the major increase in Myc-hTERT RNP correlated with cells progressing through G1 either between 10 and 18 hours post-release from G1/S (Fig. 9A) or within 10 hours post-release from M (Fig. 9B). There appeared to be no gain in Myc-hTERT RNP between 10 and 18 hours post-release from M-phase block (Fig. 9B), consistent with preferential assembly of new hTERT-hTR RNP in G1. Interestingly, total telomerase activity was not substantially increased by competitor hTERT expression (Fig. 9A, B, right), suggesting that overexpression of hTERT without hTR overexpression does not increase the amount of active RNP above its normal steady-state level.

We then tested the dynamics of hTR exchange of TCAB1. Following release of HeLa F-TCAB1 cells from synchronization at G1/S or M, cells were transfected to express competitor ZZ-TCAB1 (Fig. 10A, B, left). New expression of ZZ-TCAB1 and continued presence of F-TCAB1 were verified by immunoblot (Fig. 10A, B). The amount of hTR bound to each tagged TCAB1 was assayed 10 and 18 hours post-release from synchronization by crosslinking, IP, and RT-qPCR. In cells blocked at G1/S and released into S/G2, there was no redistribution of hTR between the pre-assembled and competitor TCAB1 by 10 hours post-release (Fig. 10A), suggesting no exchange and limited if any new TCAB1-hTR RNP assembly during this time. However, between 10 and 18 hours post-release from G1/S, after cells completed M and entered G1 as indicated by the decrease in cyclin A level, hTR exchanged between the F-TCAB1 and competitor ZZ-TCAB1 populations (Fig. 10A). The hTR bound to F-TCAB1 decreased, while hTR bound to the competitor ZZ-TCAB1 increased. These results suggest TCAB1 exchanges preferentially in cells cycling through M phase. Strengthening this conclusion, in cells released from mitotic block immediately prior to ZZ-TCAB1 expression (Fig. 10B), the hTR bound to F-

TCAB1 decreased while hTR bound to the competitor ZZ-TCAB1 increased within 10 hours post-release into G1. There was minimal change in the distribution of hTR between F-TCAB1 and ZZ-TCAB1 from 10 to 18 hours post-release from M-phase block (Fig. 10B), suggesting G1 as the period of maximal TCAB1-hTR RNP assembly.

New hTR RNP biogenesis has cell cycle coordination

The long half-life of hTR (Yi et al. 1999) suggests that most cellular hTR RNP is retained through multiple rounds of cell division. However, the initial biogenesis and folding of active RNP could occur preferentially at certain stage(s) of the cell cycle, as does transcription of budding yeast TLC1 (Dionne et al. 2013). To investigate the cell cycle timing of initial hTR RNP biogenesis, we designed RT-qPCR primers to detect 3'-extended hTR precursor (Fig. 11A). Although not every 3'-extended transcript is necessarily an intermediate to functional RNP, 3'-extended hTR provides a reasonable surrogate for mature hTR precursor because transcripts not protected by H/ACA RNP assembly are rapidly degraded (Richard et al. 2006; Egan and Collins 2012a). Precursor hTR RT-qPCR was benchmarked in parallel to mature hTR RT-qPCR (Fig. 3B) and validated for specificity in parallel using VA-13 cell extract as a negative control (Fig. 11B, left side of each set of assays). Curiously, hTR precursor level was lowest in M and highest in G1 (Fig. 11B, left) in comparison to the constant level of mature hTR across the cell cycle (Fig. 11B, right). This hTR precursor expression profile is consistent with maximal endogenous *de novo* hTR RNP biogenesis in G1. An integrated model of telomerase holoenzyme assembly coupled to cell cycle progression unifies the observations reported in this work and other relevant studies (Fig. 12; see Discussion).

Discussion

Like many chromosome replication factors, telomerase action is restricted within the cell cycle. Some of this restriction arises from S/G2-specific remodeling of telomeric chromatin, which can sequester chromosome 3' ends from access by telomerase or DNA repair proteins (de Lange 2010; Cesare and Karlseder 2012). How much cell cycle regulation is imposed directly on telomerase remains an open question. Yeast telomerase subunits have been relatively well characterized for changes in expression, interaction, and post-translational modification across the cell cycle, with numerous holoenzyme subunits implicated to have some type of regulation (Wellinger and Zakian 2012; Ribeyre and Shore 2013; Tucey and Lundblad 2014). Also, although steady-state levels of TLC1 and telomerase activity in cell extract do not vary with progression of the cell cycle, TLC1 precursor transcription is maximal in G1 (Dionne et al. 2013). These observations provide a context for this work, but the divergence of telomerase and telomere biology between yeast and human cells precludes a direct comparison. In particular, telomerase RNP assembly and nuclear trafficking are phylogenetically variable: vertebrate telomerase is an H/ACA RNP assembled in the nucleus, whereas yeast telomerases are Sm RNPs trafficked between nucleus and cytoplasm (Mitchell, Cheng, and Collins 1999; Seto et al. 1999; Egan and Collins 2012b). A further difference is the nuclear envelope breakdown that occurs prior to chromosome segregation in human but not yeast cells, which obliges hTR RNP relocalization in the nucleus with each G1. Control of telomerase recruitment to telomeres differs as well, as telomerase extends every HeLa cell telomere every cell cycle whereas only a small minority of budding yeast telomeres is elongated in each cell cycle (Zhao et al. 2011; Teixeira et al. 2004).

This study establishes a fundamental description of human telomerase holoenzyme subunit levels and interactions across the cell cycle. We developed and combined quantitative assays for hTR and hTERT-hTR and TCAB1-hTR interactions. The use of *in vivo* crosslinking captured biological interactions without RNP rearrangement in cell extract. We cross-compared results from different cell cycle synchronization methods, with cell cycle progression sampled at high temporal resolution. Our findings establish that total hTR and telomerase catalytic activity remained remarkably consistent across the cell cycle, and total TCAB1 protein level also remained constant with cell cycle progression. Against this context of invariant steady-state levels of the holoenzyme subunits and apparently non-exchanging physical interaction between hTR and hTERT, the cell cycle regulation of hTR association to TCAB1 is dramatic. TCAB1 dissociated from hTR in M-phase cells synchronized by nocodazole block. Dissociation of the TCAB1-hTR interaction also was observed in cells allowed to progress into M after release from synchronization at G1/S. Because this regulation of holoenzyme composition was captured by *in vivo* crosslinking prior to cell lysis, it does not have the caveat of sampling dependent on cell extract. A recent study suggested that hTR assembly with hTERT and TCAB1occurs *de novo* in each S phase (Lee et al. 2014), which differs from the conclusions of this work in proposed dynamics of hTERT-hTR assembly but mirrors this work in suggesting cell cycle regulation of TCAB1.

The cell cycle dynamic of TCAB1-hTR interaction can account for endogenous hTR localization changes described by *in situ* hybridization, which in landmark studies revealed hTR concentration in Cajal bodies peaking in S phase (Jády et al. 2006; Tomlinson et al. 2006). Progressive concentration of hTR in Cajal bodies over G1 would result from restoration of TCAB1-hTR interaction. Although one consequence of TCAB1-hTR interaction is hTR Cajal

body localization, we suggest that the cell cycle regulation of TCAB1-hTR interaction serves a more general role in licensing catalytically active hTERT-hTR RNP for telomere association. This suggestion arises from the observation that Cajal body disruption does not necessarily impede telomerase function: HeLa cells without coilin and thus without Cajal bodies can support telomere recruitment of telomerase and telomere length maintenance (Chen et al. 2015). Since the essential role of TCAB1 appears not to be telomerase localization to Cajal bodies *per se*, TCAB1 role in telomere maintenance remains to be determined. The significance of M-phase removal of TCAB1 from hTR also remains to be elucidated, although an obvious possibility is that this disassembly ensures release of telomerase from telomeric chromatin after each round of genome replication. Curiously, of all of the telomerase RNP biogenesis and trafficking factors tested, only NAF1 overexpression led to an increase in TCAB1-hTR interaction. This could reflect a physiological targeting of NAF1-bound RNPs to Cajal bodies, for example to accomplish the early RNP biogenesis step of hTR 5' trimethylguanosine cap modification (Fu and Collins 2006). However non-physiological consequences of NAF1 overexpression are not excluded.

The hTERT association to hTR remains at a consistent level regardless of whether cells are blocked in or progressing though different stages of the cell cycle, here conclusively demonstrated by *in vivo* crosslinking. This conclusion was anticipated by detection of telomerase activity in extracts of cells lysed after harvesting at different stages of the cell cycle (Holt et al. 1997; Wong, Kusdra, and Collins 2002). That the cellular level of assembled active RNP is not cell cycle regulated is somewhat surprising given the apparent cell cycle dependence of subunit colocalization: endogenous hTERT and hTR appear to colocalize only at telomeres. Thus, although the level of hTERT-hTR RNP is constant, it is not detected as concentrated at a particular nuclear site until TCAB1 and other interaction partners cluster the RNP at Cajal bodies and telomeric chromatin. Other than at telomeres, hTERT-hTR RNP localization is speculative. Individual subunit localizations detected for endogenous or exogenous expression reflect a combination of coassembled RNP and either hTERT-free hTR or hTR-free hTERT.

Surprisingly, in cells not in G1, minimal redistribution of hTR between pre-assembled and competitor hTERT or TCAB1 was detected. These findings suggest that there could be a non-exchangeable subunit content of telomerase RNPs, except as accomplished by cell cycle regulation of TCAB1. It is possible that the substantial steady-state pool of hTERT-free hTR RNP (Xi and Cech 2014) is not competent for active RNP assembly. This suggestion is consistent with poor assembly of active RNP by mixing hTERT and hTR cell extracts or separately folded subunits *in vitro* (Wu and Collins 2014). It will be interesting to apply the *in vivo* crosslinking approach in combination with competition assays to examine cell cycle dynamics of telomerase holoenzyme subunit interactions in budding yeast, which is suggested to include disassembly of the catalytic core (Tucey and Lundblad 2014).

At least in cultured cell lines, because hTR has a long biological half-life of many cell cycles (Yi et al. 1999), only a limited amount of new active RNP assembly needs to occur. Although speculative, based on the preferential G1 assembly of new hTERT-hTR RNP in the subunit competition experiments and the putative increased G1 level of hTR precursor, we suggest that biogenesis of active RNP could occur predominantly in G1. Contemporary with this work, hTERT mRNA was reported to increase ~3-fold in HeLa cell M phase (Xi and Cech 2014). Combining that observation with findings here, a prediction is that hTERT mRNA translation would pre-stock newly synthesized hTERT prior to new hTR RNP biogenesis. Because TCAB1 is maximally dissociated from hTR in M and early G1, and because hTR

without TCAB1 and hTERT is nucleolar (Jády, Bertrand, and Kiss 2004; Theimer et al. 2007; Zhong et al. 2011), hTR synthesized in early G1 may be trafficked to nucleoli (Fig. 12). This could account for the nucleolar association of ~7% of hTR in asynchronously cycling HeLa cells, quantified by subcellular fractionation (Mitchell, Cheng, and Collins 1999). Curiously, the fraction of hTERT associated to nucleoli also appears maximal in G1 compared to its predominantly nucleoplasmic distribution in late S/G2 in IMR90 cells stably expressing a low level of GFP-hTERT (Wong, Kusdra, and Collins 2002). Thus, as originally proposed by others many years ago (Etheridge et al. 2002), nucleoli are candidate sites of initial hTERT-hTR interaction.

As hTR RNPs gain TCAB1 association and TCAB1 returns to Cajal bodies with the elapse of G1, hTR RNPs would shift to a more nucleoplasmic and Cajal body distribution (Fig. 12). Because hTERT increases hTR Cajal body concentration (Tomlinson et al. 2008) and hTERT localization is affected by DNA damage and other signaling pathways (Wong, Kusdra, and Collins 2002; Collins 2008), there could be many inputs governing what fraction of hTERT-hTR RNP is in Cajal bodies prior to S phase. We suggest that partially dependent and partially independent of association to Cajal bodies *per se*, TCAB1 assembly with hTR licenses the catalytically active hTERT-hTR RNP for recruitment to telomeres. This licensing allows telomere extension in S phase, coupled to genome replication, and potentially also in G2, when telomeres can be accessible as substrates for DNA repair (Cesare and Karlseder 2012).

Figure 1. Crosslinking preserves cellular TCAB1-hTR RNPs and prevents new RNP formation in cell extract.
(A) Cell extract mixing using VA-13 cells expressing combinations of exogenous hTR and ZZF-hTERT. Mixing was performed at 4°C and 22°C for 0.5 or 2 hours. Telomerase activity was detected by QTRAP. Values were normalized to VA-13 coexpressing hTR and ZZF-hTERT (n=3). Note that mature hTR migrates as a doublet under the gel conditions used for northern blot detection. The U6 snRNA is a control to demonstrate comparable amounts of input extract.
(B) Cell extract mixing using 293T cells expressing combinations of exogenous hTR and F-TCAB1. hTR bound to F-TCAB1 was detected by FLAG IP and northern blot of hTR. U6 snRNA and tubulin are controls to demonstrate comparable amounts of input extract and also IP specificity. RC is an RNA precipitation recovery control.
(C) A similar experiment was carried out as in (B), except cells were formaldehyde crosslinked before cell lysis. hTR bound to F-TCAB1 was detected by FLAG IP followed by RT-qPCR. Input and F-TCAB1-bound hTR levels were each normalized to input RNA Pol II mRNA and set relative to the triple coexpression sample (n=3). All lanes were from the same blot; a gap indicates removal of extraneous samples.

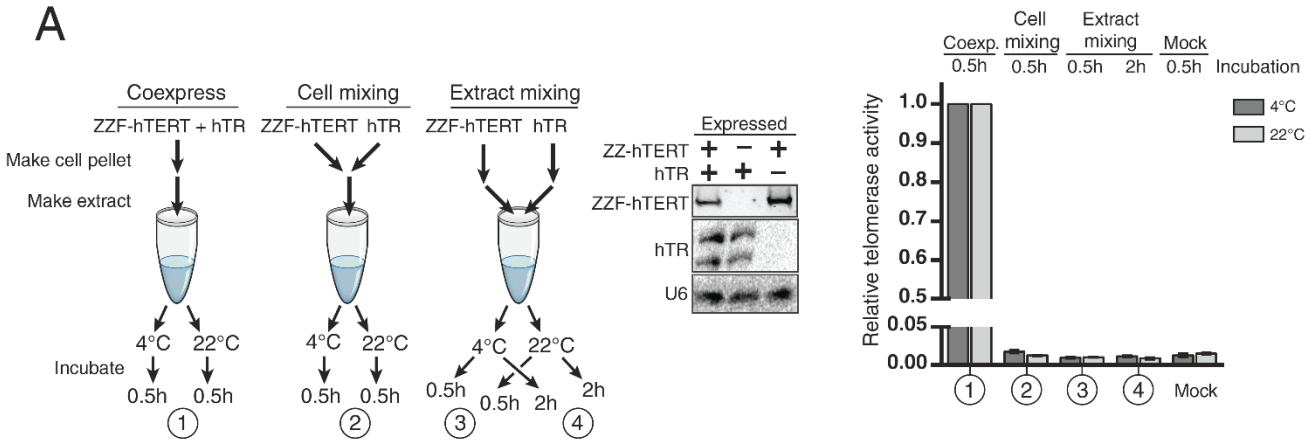
A
Coexpress
Cell mixing
Extract mixing
ZZF-hTERT + hTR
ZZF-hTERT hTR
ZZF-hTERT hTR
Make cell pellet
Make extract
4°C 22°C
Incubate
0.5h 0.5h
0.5h 0.5h
0.5h 0.5h 2h 2h
1 2 3 4
Expressed
ZZ-hTERT
hTR
ZZF-hTERT
hTR
U6
Coexp. 0.5h
Cell mixing 0.5h
Extract mixing 0.5h 2h
Mock 0.5h
Incubation
4°C
22°C
Relative telomerase activity
1.0
0.9
0.8
0.7
0.6
0.5
0.05
0.00
1 2 3 4 Mock

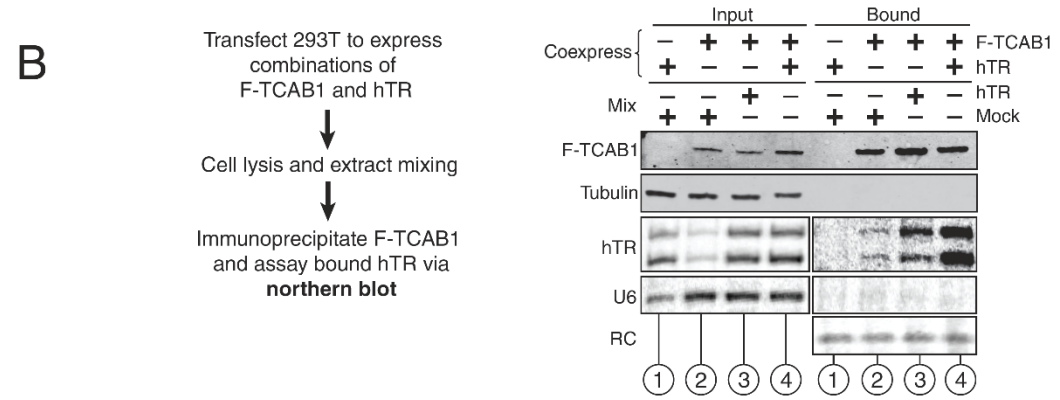
B
Transfect 293T to express combinations of F-TCAB1 and hTR
Cell lysis and extract mixing
Immunoprecipitate F-TCAB1 and assay bound hTR via **northern blot**
Input
Bound
Coexpress
F-TCAB1
hTR
Mix
hTR
Mock
F-TCAB1
Tubulin
hTR
U6
RC
1 2 3 4 1 2 3 4

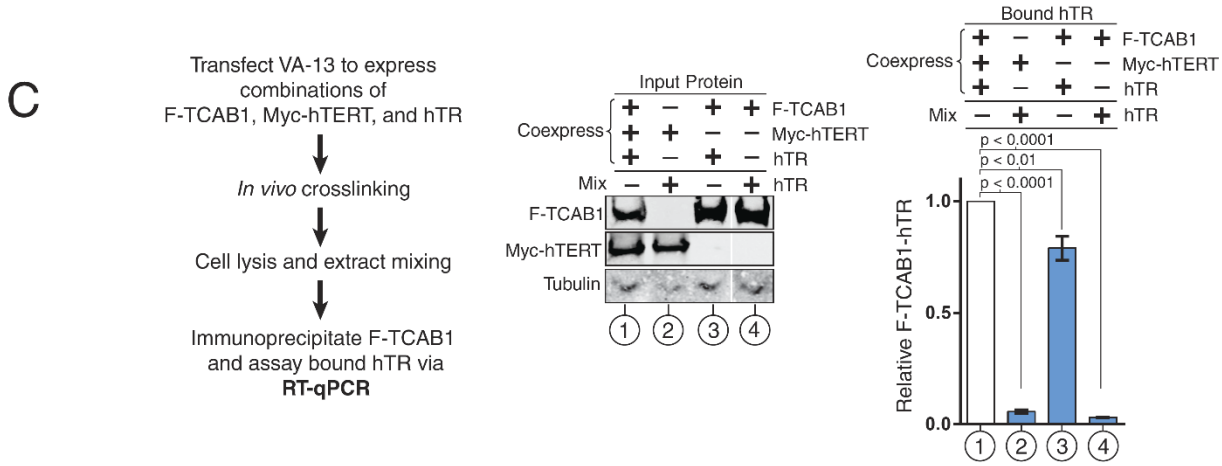
C
Transfect VA-13 to express combinations of F-TCAB1, Myc-hTERT, and hTR
In vivo crosslinking
Cell lysis and extract mixing
Immunoprecipitate F-TCAB1 and assay bound hTR via **RT-qPCR**
Input Protein
Coexpress
F-TCAB1
Myc-hTERT
hTR
Mix
hTR
F-TCAB1
Myc-hTERT
Tubulin
1 2 3 4
Bound hTR
Coexpress
F-TCAB1
Myc-hTERT
hTR
Mix
hTR
p < 0.0001
p < 0.01
p < 0.0001
Relative F-TCAB1-hTR
1.0
0.5
0.0
1 2 3 4

Figure 2. Characterization of telomerase activity using QTRAP with HeLa cell extract.
(A) QTRAP standard curve using total protein titration of HeLa cell extract (n=3).
(B, C) Readout of QTRAP measurements with HeLa, VA-13 or RNase-treated HeLa cell extract (n=6) and with sequentially diluted HeLa cell extract (n=3).

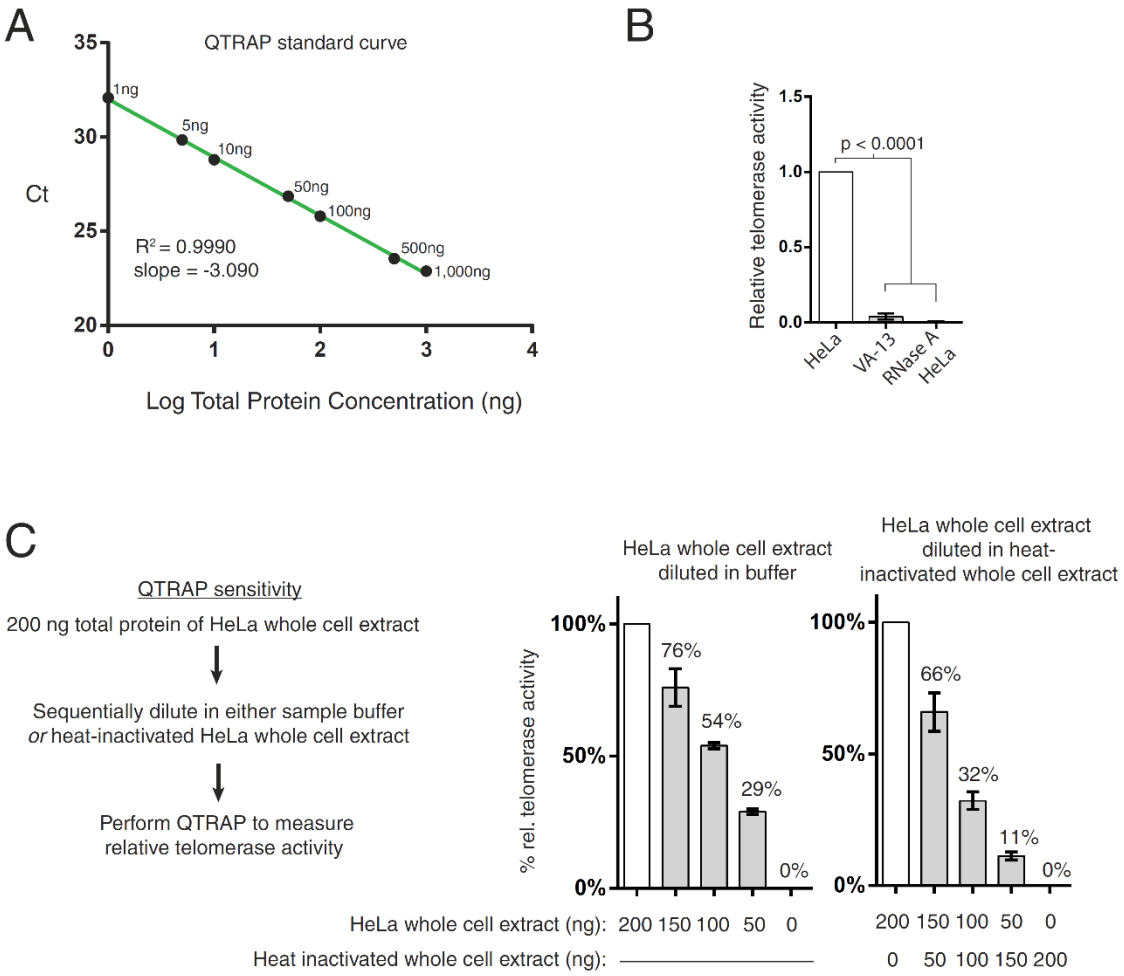

Figure 3. Characterization of RT-PCR products for hTR and reference genes.
(A) Schematic of hTR and RT-qPCR primers used for hTR cDNA generation and PCR amplification.
(B) RT-qPCR of hTR and normalization standards generates single products (+RT lane) and homogenous melt curves (n=8), shown for RNA from native cell extract. PCR amplification efficiencies were measured using the LinReg program for samples from the relevant cell extract without or with in vivo crosslinking. NTC samples lacked RNA template, and minus RT lanes lacked reverse transcriptase.
(C) Potential reference genes for cell cycle RT-qPCR measurements were compared using the NormFinder program. NormFinder stability values and rankings, in parentheses, are shown. GAPDH mRNA and hTR levels were the most consistent over the cell cycle.

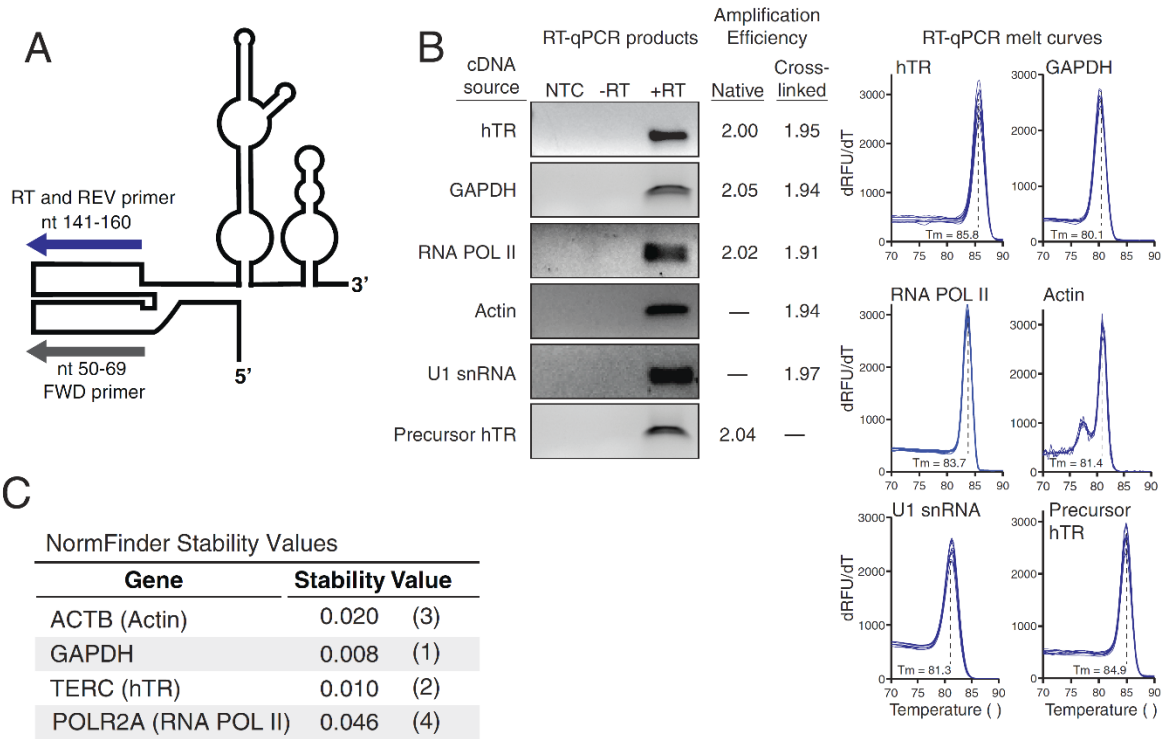

C

NormFinder Stability Values

Gene	Stability Value	
ACTB (Actin)	0.020	(3)
GAPDH	0.008	(1)
TERC (hTR)	0.010	(2)
POLR2A (RNA POL II)	0.046	(4)
U1 snRNA	0.062	(5)

Figure 4. Telomerase activity, hTR, and TCAB1 levels do not change over the cell cycle.
(A) HeLa cells were released from a double thymidine induced G1/S block and cells were harvested at time points as the cell cycle progressed. Telomerase activity was assayed by QTRAP, with values set relative to t=0 at the G1/S block (n=4). Total hTR was measured by RT-qPCR. Values were normalized to GAPDH mRNA and set relative to t=0 (n=3).
(B) Total endogenous TCAB1 protein from HeLa cells synchronized by double thymidine block was measured by immunoblot and quantified relative to tubulin protein (n=5). All lanes were from the same blot; a gap indicates removal of extraneous samples.
(C) HaCaT cells were synchronized at G1/S by double thymidine block. Telomerase activity was measured by QTRAP with values set relative to the t=0 time point (n=3). Asynchronous cell cultures are indicated as async.

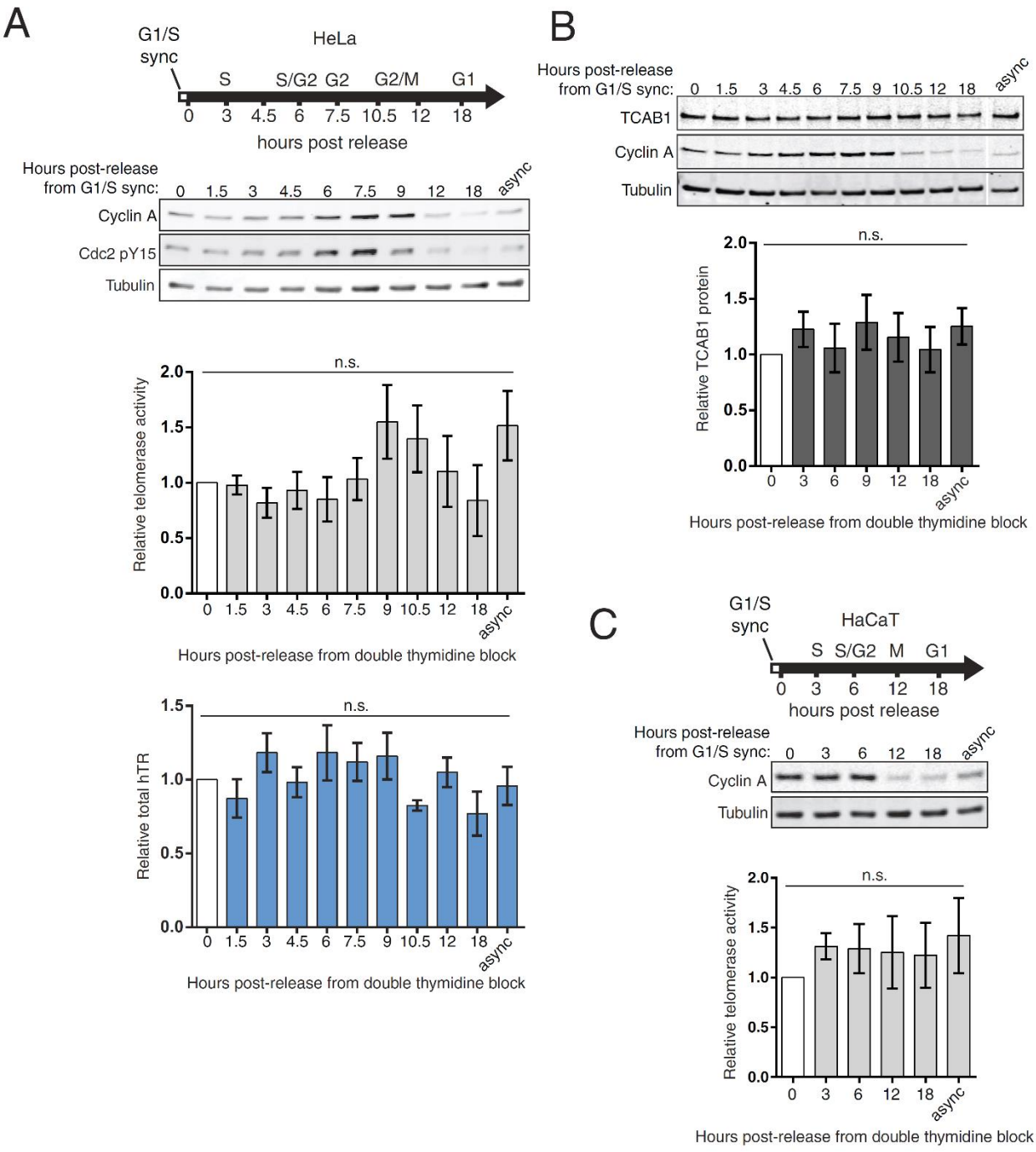
A
G1/S sync
HeLa
S
S/G2
G2
G2/M
G1
0 3 4.5 6 7.5 10.5 12 18
hours post release
Hours post-release from G1/S sync: 0 1.5 3 4.5 6 7.5 9 12 18 async
Cyclin A
Cdc2 pY15
Tubulin
n.s.
Relative telomerase activity
Hours post-release from double thymidine block
Relative total hTR
Hours post-release from double thymidine block
B
Hours post-release from G1/S sync: 0 1.5 3 4.5 6 7.5 9 10.5 12 18 async
TCAB1
Cyclin A
Tubulin
n.s.
Relative TCAB1 protein
Hours post-release from double thymidine block
C
G1/S sync
HaCaT
S
S/G2
M
G1
0 3 6 12 18
hours post release
Hours post-release from G1/S sync: 0 3 6 12 18 async
Cyclin A
Tubulin
n.s.
Relative telomerase activity
Hours post-release from double thymidine block

Figure 5. Overexpression of NAF1 affects TCAB1-hTR association.
(A) HeLa cells stably expressing ZZF-hTERT, F-TCAB1, or empty retroviral vector (control) were confirmed by immunoblot, and relative telomerase activity was measured by QTRAP (n=3).
(B) Localization of ZZF-hTERT or F-TCAB1 was detected by IF for FLAG (green) and total TCAB1 (red) compared to DNA (blue).
(C) Extract from ZZF-TERT HeLa cells transiently overexpressing the indicated individual protein was assayed via QTRAP, with values normalized to mock transfection (n=3). Only some cells stained clearly for ZZF-hTERT, with one example shown.
(D) Telomerase interactors were transiently overexpressed in the F-TCAB1 cell line. Effects on TCAB1-hTR RNP levels were assayed by RT-qPCR following F-TCAB1 IP. Bound hTR was normalized to input hTR and set relative to mock transfection (n=4). All lanes were from the same blot; a gap indicates removal of extraneous samples.

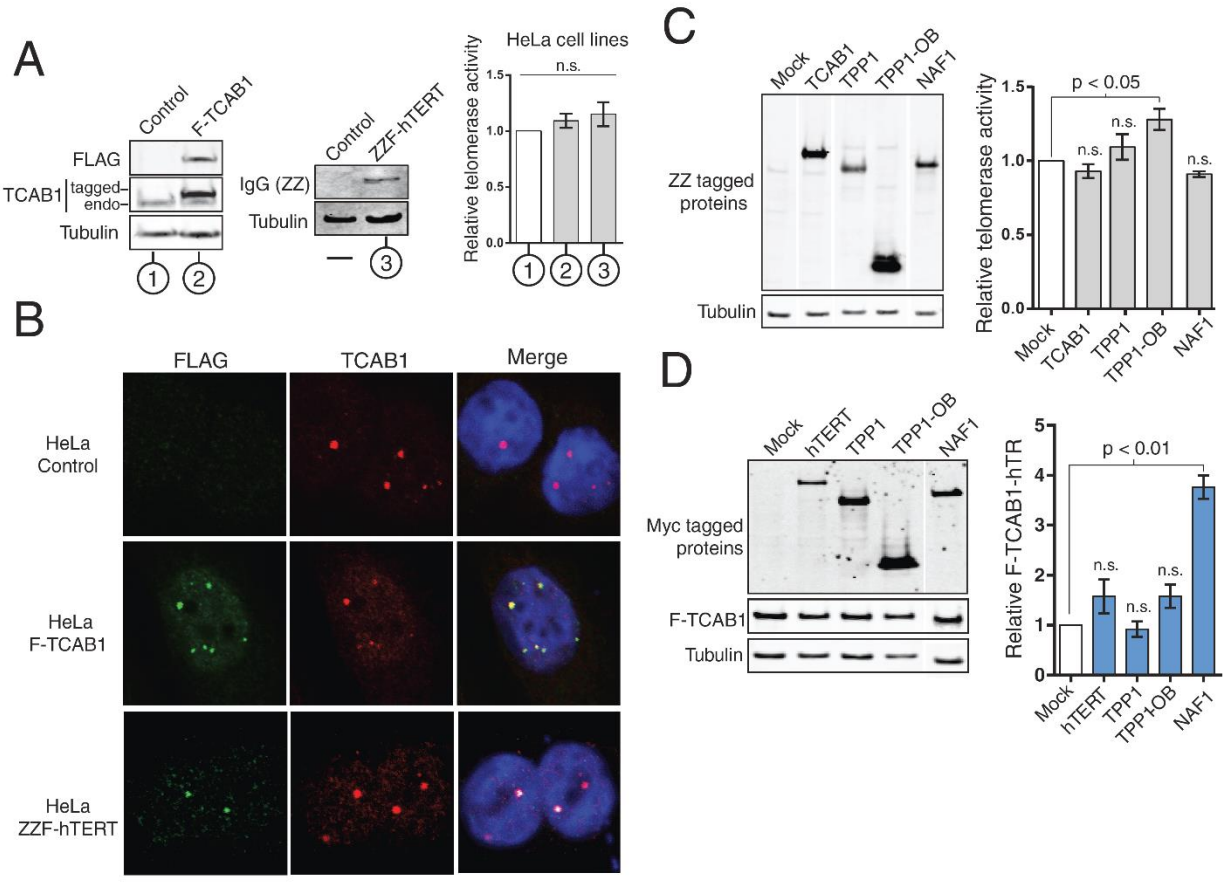

Figure 6. hTERT-hTR RNP and telomerase activity do not significantly change over the cell cycle.

(A) HeLa ZZF-hTERT cells were synchronized at G1/S by double thymidine block. The amount of hTR crosslinked to ZZF-hTERT was assayed via RT-qPCR. Bound hTR values were normalized to input GAPDH mRNA and set relative to t=0 (n=3). Input hTR normalized to input GAPDH was also invariant (not shown). Telomerase activity was measured by QTRAP, with values set relative to t = 0 (n = 3).

(B) HeLa ZZF-hTERT cells were synchronized at prometaphase using nocodazole following a single round of thymidine block and release. The amount of hTERT-hTR RNP and telomerase activity was assayed as in (A) (n = 3). Negative control sample (con) was asynchronously dividing parental HeLa cells.

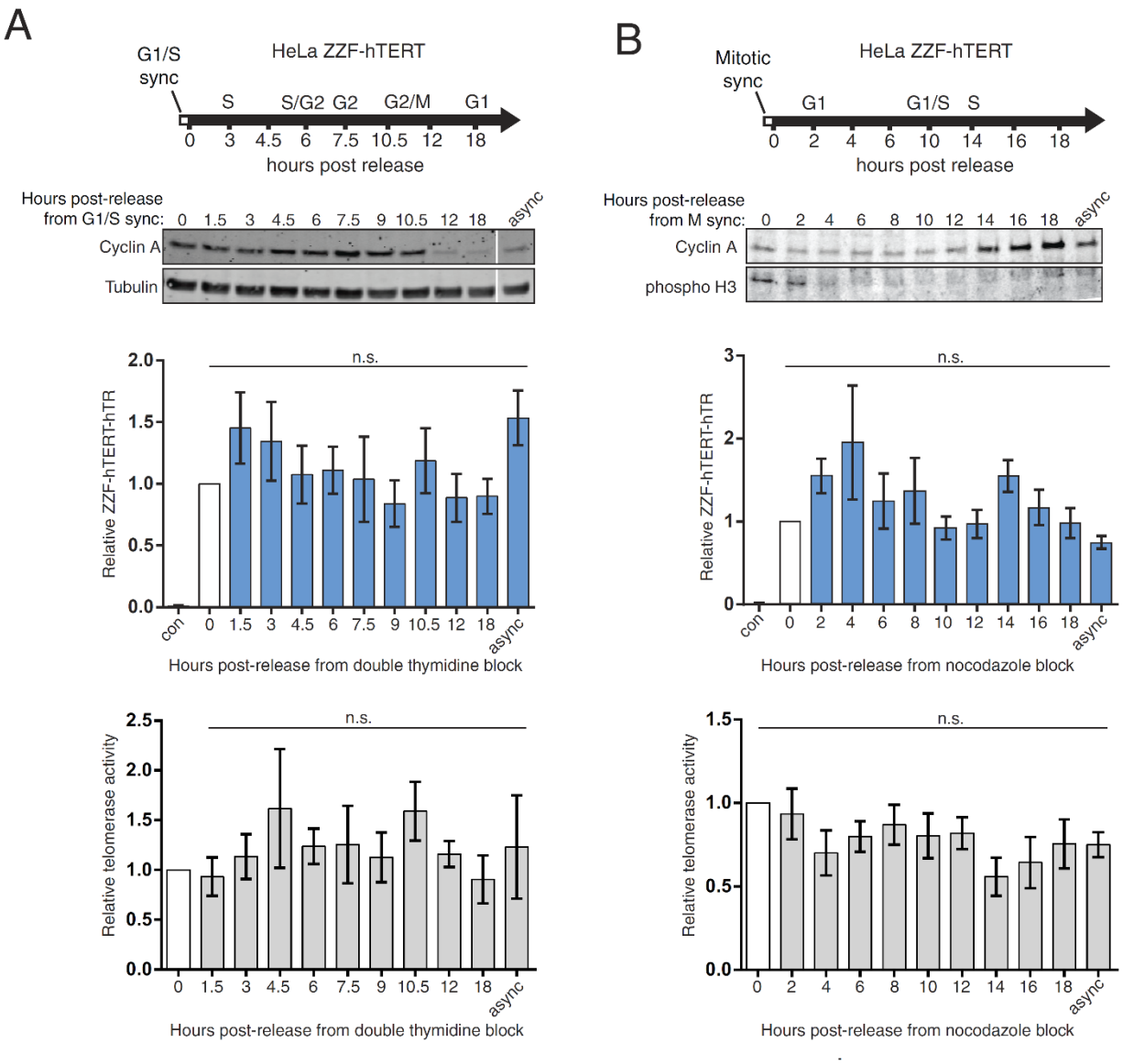

Figure 7. TCAB1-hTR RNP is altered by mitotic block.
(A) HeLa F-TCAB1 cells were synchronized at G1/S using double thymidine block. hTR crosslinked to F-TCAB1 was quantified by RT-qPCR, with values normalized to input hTR and set relative to t=0 (n=3).
(B) HeLa F-TCAB1 cells were synchronized at prometaphase using nocodazole after a single round of thymidine block, then released. F-TCAB1-hTR levels were assayed by RT-qPCR with normalization to input hTR and set relative to t=0 (n=2). Negative control sample (con) was asynchronously dividing parental HeLa cells.

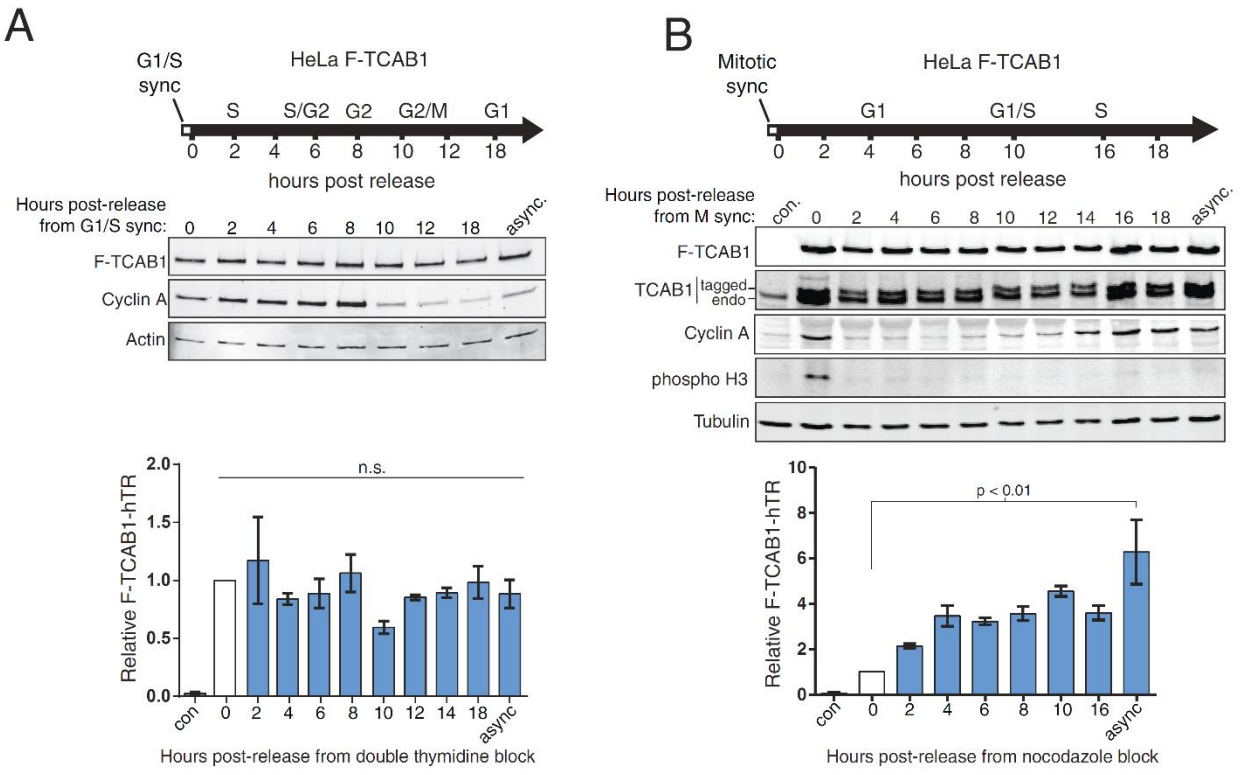

Figure 8. TCAB1 transiently changes nuclear localization and association with hTR.
(A) HeLa ZZF-hTERT cells were synchronized at G1/S using double thymidine treatment and subsequently released into mitotic block using STLC. ZZF-TCAB1-hTR RNP levels were quantified by RT-qPCR, normalized to input hTR, and set relative to t=0 (n=3).
(B) HeLa F-TCAB1 cells were synchronized at G1/S and led into mitotic block as above. F-TCAB1-hTR RNP was assayed as in (A) (n=3).
(C) IF of Coilin (green), TCAB1 (red), and DNA (black/blue) in HeLa F-TCAB1 cells under STLC induced mitotic block.
(D) IF of TCAB1 (green) and DNA (blue) in HeLa F-TCAB1 cells released from STLC mitotic block. Negative control sample (con) was asynchronously dividing parental HeLa cells.

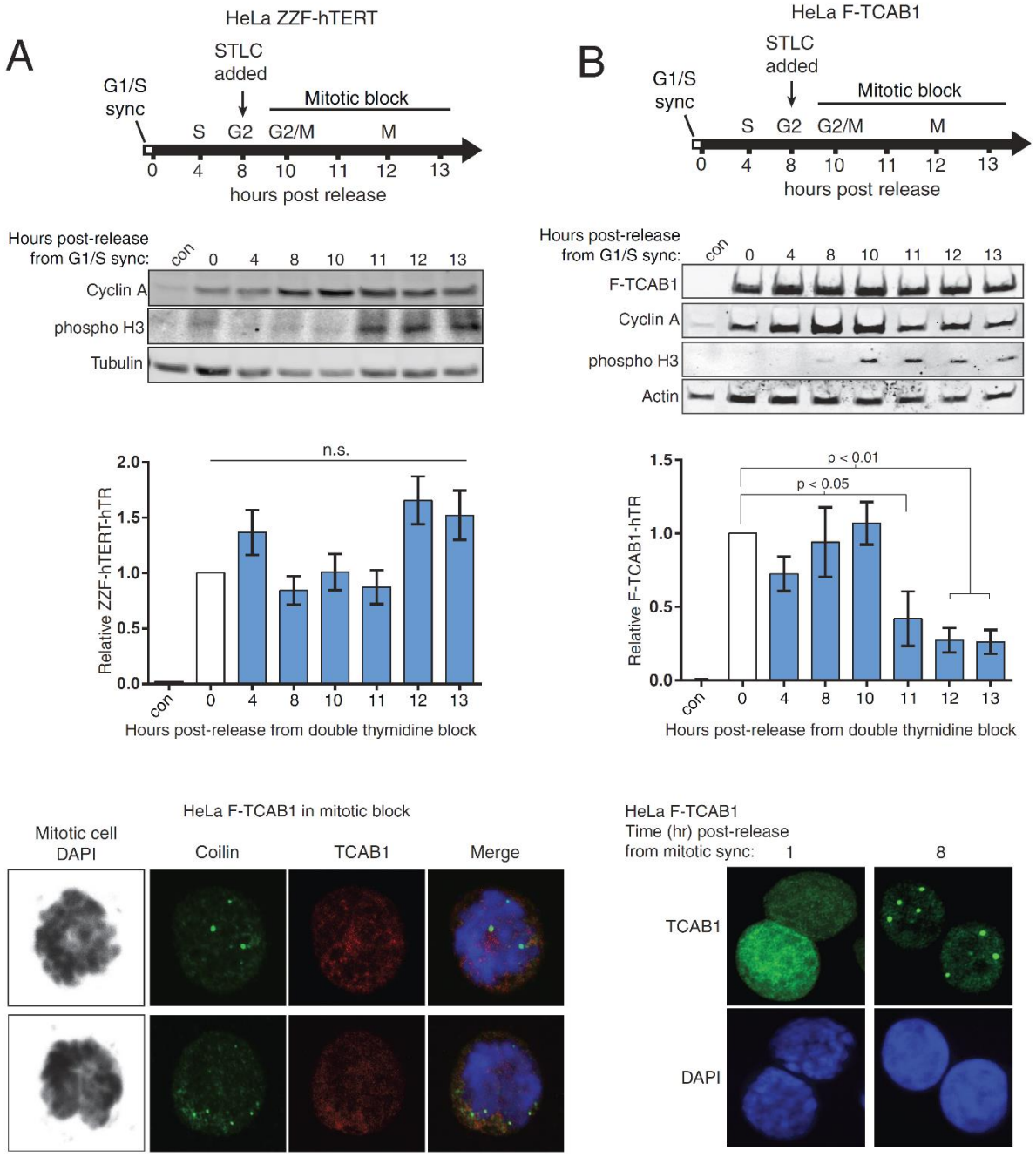
A
HeLa ZZF-hTERT
STLC added
G1/S sync
Mitotic block
S G2 G2/M M
0 4 8 10 11 12 13
hours post release
Hours post-release from G1/S sync: con 0 4 8 10 11 12 13
Cyclin A
phospho H3
Tubulin
n.s.
Relative ZZF-hTERT-hTR
Hours post-release from double thymidine block
B
HeLa F-TCAB1
STLC added
G1/S sync
Mitotic block
S G2 G2/M M
0 4 8 10 11 12 13
hours post release
Hours post-release from G1/S sync: con 0 4 8 10 11 12 13
F-TCAB1
Cyclin A
phospho H3
Actin
p < 0.01
p < 0.05
Relative F-TCAB1-hTR
Hours post-release from double thymidine block
HeLa F-TCAB1 in mitotic block
Mitotic cell DAPI
Coilin
TCAB1
Merge
HeLa F-TCAB1
Time (hr) post-release from mitotic sync: 1 8
TCAB1
DAPI

Figure 9. The hTERT-hTR RNP does not undergo subunit exchange.
(A) HeLa ZZF-hTERT cells were synchronized at G1/S using double thymidine block. Cells were released from block and, after 1 hour, were transfected with empty vector (no competitor, mock) or competitor Myc-hTERT plasmid. Levels of hTR bound to ZZF-hTERT and the competing Myc-hTERT were assayed using RT-qPCR at 10 and 18 hours post-release. hTR values were normalized to input hTR and set relative to the corresponding mock transfection sample (n=3). QTRAP used total cell extract (n=3).
(B) HeLa ZZF-hTERT cells were synchronized at prometaphase using STLC following a single round of thymidine block. One hour post-release, cells were transfected with empty vector or competitor Myc-hTERT plasmid. Bound hTR was assayed as above (n=3).

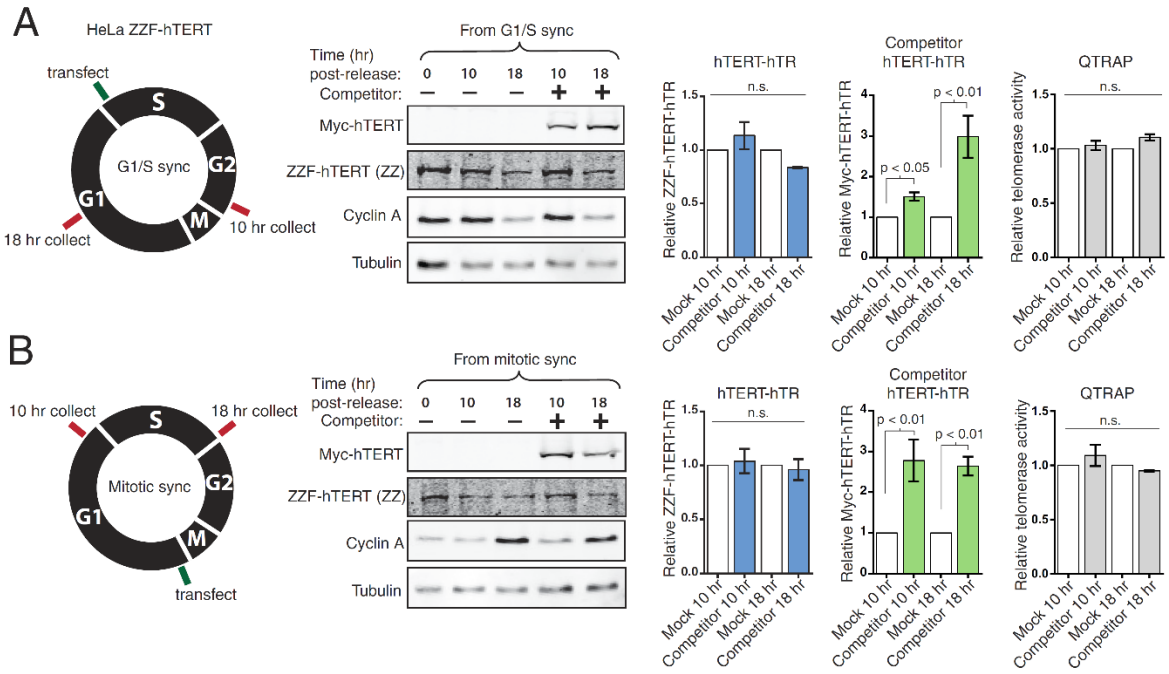

Figure 10. The TCAB1-hTR RNP dissociates and reassembles with progression through mitosis.

(A) HeLa F-TCAB1 cells were synchronized at G1/S using double thymidine block. Cells were released from block and, after 1 hour, were transfected with empty vector (no competitor, mock) or competitor ZZ-TCAB1 plasmid. Levels of hTR bound to F-TCAB1 and the competing ZZ-TCAB1 were assayed by RT-qPCR 10 and 18 hours post-release. hTR values were normalized to input hTR and set relative to the corresponding mock transfection sample (n=6 at 10 hours, n=3 at 18 hours), unpaired *t*-test).

(B) HeLa F-TCAB1 cells were synchronized at prometaphase using STLC following a single round of thymidine block. One hour post-release, cells were transfected with empty vector or competitor ZZ-TCAB1 plasmid. Bound hTR was assayed as above (n=6 at 10 hours, n=3 at 18 hours, unpaired *t*-test).

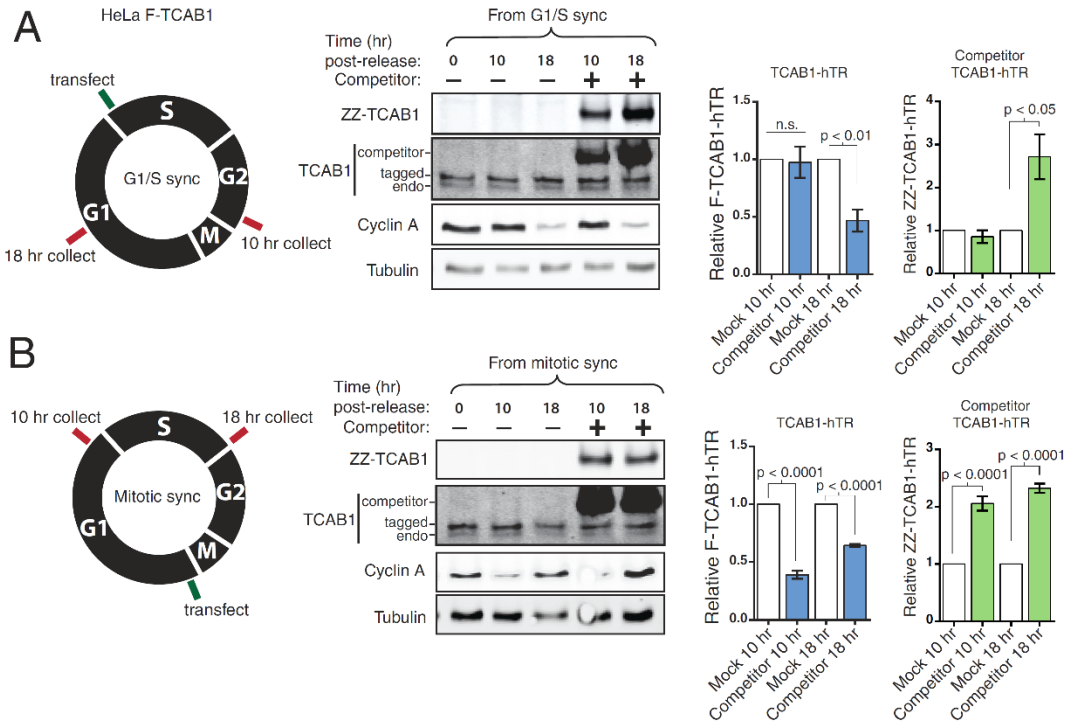

Figure 11. New hTERT-hTR RNP may be assembled predominantly in G1.
(A) RT-qPCR primers were designed to detect the immediate downstream region of the TERC (hTR) gene present only on the hTR precursor before 3' end processing to mature hTR.
(B) Precursor hTR detection in HeLa cells over the cell cycle. HeLa cells were held in S phase by a single round of thymidine block (S sample) and released. At 3 hours post-release (S/G2 sample), STLC was added for mitotic block. At 9 hours after release, an M sample was collected. Mitotic block was subsequently released and time points were collected after the hours of release indicated. The G1 immunoblot sample is 4 hours post-release from mitotic block. Precursor hTR and total hTR levels were measured by RT-qPCR. Values were normalized to GAPDH mRNA and set relative to the sample of cells dividing asynchronously (n=3).

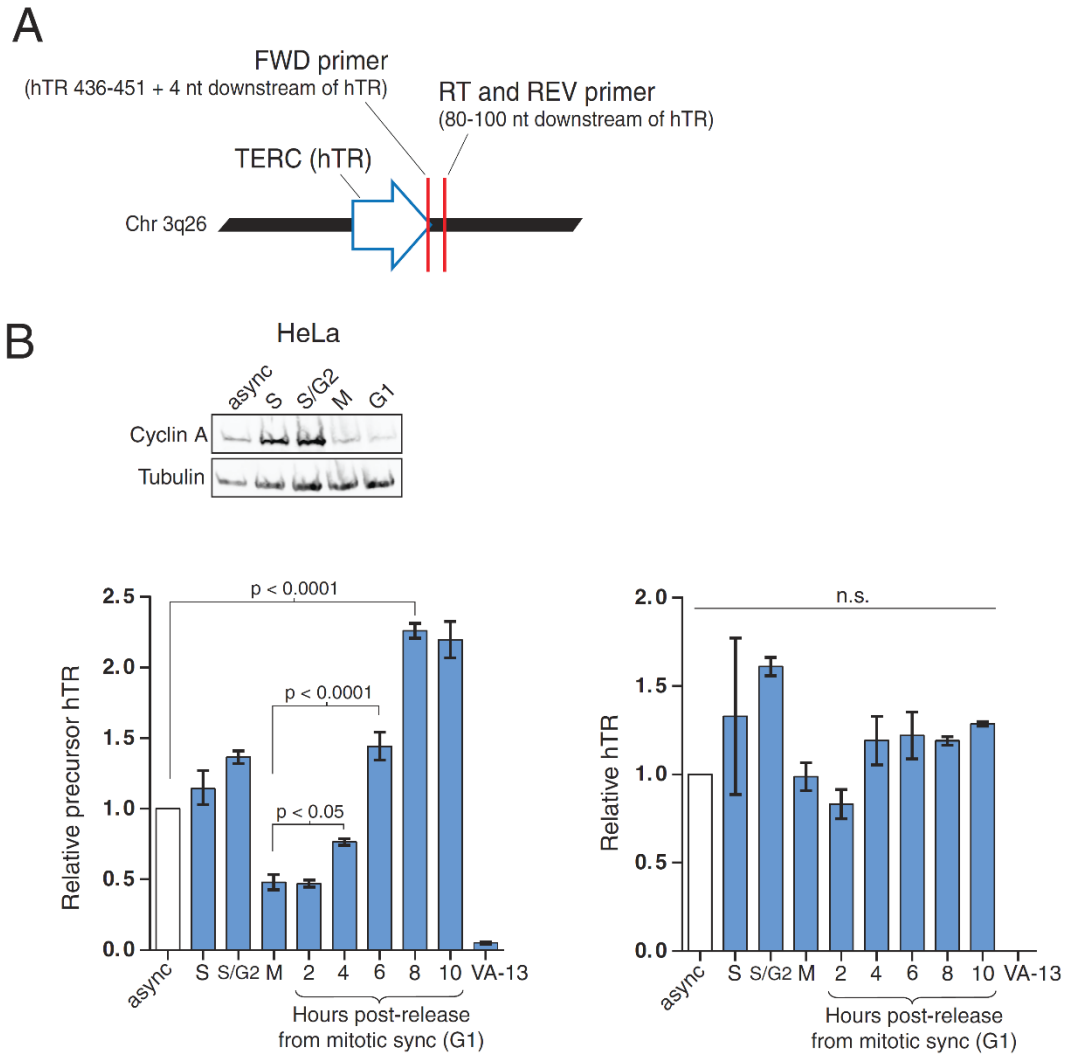

Figure 12. Model for telomerase holoenzyme subunit assembly and disassembly.
While the catalytically active core of telomerase RNP remains intact, TCAB1 dissociates and is reassembled with progression through M and G1, respectively. New hTR RNP biogenesis may peak in G1, accompanied by RNP assembly with hTERT.

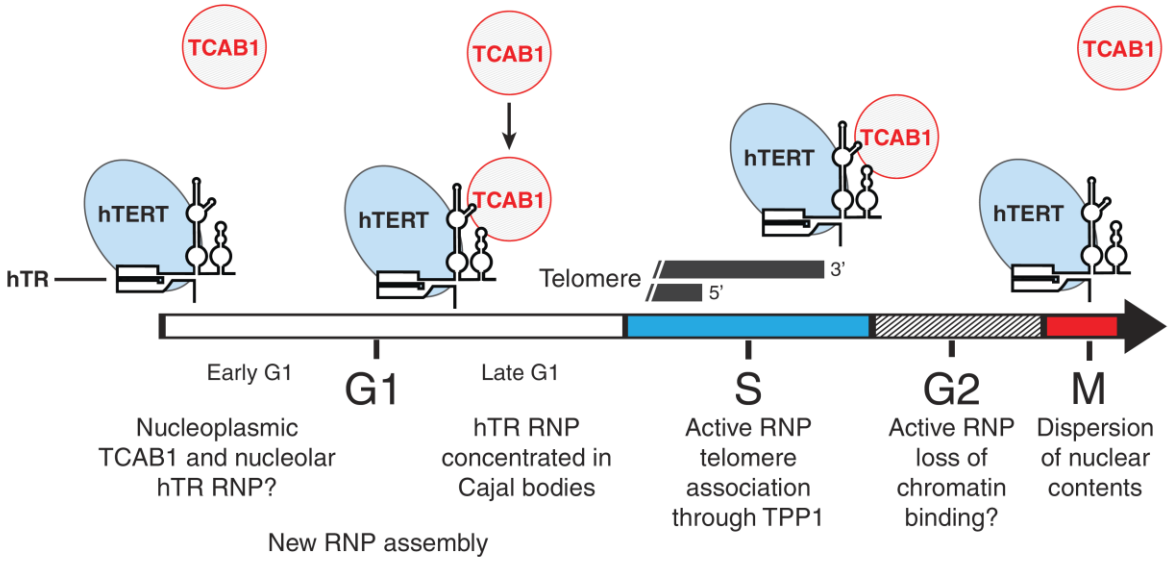

CHAPTER THREE

Minimized human telomerase maintains telomeres and resolves endogenous roles of H/ACA proteins, TCAB1, and Cajal bodies

Abstract

We dissected the importance of human telomerase biogenesis and trafficking pathways for telomere maintenance. Biological stability of human telomerase RNA (hTR) relies on H/ACA proteins, but other eukaryotes use other RNP assembly pathways. To investigate additional rationale for human telomerase assembly as H/ACA RNP, we developed a minimized cellular hTR. Remarkably, with only binding sites for telomerase reverse transcriptase (TERT), minimized hTR assembled biologically active enzyme. TERT overexpression was required for cellular interaction with minimized hTR, indicating that H/ACA RNP assembly enhances endogenous hTR-TERT interaction. Telomere maintenance by minimized telomerase was unaffected by elimination of the telomerase holoenzyme Cajal body chaperone TCAB1 or the Cajal body scaffold protein Coilin. Surprisingly, wild-type hTR also maintained and elongated telomeres in TCAB1 or Coilin knockout cells, with distinct changes in telomerase action. Overall we elucidate trafficking requirements for telomerase biogenesis and function and expand mechanisms by which altered telomere maintenance engenders human disease.

Introduction

Eukaryotic chromosome stability relies on end-protective telomeres (Arnoult and Karlseder 2015). In most organisms, end-protective telomeric chromatin assembles on a tract of simple-sequence DNA repeats (de Lange 2010), for example the human repeat of TTAGGG on the strand with 3'OH terminus. Maintenance of this telomeric repeat array requires *de novo* repeat synthesis by the ribonucleoprotein (RNP) reverse transcriptase telomerase to balance the repeat erosion inherent in DNA-dependent DNA-polymerase replication of the genome (Blackburn, Greider, and Szostak 2006; Hug and Lingner 2006). Telomerase extends chromosome 3' ends by copying a template within the telomerase RNA subunit (hTR in human cells), using an active site in the telomerase reverse transcriptase protein (TERT). The intricate co-folding and co-function of telomerase RNA and TERT obliges a step-wise RNP assembly process and generates a network of protein- and RNA-domain interactions (Blackburn and Collins 2011, (Schmidt and Cech 2015).

Cellular RNP biogenesis involves transit through and concentration in specific nuclear bodies (Mao, Zhang, and Spector 2011; Machyna, Heyn, and Neugebauer 2013). Trafficking pathways differ depending on the diverse steps of RNA processing, modification, and RNP assembly that give a transcript its fate and function. Among the best-studied RNP transit points are Cajal bodies, defined as foci of the protein Coilin (Nizami, Deryusheva, and Gall 2010; Machyna, Neugebauer, and Stanek 2015). Enzymes resident in Cajal bodies catalyze numerous RNA processing and modification reactions as well as RNP assembly and remodeling (Machyna, Heyn, and Neugebauer 2013). Beyond RNA processing and RNP biogenesis factors, Cajal bodies also recruit regulatory complexes such as CDK2-cyclinE (Liu et al. 2000) and have widespread influence on gene expression (Wang et al. 2016). Despite the multiplicity of functions ascribed to Cajal bodies, including critical roles in vertebrate telomerase function described below, it remains unclear whether their formation is cause or consequence of associated RNP biogenesis pathways.

Curiously, ciliate, fungal, and vertebrate telomerases follow entirely different RNP biogenesis pathways, which are directed by telomerase RNA interaction with a La-motif protein, Sm proteins, or H/ACA proteins, respectively (Egan and Collins 2012b; Schmidt and Cech 2015). In human cells, telomerase shares the same mature H/ACA proteins (dyskerin, NHP2, NOP10, GAR1) and H/ACA RNP biogenesis chaperones as the intron-encoded small nucleolar (sno) or small Cajal body (sca) RNPs that catalyze cleavage and pseudouridylation of ribosomal and small nuclear RNAs (Kiss, Fayet-Lebaron, and Jády 2010). Because precursor hTR is released from its site of synthesis as an autonomous transcript rather than the spliced intron lariat of other human H/ACA RNAs, it is sensitized to degradation in dyskeratosis congenita (DC) patient cells with a mutation of an H/ACA protein (Egan and Collins 2012a; Armanios and Blackburn 2012; Sarek et al. 2015). Also, unlike other H/ACA RNAs, hTR requires a 5' trimethylguanosine cap to prevent 5'-3' exonuclease processing (Mitchell, Cheng, and Collins 1999). Models for vertebrate telomerase RNA trafficking suggest an initial transit of Cajal bodies, where 5' trimethylguanosine cap modification is thought to occur, followed by localization to nucleoli (Egan and Collins 2012b; Schmidt and Cech 2015). Subsequent RNP trafficking from nucleoli to steady-state concentration in Cajal bodies depends on binding of the Cajal body chaperone and telomerase holoenzyme protein TCAB1/WDR79/WRAP53 to an hTR 3' stem-loop CAB-box motif (Venteicher et al. 2009; Tycowski et al. 2009; Zhong et al. 2011), which is present in both stem-loops of an H/ACA scaRNA (Kiss, Fayet-Lebaron, and

Jády 2010). Overall, this trafficking complexity could represent only a subset of the necessary cellular directions for human telomerase biogenesis and function.

The human telomerase holoenzyme subunits that localize active RNP to Cajal bodies are considered crucial for telomerase action at telomeres (Schmidt and Cech 2015). Transient telomere colocalization with a Cajal body can be detected in S-phase, when telomerase acts at chromosome ends (Jády et al. 2006; Tomlinson et al. 2006). Evidence for Cajal body delivery of telomerase to telomeres builds from studies depleting TCAB1 or Coilin using RNA interference, which reduced or eliminated hTR colocalization with telomeres and induced telomere shortening (Venteicher et al. 2009; Zhong et al. 2011; Stern et al. 2012; Zhong et al. 2012). DC patient cells with biallelic TCAB1 mutations have short telomeres and fail to maintain telomere length even with the up-regulated telomerase expression in induced pluripotent cells (Batista et al. 2011). With all of this experimental support for Cajal body delivery of human telomerase to telomeres, it is puzzling that mouse telomerase RNA does not localize to Cajal bodies (Tomlinson et al. 2010a). Also, recently, Coilin gene knock-out (KO) in HeLa cells generated two clonal cell lines that maintained telomeres (Chen et al. 2015).

Here we address the significance of human telomerase biogenesis and trafficking pathways for active RNP assembly and function at telomeres. As a new approach, we first bypassed the endogenous hTR stability requirement for H/ACA proteins. Remarkably, we found that a minimal hTR (hTRmin) containing only binding sites for TERT can assemble active RNP in cells, and this active RNP can maintain stable telomere length homeostasis. TERT overexpression was required for cellular assembly with hTRmin, suggesting that hTR H/ACA RNP assembly enhances TERT interaction at scarce endogenous telomerase subunit levels. KO of TCAB1 or Coilin did not alter hTRmin RNP function at telomeres. Surprisingly, TCAB1 KO or Coilin KO was also permissive for hTR telomerase to maintain telomeres. In cancer and pluripotent stem cell lines with endogenous hTR and TERT expression, TCAB1 KO resulted in a slow decline of telomere length followed by stable telomere length homeostasis. We conclude that aside from conferring hTR stability and facilitating active telomerase assembly in cells with scarce TERT, hTR assembly as H/ACA RNP is not essential. Also, Cajal body localization is not essential for hTRmin or hTR telomerase to maintain stable telomere length homeostasis. Our findings illuminate the influences of nuclear trafficking on human telomerase biogenesis and action at telomeres, account for why telomerase biogenesis pathways can be so divergent in eukaryotic evolution, and give new interpretation to the mechanisms by which different telomerase subunit mutations impose human disease.

Materials and methods

Cell culture

HCT116, 293T, VA-13, and U2OS cells were cultured in DMEM with GlutaMAX (Thermo) supplemented with 10% FBS and 100 □g/ml Primocin (Invivogen). The hESC line WIBR#3 (NIH stem cell registry #0079) was maintained on inactivated mouse embryonic fibroblasts in DMEM/F12 under conditions previously described (Chiba and Hockemeyer 2015). Transient transfections were performed using calcium phosphate or Lipofectamine 2000 (Thermo). Genome engineering and lentiviral transduction methods, plasmids, and primers are detailed in Supplementary file 1.

Northern blots

RNA was purified using TRIzol (Thermo) and resuspended in distilled water. Concentration was determined by absorbance at 260 nm. Formamide loading buffer was added to RNA samples, followed by heat denaturation at 95ºC for 1 min and ice for 5 min before loading on a denaturing gel (5% of 19:1 acrylamide:bis-acrylamide, 0.6X TBE, 32% formamide, and 5.6 M urea). Following electrophoresis, RNA was transferred to nylon membrane by electroblotting. RNA was then UV crosslinked and the membrane was blocked in Church's buffer (1% BSA, 1 mM EDTA, 0.5 M $NaP0_4$, 7% SDS) with 15% formamide at 50ºC. ^{32}P-labeled, 2'O-methyl RNA probe complementary to the hTR template region was then added (Fu and Collins 2003). In some experiments, ^{32}P-labeled DNA oligonucleotides complementary to regions in the hTR pseudoknot (5'-TAGAATGAACGGTGGAAGGCGGCAGGCCGAGGCT-3') and hTR CR4/5 (5'-TCGCGGTGGCAGTGGGTGCCTCCGGAGAAGCCC-3') were also added to enhance signal detection. Membranes were hybridized overnight at 50ºC, followed by extensive washing with 1X SSC + 0.1% SDS at 50ºC. Blots were then exposed on phosphorimager screens and subsequently scanned on a Typhoon (GE Healthcare). Scans were processed using ImageJ software (NIH). The Northern blot loading control (LC) is a non-specifically detected cellular RNA.

Immunoblots

Protein was resolved in 10% Bis-Tris SDS-PAGE gels in MOPS buffer (250 mM MOPS pH 7.0, 250 mM Tris, 5 mM EDTA, 0.5% SDS) before being transferred to nitrocellulose membrane. The membranes were then blocked in immunoblot buffer consisting of 4% nonfat milk (Carnation) in TBS buffer (150 mM NaCl, 50 mM Tris pH 7.5). Membranes were then incubated with primary antibodies diluted in immunoblot buffer at 4ºC overnight. After primary antibody incubation, membranes were washed extensively in TBS, followed by secondary antibody incubation in immunoblot buffer for 1 hour at room temperature. After washing in TBS, blots were scanned using a LI-COR Odyssey imager. Immunoblot primary antibodies included mouse anti-tubulin (1:500, DM1A, Calbiochem), mouse anti-FLAG (1:4,000, F1804, Sigma-Aldrich), rabbit anti-TCAB1 (1:2,000, NB100-68252, Novus Biologicals), mouse anti-Coilin (1:250, IH10, Abcam), and mouse anti-TERT (1:2000 (Wu et al. 2015)). Secondary antibodies included goat anti-mouse Alexa Fluor 680 (1:2,000, Life Technologies) and goat anti-rabbit IR Dye 800 (1:10,000, Rockland Immunochemicals).

Immunopurification

HLB150 buffer (20 mM HEPES pH 8.0, 2 mM $MgCl_2$, 0.2 mM EGTA, 10% glycerol, 1 mM DTT, 0.1% Igepal, Sigma protease inhibitor cocktail, 150 mM NaCl) was used throughout. Samples were normalized to 2 mg/ml and 200 □l was incubated at 4ºC for 1-2 hours with 4 □l magnetic anti-FLAG M2 beads (Sigma) or 4 □l magnetic Protein A/G beads (BioTools) pre-bound with antibody against TCAB1 (Novus Biologicals), antibody against FLAG (Sigma), or rabbit IgG (Sigma). After binding and washing, the beads were resuspended in 20 □l HLB150 buffer. For hotTRAP, the resuspended beads were diluted 1:10 in HLB150, and 2 □l of the diluted sample was used per hotTRAP reaction. For Northern blot analysis, the washed beads were processed with TRIzol (Thermo).

Microscopy

Live cell imaging was performed on a Zeiss Axio Observer A1 with a 40X phase contrast objective. For RNA and protein localization, cells were fixed in 4% paraformaldehyde for 10 min at room temperature. Cells were then washed with PBS twice, before additional fixation and permeabilization with 100% methanol for 10 min at room temperature. For RNA FISH, the methanol was aspirated and RNA probes in RNA FISH buffer were directly added to cells. Detection of hTR and hTRmin used Cy3-labeled RNA probes complementary to the template, pseudoknot, and CR4/5 spanning hTR nt 36-70, 129-162, and 249-281, respectively. Ten ng of each probe was diluted in RNA FISH buffer consisting of 2X SSC, 10% formamide, and 10% dextran sulfate. Probes were incubated with samples overnight at 37ºC in a humidified chamber. Samples were then washed 6 times with 2X SSC before being mounted on coverslips using ProLong Gold with DAPI (Thermo). For immunofluorescence, cells were washed three times in PBS following methanol incubation and then rehydrated and blocked in 4% BSA in PBS for 1 hour at room temperature or overnight at 4ºC. Primary antibodies diluted in 4% BSA in PBS were then added and incubated with samples for 1 hour at room temperature. Primary antibodies used included rabbit anti-TCAB1 (1:300, NB100-68252, Novus Biologicals), mouse anti-Coilin (1:250, IH10, Abcam), and mouse anti-SMN (1:300, sc-15320, Santa Cruz Biotechnology). After washing in PBS, samples were incubated with Alexa Fluor 488 or Alexa Fluor 568 (Thermo) secondary antibodies diluted in 4% BSA in PBS for 1 hour at room temperature. Samples were then washed in PBS and mounted on coverslips using ProLong Gold with DAPI. Images were acquired using a Zeiss LSM510 Meta confocal microscope with a ×100/1.49 Apo objective, with 364-, 488-, and/or 543-nm laser excitation.

Telomerase activity assays

Cell extract was prepared by hypotonic freeze thaw lysis and salt extraction. Primer extension and hotTRAP were performed as previously described (Sexton et al., 2014). Unless otherwise noted, 200 ng total protein was used per hotTRAP or QTRAP reaction, quantified using the Bio-Rad protein assay. An internal control (IC) to normalize PCR amplification was always included in hotTRAP assays. QTRAP used the iTaq universal SYBR green Supermix (Bio-Rad) and a CFX96 Touch Real-Time PCR Detection System (Bio-Rad) as previously described (Vogan and Collins 2015). Relative telomerase activity measured by QTRAP was calculated by delta Ct to a reference sample. All error bars shown are standard error of the mean and statistical significance was calculated using ANOVA with Tukey's multiple comparison test in GraphPad Prism 6.

Southern blots

Cell pellets were lysed in RIPA buffer (150 mM NaCl, 50 mM Tris at pH 7.5, 1 mM EDTA,1% Triton X-100, 0.5% sodium deoxycholate, 0.1% SDS, 1 mM DTT), treated with RNase A for 30 min at 37ºC, followed by proteinase K treatment for 4 hours to overnight at 50ºC. DNA was then purified using phenol-isoamyl alcohol-chloroform, followed by precipitation with isopropanol and NaCl. After pelleting, the DNA was washed twice with ethanol and resuspended in TE buffer (10 mM Tris, 1 mM EDTA). DNA concentration was determined by absorbance at 260 nm. Two to 8 □g of DNA was then digested with MboI and AluI for 6 hours to overnight before electrophoresis in a 0.7% agarose gel in 1X TAE. The agarose gel was then vacuum dried at 50ºC for 1 hour. The dried gel was then denatured with 0.5 N NaOH, 1.5 M NaCl for 30 min at 50ºC. The gel was washed twice with 4X SSC + 0.1% SDS and subsequently blocked with Church's buffer for 30 min at 50ºC. ^{32}P-end-labeled telomeric repeat probe $(T_2AG_3)_3$ and ^{32}P-labeled probe made by random-priming of HinDIII lambda phage digest ladder (NEB) and/or the O'generuler 1 kbp plus DNA ladder (Thermo) were added. Probes were hybridized overnight at 50ºC. The membrane was then extensively washed in 4X SSC + 0.1% SDS at 40ºC before screen exposure and imaging on a Typhoon scanner (GE Healthcare).

Genome engineering

Single-guide RNA sequences for Cas9 targeting of protein coding genes were designed for selection cassette insertion downstream of the start codon. Optimal guide sequences were generated using the CRISPR Design tool (http://crispr.mit.edu/). Guide sequences were then inserted into the PX330 plasmid (Cong et al., 2013). TERC guide sequence, followed by the PAM: 5'-TTCAGCGGGCGGAAAAGCCT CGG-3'. TCAB1 exon 2 guide sequence, followed by the PAM: 5'-TTTATTCATCGGGGAAGCGT GGG -3'. TCAB1 exon 8 guide sequence, followed by the PAM: 5'- TGAGAAGAAGCGGTTGCCAT CGG-3'. COIL exon 1 guide sequence, followed by the PAM: 5'-AAGCCGTAGCCTAACCGTCT CGG-3'. Donor plasmid constructs were designed by flanking a puromycin resistance cassette or a hygromycin resistance cassette with sequence 500-600 bp upstream and downstream of the genomic DNA cut site. The TCAB1 targeting sites do not overlap with the upstream p53 gene.

Zinc-finger nuclease (ZFN) mediated disruption of the TERT gene and transgene integration at AAVS1 have been previously described (Sexton et al., 2014). For disruption of TERT gene exon 1, a donor plasmid carrying a hygromycin resistance cassette flanked by homology arms of approximately 500 bp upstream and downstream of the cut site was transfected with plasmids expressing the TERT-targeting ZFN. For AAVS1 transgene integration, donor plasmids carrying the transgene(s) with an upstream neomycin or puromycin resistance cassette, together flanked AAVS1 homology arms, were transfected with plasmids expressing the AAVS1-targeting ZFN.

Genome engineering in HCT116 cells was performed by Lipofectamine 3000 transfection according to manufacturer guidelines (Thermo) using a 2:1 ratio of donor plasmid to nuclease plasmid. HCT116 cell lines were selected with 300 ug/ml hygromycin, 1 ug/ml puromycin, or 300 ug/ml G418. hESC gene editing was performed by electroporation as previously described (Sexton et al., 2014; (Chiba and Hockemeyer 2015).

Lentiviral transduction

Lentivirus was produced in 293T cells by calcium phosphate transfection with the packaging plasmid, psPAX2, the envelope plasmid, pMD2.G, and with transgene constructs in the DUET011 backbone (Zhou et al., 2007). Cell transfection media was replaced at 24 hours post-transfection and virus was harvested 48 hours post-transfection. Virus-containing media was applied to HCT116 cells in the presence of 5 □g/ml polybrene (Sigma) for 24 hours before a media change. At 48 hours post-infection, transduced cells were selected with 300 □g/ml hygromycin.

PCR genotyping

Genomic DNA was prepared as described above for telomere restriction fragment analysis. Between 50-100 ng of genomic DNA was used as the template for PCR using the Q5 polymerase (NEB). For PCR confirmation of gene editing, PCR primers were designed to generate amplicon size differences between loci with or without a drug resistance cassette. Paired PCR primers complementary to genomic loci had one primer complementary to a region also in the donor plasmid and the other primer complementary to a region beyond the donor plasmid homology. A third primer against either the hygromycin or puromycin resistance cassette was included that would generate an amplicon size for cassette-containing alleles that was either smaller or larger than amplicons from alleles lacking the cassette.

For TCAB1 exon 2 and Coilin exon 1 PCRs, a hygromycin cassette primer (PGK hygro: 5'-AGGCTGATCAGCGGTTTAAACTTAGCCTCCCCTACCCGGTAGAATTC-3'; or hygro pA: 5'-CTAGTGGATCCGAGCTCGGTACCAGATGCGGTGGGCTCTATGGC-3') was paired with the following locus-specific primers:

Coil_FWD: 5'-TAGTGGATCCGAGCTCGGTACCACCACTGCTCCTGGCCTCTAGTTAC-3', Coil_REV: 5'-AGGCTGATCAGCGGTTTAAACTTAAGAACTGAAGCCGAAGCGCTGG-3', TCAB_FWD1: 5'-CTAGTGGATCCGAGCTCGGTACCAGGAAGGCTTTCCGTAATATCACACCCTAACG-3', and TCAB_REV1: 5'-AGGCTGATCAGCGGTTTAAACTTACAGAAAGTTCTTGCTCCTCGATTCGAGGACTC-3'. An alternative set of TCAB1 locus primers was also used for additional validation of the lines: TCAB1_FWD2: 5'-CTAGTGGATCCGAGCTCGGTACCAGCGGTGCTAAGGAACACAGTGCTTTCAAAAG-3', and TCAB1_REV2: 5'-AGGCTGATCAGCGGTTTAAACTTAGGCATCCCTCTCCTAGAAAACTGG-3'.

For TCAB1 exon 8 PCR, a primer against the puromycin resistance cassette (PGK_PURO: 5'-GGCGCACCGTGGGCTTGTACTCGGTCATGGTGGCGGGATGCAGGT CGAAAGGCCCG-3') was combined with two loci primers (TCAB1_ex8_FWD: 5'-CCAAGGCCAACCAGCTGGTCAAAGGACTGCTTC-3', and TCAB1_ex8_REV:5'-CTCAGCATCCTGGAGACAAGGAACAGGACCTGGAGT-3'). For TERT locus PCR, another primer against the hygromycin cassette was used (TERT_hygro: 5'-CTCACCGCGACGTCTGTCGAGAAG-3') with the following locus-specific primers: TERT_FWD 5'-CTAGTGGATCCGAGCTCGGTACCAGCGGCGCGAGTTTCAGGCAG-3', and TERT_REV 5'-AGGCTGATCAGCGGTTTAAACTTAAACGGCAGACTTCGGCTGGCAC-3'.

For TERC locus PCR, a puromycin resistance cassette primer (5'-TGAAGCCGAGCCGCTCGTAGAA-3') was combined with locus-specific primers: hTR_FWD 5'-GTGGATCCGAGCTCGGTACCACCCACTGAGCCGAGACAAGATTC-3' and hTR_REV 5'-GAAAGCGAACTGCATGTGTGAGCCG-3'. Some of the primers had 5' regions complementary to the pcDNA3.1 vector to facilitate cloning, for which DNA was gel-excised, purified, and ligated into pcDNA3.1 (Thermo). DH5a cells were then transformed and several colonies were sequenced.

Results

Human telomerase can be liberated from H/ACA RNP assembly

To test the significance of H/ACA RNP biogenesis for human telomerase function at telomeres, we sought to bypass the essential role of this pathway in protection of hTR from degradation while preserving hTR-TERT interaction and RNP catalytic activity. The H/ACA-motif 5' stem of hTR (Figure 1A) separates two hTR regions that are critical for binding of TERT and catalytic activity: the template/pseudoknot (t/PK) and conserved regions (CR) 4/5 (Zhang, Kim, and Feigon 2011). Previously we joined these two regions with a spacer to create hTRmin (Figure 1B), which in combination with TERT reconstitutes a minimized active telomerase in rabbit reticulocyte lysate (Wu and Collins 2014). To allow cellular accumulation of hTRmin, the most successful strategy was to append 3' processing and protection motifs from the human long non-coding RNA MALAT1 (Brown et al., 2012; Brown et al., 2014).

The overall design strategy to optimize hTRmin accumulation involved testing combinations and variations of RNA modules (Figure 1C). For example, we interchanged the hTRmin 5' end as no leader, endogenous hTR quadruplex-forming leader (LeaderG), or a mutant leader (LeaderC) that eliminates one of the four adjacent guanosine tracts (Sexton and Collins 2011). We also tested 6 or 14 nucleotide (nt) lengths of single-stranded RNA spacer separating the t/PK and CR4/5 regions. For 3'-end formation, we tested the MALAT1 triplex motif with or without an adjacent RNase P cleavage site mimicking a pre-tRNA (Brown et al. 2012). We also omitted or included a hepatitis delta virus ribozyme (HDV RZ), which can increase hTR accumulation by stabilizing the precursor 3' end with an exonuclease-resistant 2',3' cyclic phosphate (Egan and Collins 2012a).

We first assessed hTRmin accumulation in transiently transfected 293T cells, using an expression context previously optimized for hTR that exploits the U3 snoRNA promoter to direct transcription by RNA Polymerase II (Fu and Collins 2003). Accumulation of hTRmin to a level detectable by Northern blot required both the RNA triplex and the RNase P site (Figure 1D). We next tested if this cellular hTRmin could form active RNP. We transiently co-expressed hTRmin or hTR with 3xFLAG-tagged (F) TERT in the telomerase-negative U2OS cell line and assayed for telomeric primer extension by immunopurified TERT. Cellular reconstitution with hTRmin yielded lower RNA accumulation and proportionally lower overall activity than reconstitution with hTR, but hTRmin and hTR telomerase RNPs had similar profiles of repeat synthesis (Figure 1 – figure supplement 1A). For continued optimization, we next compared hTRmin accumulation with no 5' leader, LeaderG, or LeaderC and with 6 nt versus 14 nt spacer (Figure 1C), all with the RNA triplex and RNaseP cleavage site. The presence of a 5' leader increased accumulation, and the quadruplex-mutant LeaderC was as good or better than the native hTR LeaderG (Figure 1E). Also, the 6 nt spacer between t/PK and CR4/5 was as good or better than the 14 nt spacer (Figure 1E). HDV RZ addition downstream of the MALAT1 3' processing elements improved hTRmin accumulation from some transfected constructs but did not notably increase accumulation of the optimal LeaderC-containing hTRmin with 6 nt spacer (Figure 1E), which in subsequent experiments we designate LhTRmin for distinction from the leader-less hTRmin.

To confirm that removal of the H/ACA motif eliminated all interactions with H/ACA proteins, we expressed epitope-tagged TERT, dyskerin, or TCAB1 with hTR or LhTRmin in telomerase-negative VA-13 cells, immunopurified the tagged protein using FLAG antibody

resin, and detected bound RNA by Northern blot (Figure 1F). As expected, TERT, dyskerin, and TCAB1 each bound hTR whereas only TERT bound LhTRmin. As in 293T cells, in VA-13 cells both leader-free hTRmin and LhTRmin accumulated, with LhTRmin being optimal (Figure 1G). The robust 3' end protection activity of the MALAT1 triplex was evident when it was appended to full-length hTR (Figure 1G; note that mature hTR sometimes migrates as a doublet due to in-gel folding). To compare the cellular localizations of LhTRmin and hTR, we overexpressed LhTRmin or hTR with TERT by transient transfection. While hTR concentrated in nuclear puncta as expected, LhTRmin distributed throughout the nucleoplasm (Figure 1H). Transfection of cells lacking endogenous hTR (see below) confirmed that hTRmin and LhTRmin have a diffuse nucleoplasmic distribution distinct from that of hTR or hTR with a CAB-box mutation (Figure 1 – figure supplement 1B). Together the studies above establish that cellular hTRmin and LhTRmin escape the confines of H/ACA RNP assembly.

We next tested whether hTRmin or LhTRmin could accumulate when stably expressed from an integrated transgene. In the near-diploid HCT116 human colon carcinoma cell line, we used a zinc finger nuclease that introduced a double-stranded DNA break at the AAVS1 safe-harbor locus (Hockemeyer et al. 2009) to integrate an RNA expression cassette and a neomycin resistance cassette. After selection, the polyclonal population of targeted cells was assayed for RNA accumulation by Northern blot. Consistent with results from transient transfection, LhTRmin accumulation exceeded that of hTRmin, with or without a downstream HDV RZ (Figure 1I). Stably expressed hTRmin was barely detectable, and even LhTRmin accumulated to a level lower than endogenous hTR (Figure 1I). Therefore, the MALAT1 3' processing elements do not confer as much accumulation to minimized hTR as does an embedded H/ACA RNP.

Catalytically active telomerase supports telomere maintenance without H/ACA proteins or TCAB1

Successful cellular biogenesis of hTRmin telomerase RNP allowed us to test whether H/ACA proteins have post-biogenesis influences on telomerase function at telomeres. We first programmed Cas9 for cleavage of the endogenous hTR locus (TERC) in HCT116 cells in the presence of donor plasmid that would integrate a puromycin resistance cassette (Figure 2A). After selection, clonal cell lines were established and screened by PCR for biallelic gene disruption (Figure 2 – figure supplement 1A). Two independent cell lines with homozygous TERC KO were confirmed to lack telomerase catalytic activity in cell extract, as assayed by the PCR-based telomeric repeat amplification protocol performed with radiolabeled dGTP (hotTRAP) (Figure 2B and Figure 2 – figure supplement 1B, left). Initially, these two hTR KO clonal cell lines showed no growth defect.

In each hTR KO cell line, we targeted transgene integration at AAVS1 with expression cassette(s) encoding GFP, N-terminally F-tagged TERT, hTR, LhTRmin, hTRmin, or LhTRmin or hTRmin coexpressed with TERT (Figure 2C). RNA expression was directed by the U3 snoRNA promoter, and protein expression was driven by the strong and constitutive CAGGS promoter. Polyclonal populations of transgene-containing cells were selected and immediately assayed for telomerase subunit expression and telomerase activity (Figure 2D). TERT overexpression (OE) was detected by immunoblot, and transgene-encoded RNA expression was detected by Northern blot. Telomerase catalytic activity was assayed by hotTRAP.

Transgene expression of wild-type hTR restored telomerase catalytic activity to the hTR KO cells, rescuing endogenous TERC locus disruption (Figure 2D, lane 3). Transgene expression of GFP, LhTRmin, hTRmin, or TERT alone did not (Figure 2D, lanes 2 and 4-6). However, LhTRmin or hTRmin with TERT OE did generate active telomerase (Figure 2D, lanes 7-8). TERT co-expression did not affect hTRmin biological accumulation (Figure 2D, compare lanes 4-5 to lanes 7-8). Parallel results were confirmed using the independent hTR KO clonal cell line (Figure 2 – figure supplement 1B,C). In addition, we tested telomerase activity rescue of hTR KO cells or hTR KO cells with AAVS1 TERT OE by lentiviral introduction of LhTRmin. Only with TERT OE did lentiviral expression of LhTRmin produce active telomerase, whereas lentiviral expression of hTR rescued hTR KO without TERT OE (Figure 2 – figure supplement 1D,E). Telomerase activity levels in the hTRmin telomerase cell lines were within an order of magnitude of the telomerase level in parental HCT116 cells (Figure 2 – figure supplement 1B,C). From these experiments we conclude that hTR assembly as H/ACA RNP strongly stimulates hTR interaction with TERT when both subunits are at very low expression levels, but this role of H/ACA RNP assembly can be bypassed by increasing the cellular availability of TERT.

The hTR KO cell lines lacking active telomerase ultimately entered an interval of pervasive cell death with dramatic membrane blebbing (Figure 2E, yellow arrowheads) at ~70 days post-targeting, corresponding to ~70 population doublings. In stark contrast, all of the telomerase-positive polyclonal cell cultures and clonal cell lines proliferated over many months of continuous passage with normal morphology and doubling time (Figure 2F). Therefore, the catalytically active hTRmin telomerase RNPs conferred indefinite cellular proliferative capacity.

We next tested the hTR KO cell lines with AAVS1 transgenes for rescue of telomere shortening. As expected, hTR KO cells re-expressing hTR rapidly gained telomere length, whereas hTR KO cells expressing the negative control GFP did not (Figure 3A, lanes 1-3 and Figure 3 – figure supplement 1A). All cell cultures lacking active telomerase had short telomeres that continued to shorten until eventually all cells in the culture died (Figure 3A,B). Telomere length was heterogeneous in the polyclonal population of hTR KO cells rescued by LhTRmin with TERT OE (Figure 3A, lane 7 and Figure 3 – figure supplement 1B). We generated clonal cell lines from the hTR KO cell lines complemented by LhTRmin or hTRmin with TERT OE and characterized their maintenance of telomere length. These clonal cell lines had distinct but stable telomere lengths (Figure 3C,D and Figure 3 – figure supplement 1C).

To investigate the clonal cell line variance in telomere length at length homeostasis, we profiled levels of telomerase subunits and activity across the clonal cell lines. All of the LhTRmin cell lines had higher steady-state RNA accumulation than the hTRmin lines (Figure 3E). LhTRmin levels varied more than hTRmin, and TERT levels varied more in LhTRmin lines than hTRmin lines (Figure 3E and Figure 3F, symbols). Telomerase activity measured by fluorescence quantification of telomeric repeat amplification (QTRAP) (Figure 3F, bars and Figure 3 – figure supplement 1D for replicates) or hotTRAP (Figure 3 – figure supplement 1E) was generally greatest in cell lines with high telomerase subunit expression (Figure 3F, compare symbols to bars). Higher telomerase activity in cell extract correlated generally but not absolutely to longer telomere length at homeostasis (compare Figure 3F, bars to Figure 3C). We suggest that differences in telomerase subunit expression levels could in part reflect epigenetic differences introduced upon transgene integration, which was an independent event in each clonal cell line. In addition, differences in subunit expression levels could result from the stochastic fluctuation established to occur in many model systems, including HeLa cells (Bryan et al. 1998).

TCAB1 and Cajal bodies contribute non-essential regulations of telomerase

We confirmed that the hTRmin telomerase RNP assembled in the stable cell lines did not have the endogenous hTR RNP interaction with TCAB1, tested by immunopurification of TCAB1 from cell lysate and subsequent telomerase activity assay (Figure 4 – figure supplement 1A). However, because telomere-associated telomerase would be a small fraction of the total telomerase RNP pool, we sought another approach to demonstrate that hTRmin telomerase maintained telomeres without a requirement for TCAB1-mediated recruitment to Cajal bodies. To this end, we disrupted the genes encoding TCAB1 and Coilin in HCT116 cells expressing hTRmin telomerase.

We programmed Cas9 for cleavage of the endogenous TCAB1 or Coilin locus in the presence of donor plasmid that would integrate a hygromycin resistance cassette (Figure 4A). Targeting and selection were highly efficient, resulting in polyclonal populations of LhTRmin TERT OE cells and hTRmin TERT OE cells with little TCAB1 or Coilin, as detected by immunoblot (Figure 4B) or immunofluorescence (Figure 4C). TCAB1 KO cells retained a normal level of Coilin, and Coilin KO cells retained a normal level of TCAB1 (Figure 4B). Cells lacking TCAB1 retained Cajal bodies (Figure 4C), in agreement with some previous findings (Venteicher et al. 2009; Zhong et al. 2011) but contrary to others (Mahmoudi et al. 2010; Wang et al. 2016). Also, nuclear foci of SMN remained detectable in the TCAB1 KO cells but not Coilin KO cells (Figure 4 – figure supplement 1B). We conclude that in HCT116 cells, TCAB1 KO did not disrupt Cajal bodies, and Coilin KO did not induce TCAB1 degradation.

We isolated clonal cell lines from the polyclonal KO cell populations and validated homozygous TCAB1 or Coilin KO by genomic locus PCR and protein immunoblots (Figure 4D and Figure 4 – figure supplement 1C,D). These clonal cell lines retained telomerase catalytic activity in cell extract (Figure 4E) and stably maintained telomeres (Figure 4F and Figure 4 – figure supplement 1E). Some heterogeneity was evident comparing the telomere lengths maintained in different clonal cell lines, which could result from stochastic variation (Bryan et al. 1998). Importantly, neither TCAB1 KO nor Coilin KO affected cell viability, morphology, or proliferation in a readily detectable manner. These findings support the conclusion that an RNP of minimized hTRmin and TERT functions at telomeres without dependence on H/ACA RNP biogenesis or localization pathways.

In parallel, we generated TCAB1, Coilin, and TERT KO HCT116 cells with endogenous hTR expression using Cas9 for TCAB1 and Coilin or a zinc finger nuclease developed previously for TERT (Sexton et al., 2014). Clonal cell lines with homozygous KO were identified using genomic locus PCR (Figure 4 – figure supplement 1C,D and Figure 5 – figure supplement 1A) and validated for loss of TCAB1 or Coilin but not hTR (Figure 5A,B). TERT KO was validated by loss of telomerase activity from cell extract (Figure 5C). As expected, TCAB1 KO cells retained Coilin, and Coilin KO cells retained TCAB1 (Figure 5A). We also confirmed that immunopurification of TCAB1 from Coilin KO cell extract, but not from TCAB1 KO cell extract, enriched active telomerase (Figure 5 – figure supplement 1B). The loss of TCAB1 or Coilin did not alter telomerase activity in cell extract by more than a few-fold extent that could be within the range of clonal variation (Figure 5D and Figure 5 figure supplement 1C). HCT116 cells with TCAB1 KO or Coilin KO showed no change in growth rate, cell viability, or morphology over more than half a year of continuous culture. In contrast, the TERT KO cells underwent cell death at ~70 days after targeting, paralleling the fate of the hTR KO HCT116 cells.

As expected the TERT KO cells experienced rapid, progressive telomere attrition (Figure 5E). Surprisingly, telomeres shortened more gradually in the TCAB1 KO clonal cell lines, followed by stable telomere length homeostasis (Figure 5F). The starting point of telomere length in TCAB1 KO clonal cell lines mirrored the amount of telomerase activity in cell extract (compare Figure 5D and Figure 5F, left panel), but after more than half a year of continuous growth, telomere lengths in all of the TCAB1 KO clonal cell lines stabilized at a few kbp shorter than telomeres in the parental cell line (Figure 5F, right panel). In comparison, telomeres in Coilin KO clonal cell lines cultured in parallel remained near the length of telomeres in the parental HCT116 cells (Figure 5G). We conclude that in HCT116 cells, neither TCAB1 nor Coilin is required for a stable telomere length homeostasis.

Stable telomere length maintenance in the TCAB1 KO cells with endogenous telomerase was unexpected. To determine whether this finding is general, we investigated the consequence of TCAB1 or Coilin KO in the human embryonic stem cell (hESC) line WIBR#3 (Chiba and Hockemeyer, 2015). Clonal hESC lines with TCAB1 or Coilin KO were generated using the same approach that was successful in HCT116 cells (Figure 5 – figure supplement 2A). As observed for HCT116 cells, hESC lines lacking TCAB1 or Coilin were viable with no evident change in cell morphology or proliferation. TCAB1 accumulated in Coilin KO cells, and Coilin accumulated in TCAB1 KO cells (Figure 5H). Neither TCAB1 KO nor Coilin KO affected telomerase activity assayed in cell extract beyond the range of clonal variation (Figure 5I and Figure 5 – figure supplement 2B). Coilin remained localized to Cajal bodies in TCAB1 KO cells (Figure 5 – figure supplement 2C). Over many months of continuous culture, hESCs lacking TCAB1 experienced very gradual telomere shortening followed by telomere length maintenance (Figure 5J). The rate of telomere shortening was slow compared to telomere shortening in TERT KO hESC (Sexton et al., 2014). The hESCs lacking Coilin retained telomere lengths comparable to the parental hESC culture (Figure 5K). Clonal hESC lines that had undergone targeting but retained the wild-type genotype also did not demonstrate telomere shortening (Figure 5J, lanes labeled wild-type).

To confirm that telomere shortening in TCAB1 KO cells was directly linked to the loss of TCAB1, we introduced a TCAB1 transgene to TCAB1 KO cells by integration at AAVS1. TCAB1 KO HCT116 cells ectopically expressing F-tagged TCAB1 regained telomere length (Figure 5 – figure supplement 3A,B). Likewise, TCAB1 KO hESCs ectopically expressing F-tagged TCAB1 regained telomere length (Figure 5 – figure supplement 3C,D). As a control for complete TCAB1 loss-of-function, we targeted the TCAB1 KO cells above, which have an exon 2 disruption shortly after the translation start codon (Figure 4A), for successful homozygous disruption of downstream exon 8 (Figure 5 – figure supplement 3E). Cells with homozygous disruptions of exon 2 and exon 8 showed no proliferation defect, no change in telomere length from the exon 2 KO, and no loss of Cajal bodies (Figure 5 – figure supplement 3F,G). Overall, based on the assays described above, we conclude that TCAB1 and Cajal bodies are not essential for hTR telomerase to maintain telomeres at a stable length homeostasis.

TCAB1 is not required for rapid telomere elongation by telomerase overexpression

In human somatic cells that remain telomerase-positive, stimulation to proliferate can be accompanied by dramatic telomerase activation and telomere length gain (Weng, Granger, and Hodes 1997). This rapid increase in telomere length could depend on telomerase assistance by

TCAB1 and/or Cajal bodies in a manner not required for maintaining length homeostasis. We therefore tested TCAB1 and Coilin KO cells for their ability to support rapid telomere elongation upon increase in telomerase expression, achieved by integrating transgenes for hTR and TERT overexpression at AAVS1.

The parental, TCAB1 KO, and Coilin KO HCT116 cells with integrated hTR and TERT transgenes acquired ~2-fold elevated hTR and ~5-fold elevated telomerase catalytic activity (Figure 6A). These High-Telomerase (HiT) polyclonal cell cultures had increased telomere length by the first time point after selection (Figure 6B). Telomere elongation was rapid in TCAB1 KO HiT cell cultures, reaching the limit of length discrimination almost immediately. Rapid telomere elongation in TCAB1 KO cells is consistent with telomere elongation in wild-type HeLa cells by overexpression of CAB-box-mutant hTR (Fu and Collins 2007; Cristofari et al. 2007). In comparison, Coilin KO HiT cells had less telomere elongation (Figure 6B). These results were replicated in an independently performed HiT conversion of the same cell lines (not shown). Telomeres in both TCAB1 KO and Coilin KO cells elongated upon expression of a truncated POT1 compromised for binding to single-stranded telomeric-repeat DNA (Loayza and De Lange 2003), expressed by transgene integration at AAVS1 (data not shown). No obvious hTR foci were detected in HCT116 HiT cells lacking TCAB1 or Coilin (Figure 6C), indicating that the hTR foci detected in HeLa cells lacking Coilin (Chen et al. 2015) are challenging to detect. We conclude that if telomerase is abundant, TCAB1 is not required to support telomerase-mediated elongation of even relatively long telomeres. Integrating all of the findings of this study, we conclude that human telomerase H/ACA RNP assembly is essential not only for biological stability of hTR but also for active RNP biogenesis at scarce subunit expression levels. In addition, H/ACA RNP assembly gives endogenous-level hESC telomerase the ability to maintain long telomeres. Remarkably, all of these H/ACA RNP assembly roles can be bypassed using hTRmin (Figure 7). This plasticity of telomerase RNP biogenesis and holoenzyme composition informs mechanisms of telomerase diversification across eukaryotes.

Discussion

Telomerase holoenzymes from different eukaryotes share the cellular requisites of stable RNP biogenesis and active RNP recruitment to telomeres in S-phase, but the mechanisms that underlie these requirements for telomerase function vary greatly (Egan and Collins 2012b). We set out to uncover the rationale for vertebrate telomerase evolutionary gain of H/ACA RNP biogenesis. H/ACA RNP biogenesis confers hTR biological stability, but across eukaryotes, telomerase RNA stability can be conferred by diverse other RNP assembly pathways. To bypass the essential role of H/ACA proteins in hTR cellular stability, we designed hTRmin RNAs containing the activity-essential hTR motifs and a 3' triplex structure but not an H/ACA motif. Although hTRmin did not bind H/ACA proteins or TCAB1, it did assemble catalytically active telomerase. The opposite TER redesign strategy was used to test the significance of the relative positioning of a large number of holoenzyme protein binding motifs in *S. cerevisiae* TLC1 (Zappulla et al. 2005). *S. cerevisiae* Mini-T retains all of the holoenzyme protein interactions but condenses the length of spacing between them (Zappulla et al. 2005).

Initially we expected the biological function of hTRmin-TERT RNPs to require tethering to Cajal bodies or telomeres. Instead, hTRmin-TERT RNPs supported stable telomere maintenance without any supplementary trafficking instructions (Figure 7, left). Therefore, most telomerase holoenzyme proteins may serve indirect roles in telomerase function that are readily adapted to evolutionary divergence of nuclear architecture and its cell cycle regulation. Other than hTR biological stability, the contributions of H/ACA RNP assembly, TCAB1, and Cajal bodies to endogenous human telomerase function could all be accounted for by changes in subunit and RNP distribution within the nucleus (Figure 7, right).

Studies here point to stabilization and efficient interaction of low-abundance telomerase subunits as a main rationale for the vertebrate telomerase H/ACA RNP biogenesis pathway. Cellular assembly of minimized hTRmin into catalytically active telomerase RNP required a higher than endogenous expression level of TERT. One simple model for this influence would be that H/ACA RNP biogenesis directs trafficking of assembly-competent hTR to meet assembly-competent TERT. Based on the cell cycle regulation of human telomerase subunit synthesis and subunit exchange in assembled RNPs, we have suggested that active RNP assembly may occur with only newly synthesized TERT and/or hTR subunits prior to their steady-state distribution (Vogan and Collins 2015). Newly synthesized subunits could meet in Cajal bodies, as pre-mature hTR transits to acquire 5' cap trimethylation, or in nucleoli. Additional non-exclusive possibilities for cellular role(s) of hTR H/ACA RNP assembly in active RNP biogenesis include hTR folding, which would parallel the precedent from ciliate telomerase biogenesis (Stone et al. 2007), and/or exclusion of non-productive hTR-protein interactions.

In both HCT116 cells and hESCs, TCAB1 KO led to telomere shortening followed by telomere length homeostasis. As one model to account for these results, TCAB1 could influence the subnuclear distribution of active RNP between nucleoli and nucleoplasm (Figure 7, right). This change in distribution would have different influence on the amount of new telomeric repeat synthesis depending on telomerase expression level and other variables across human cell types. Of note, we have not ruled out an influence of TCAB1 related to its proposed function in DNA damage repair (Henriksson and Farnebo 2015). However, in studies here it is striking that TCAB1 KO affected telomere length only in cells with hTR telomerase, not in cells with hTRmin telomerase. Therefore, TCAB1 functions directly related to active telomerase assembly and trafficking are more logical hypotheses.

Consistent with a contemporary study of Coilin KO in HeLa cells (Chen et al. 2015), we found that Coilin KO in HCT116 cells or in hESCs was permissive for stable telomere length maintenance. Coilin KO clonal cell lines generated in this work had telomere lengths similar to the parental cell lines. Because Coilin KO cells with endogenous telomerase levels have apparently unperturbed telomere length homeostasis, we suggest that they will be useful for visually tracking telomerase interactions with telomeres without the complication of Cajal body clustering of active with inactive hTR. Curiously, Coilin KO HCT116 cells had dampened telomere elongation upon an increase in telomerase expression. This could reflect less synergistic telomerase RNP loading on telomeres. Alternately, Cajal bodies could coordinate telomerase with other factors important for telomere synthesis, or they could safeguard telomere integrity. Our results support a paradigm of nuclear bodies as zones that draw factors together to fine-tune the likelihood of their physical association or functional cooperation rather than their interaction or reaction specificity.

Previous studies did not anticipate the genetic consequences of TCAB1 and Coilin KOs. For example, opposite the impact of TCAB1 and Coilin KOs on telomere lengths described above, previous studies found that endogenous hTR colocalization with telomeres was reduced more by Coilin depletion than TCAB1 depletion and overexpressed hTR colocalization with telomeres was reduced more by TCAB1 depletion than by Coilin depletion (Zhong et al. 2012; Stern et al. 2012). Also, TCAB1 mutations result in severe DC (Zhong et al. 2011; Egan and Collins 2012a; Armanios and Blackburn 2012). We suggest that TCAB1 mutations reduce telomere length in early human development and in somatic cells with long telomeres. Overall, insights from this work inform strategies of therapy for human disease.

Figure 1. Human telomerase RNA can accumulate without H/ACA RNP biogenesis.
(A,B) Diagrams of hTR and hTRmin secondary structure and bound proteins.
(C) Parts list for a cellular minimal telomerase RNA. Components are presented in 5' to 3' order.
(D,E) Northern blot assay for RNA accumulation in transfected 293T cells. Endogenous hTR was also detected. Loading control (LC) is a cellular RNA non-specifically detected by the Northern blot probe used for normalization. In (D), all hTRmin variants are without a 5' leader and with a 6 nt spacer. In (E), all constructs had the RNA triplex and RNase P site. hTRmin accumulation was normalized to LC to quantify relative accumulation (Rel).
(F) Copurification of hTR or LhTRmin with tagged telomerase holoenzyme subunits co-overexpressed in transfected VA-13 cells. RNPs were purified from cell lysate using FLAG antibody resin and analyzed by immunoblot and Northern blot. F indicates 3xFLAG peptide, ZZ indicates tandem Protein A domains.
(G) Northern blot assay for RNA accumulation in transfected VA-13 cells. RNA folding during extensive gel electrophoresis gives mature hTR two mobilities (a doublet of bands).
(H) FISH detection of hTR or LhTRmin in transfected HCT116 cells. Untagged TERT was coexpressed.
(I) Northern blot assay for RNA expressed from transgenes integrated at ; in HCT116 cells. Endogenous hTR was also detected.

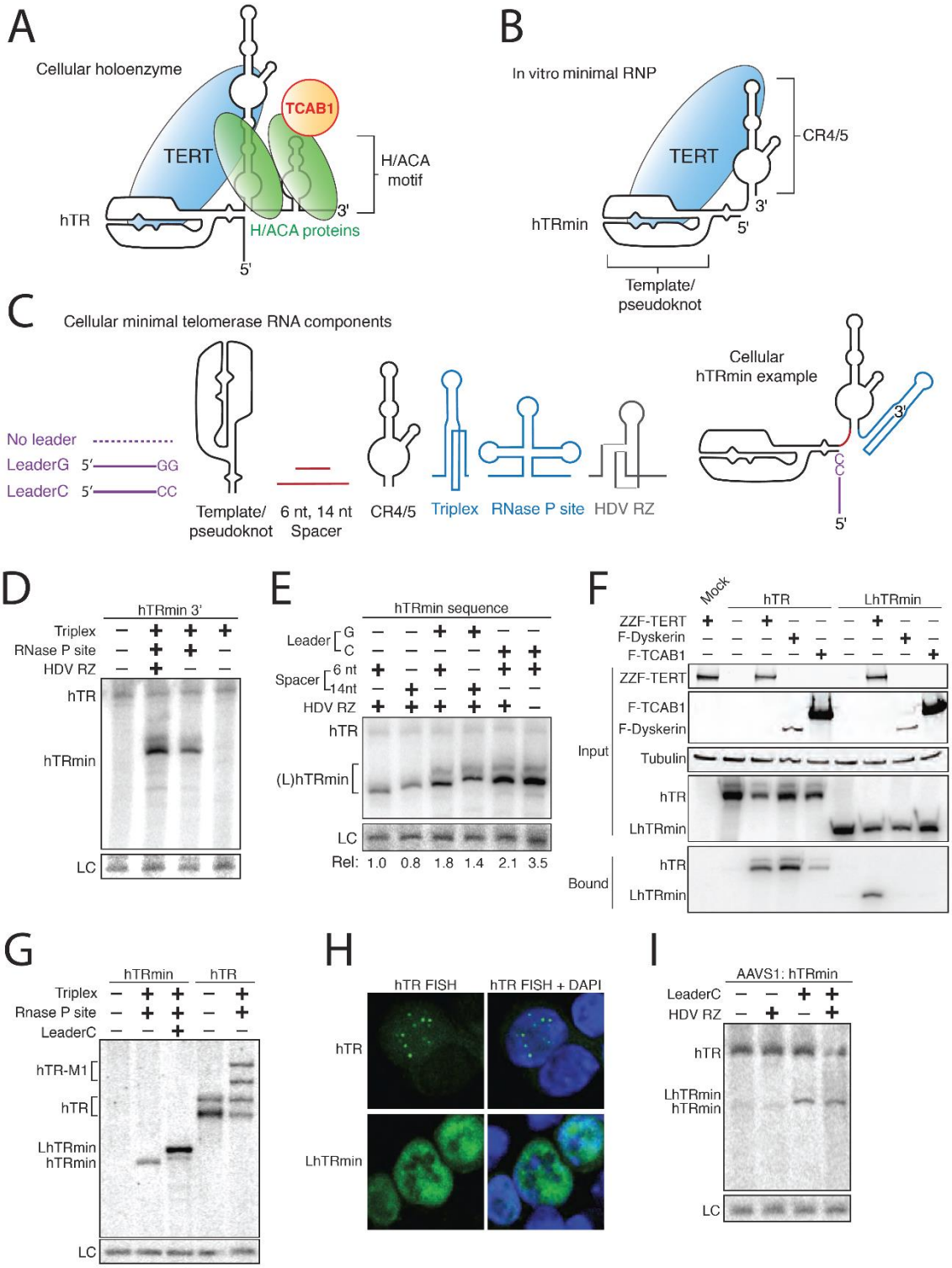
A
Cellular holoenzyme
TCAB1
TERT
H/ACA motif
hTR
3'
H/ACA proteins
5'
B
In vitro minimal RNP
CR4/5
TERT
hTRmin
3'
5'
Template/ pseudoknot
C
Cellular minimal telomerase RNA components
No leader
LeaderG 5'—GG
LeaderC 5'—CC
Template/ pseudoknot
6 nt, 14 nt Spacer
CR4/5
Triplex
RNase P site
HDV RZ
Cellular hTRmin example
3'
CC
5'
D
hTRmin 3'
Triplex
RNase P site
HDV RZ
hTR
hTRmin
LC
E
hTRmin sequence
Leader G C
Spacer 6 nt 14nt
HDV RZ
hTR
(L)hTRmin
LC
Rel: 1.0 0.8 1.8 1.4 2.1 3.5
F
Mock
hTR
LhTRmin
ZZF-TERT
F-Dyskerin
F-TCAB1
Input
ZZF-TERT
F-TCAB1
F-Dyskerin
Tubulin
hTR
LhTRmin
Bound
hTR
LhTRmin
G
hTRmin
hTR
Triplex
Rnase P site
LeaderC
hTR-M1
hTR
LhTRmin
hTRmin
LC
H
hTR FISH
hTR FISH + DAPI
hTR
LhTRmin
I
AAVS1: hTRmin
LeaderC
HDV RZ
hTR
LhTRmin
hTRmin
LC

Figure 1 – figure supplement 1. Cellular assembly of hTRmin telomerase.
(A) U2OS cells were transiently transfected with constructs encoding F-TERT and either hTRmin, hTR, or empty vector (mock). TERT was immunopurified on anti-FLAG agarose from cell extract 48 hours post-transfection. An aliquot of the bound samples were treated with TRIzol to purify RNA, which was analyzed by Northern blot. In parallel, bound samples were tested for telomerase activity by primer extension using ^{32}P dGTP for radiolabeling. Products were precipitated and resolved by denaturing gel electrophoresis. A radioactive oligonucleotide recovery control (RC) was added prior to precipitation. For the hTR cell extract, different amounts of extract were assayed relative to the hTRmin sample set at 100%. All lanes are from the same gel.
(B) HCT116 hTR KO#2 cells were transiently transfected to express hTR, CAB-box-mutant hTR (G414C), LhTRmin, or hTRmin. FISH was performed to detect the RNAs (green). Nuclei were counterstained with DAPI (blue).

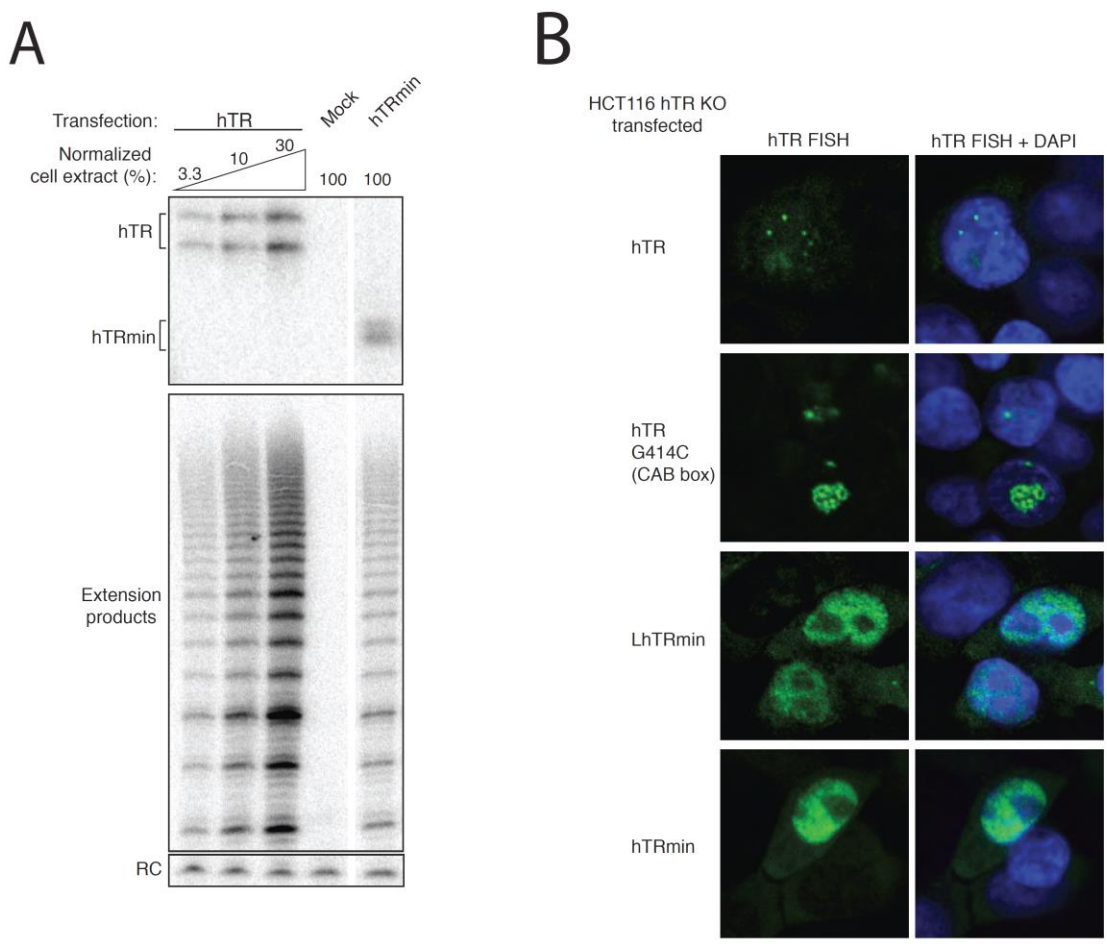

Figure 2. An hTRmin RNP can functionally substitute for hTR.
(A) Schematic of Cas9-mediated disruption of the hTR locus with a PURO selection cassette.
(B) Northern blot and hotTRAP assays of hTR KO#1 and KO#2 clonal HCT116 cell lines. An internal control (IC) to normalize PCR amplification was always included in hotTRAP assays.
(C) AAVS1 donor constructs used for transgene rescue of hTR KO HCT116 cells. RNA expression used the U3 promoter and terminated within 500 bp of transplanted genomic region from immediately downstream of endogenous hTR (g500). mRNA expression used the CAGGS promoter terminated with a polyadenylation element (pA).
(D) Immunoblot, northern blot, and hotTRAP characterization of HCT116 cell lines 51 days after hTR KO targeting.
(E) Brightfield microscopy images of HCT116 cell lines during the die-off interval of telomerase-negative cell cultures. Yellow arrowheads indicate membrane blebbing.
(F) Chart of survival fate of HCT116 hTR KO cell lines with the indicated transgene at AAVS1.

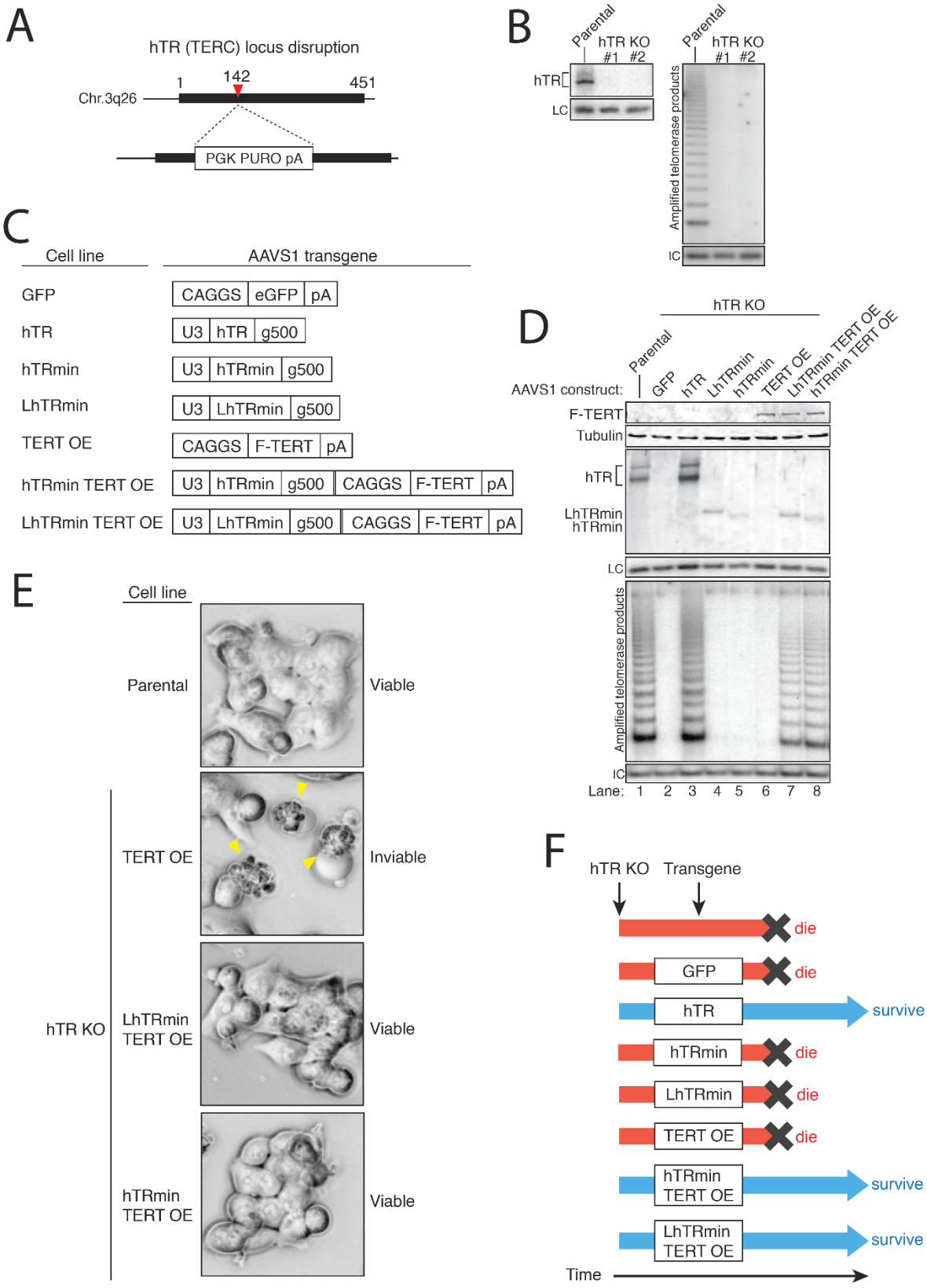
A
hTR (TERC) locus disruption
Chr.3q26
1
142
451
PGK PURO pA
B
Parental
hTR KO
#1 #2
hTR
LC
Amplified telomerase products
IC
C
Cell line
AAVS1 transgene
GFP
CAGGS eGFP pA
hTR
U3 hTR g500
hTRmin
U3 hTRmin g500
LhTRmin
U3 LhTRmin g500
TERT OE
CAGGS F-TERT pA
hTRmin TERT OE
U3 hTRmin g500 CAGGS F-TERT pA
LhTRmin TERT OE
U3 LhTRmin g500 CAGGS F-TERT pA
D
hTR KO
Parental
GFP
hTR
LhTRmin
hTRmin
TERT OE
LhTRmin TERT OE
hTRmin TERT OE
AAVS1 construct:
F-TERT
Tubulin
hTR
LhTRmin
hTRmin
LC
Amplified telomerase products
IC
Lane: 1 2 3 4 5 6 7 8
E
Cell line
Parental
Viable
hTR KO
TERT OE
Inviable
LhTRmin
TERT OE
Viable
hTRmin
TERT OE
Viable
F
hTR KO
Transgene
die
GFP
die
hTR
survive
hTRmin
die
LhTRmin
die
TERT OE
die
hTRmin
TERT OE
survive
LhTRmin
TERT OE
survive
Time

Figure 2 – figure supplement 1. Generation of cell lines expressing hTRmin telomerase.
(A) Schematic and assay results for PCR detection of hTR locus KO.
(B) Telomerase activity comparison by hotTRAP for the hTR KO cell lines with TERT OE alone or in combination with hTRmin or LhTRmin. Input total protein is whole cell lysate. Assays were from polyclonal populations following selection for transgene integration and extended post-targeting culture (114 days post-targeting for hTR KO).
(C) QTRAP comparison of telomerase activity levels in the hTR KO cell lines rescued by AAVS1 hTRmin TERT OE or LhTRmin TERT OE. Values are set relative to parental HCT116 (n = 3).
(D) Immunoblot, northern blot, and hotTRAP characterization of HCT116 hTR KO cells with or without TERT OE from an AAVS1 transgene and with lentiviral hTR, LhTRmin, or GFP.
(E) Time course of TRF in the HCT116 hTR KO with TERT OE and lentiviral LhTRmin or negative control GFP. Days post-targeting is relative to hTR KO; 65 days post-targeting was the last time point of collection prior to die-off of the telomerase-negative cells.

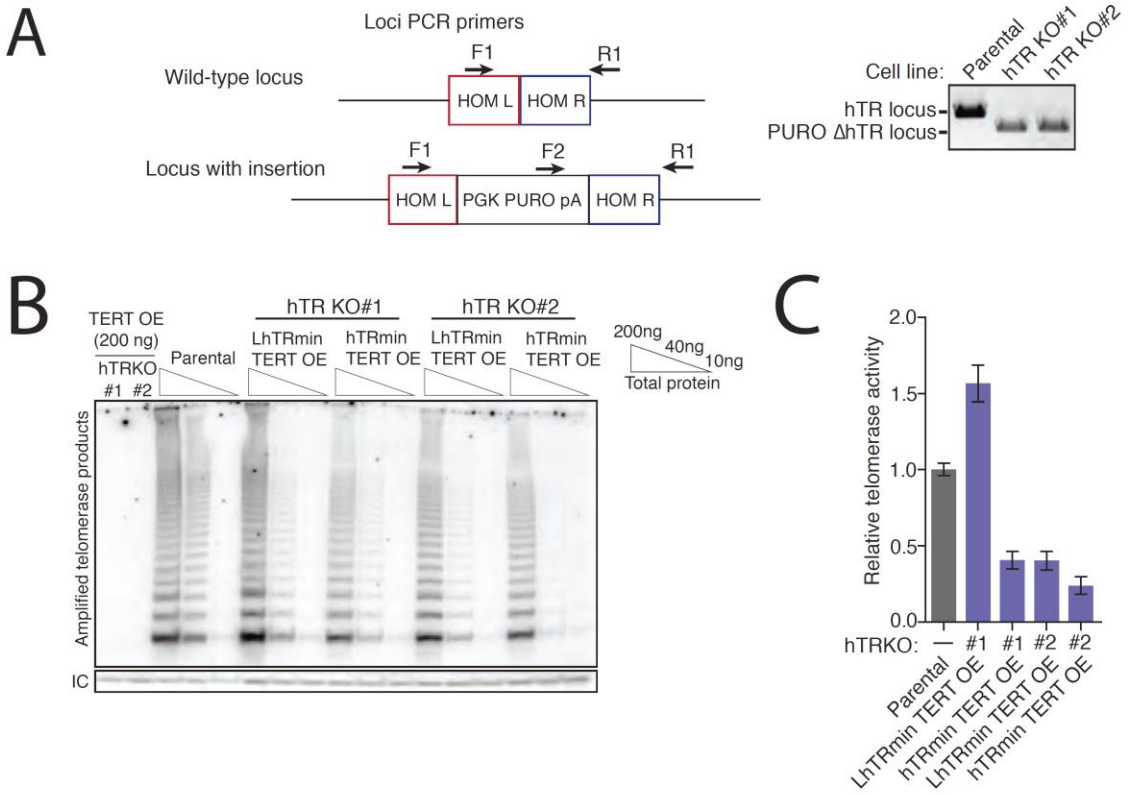
A
Loci PCR primers
F1
R1
Wild-type locus
HOM L
HOM R
F1
F2
R1
Locus with insertion
HOM L
PGK PURO pA
HOM R
Cell line:
Parental
hTR KO#1
hTR KO#2
hTR locus
PURO ΔhTR locus
B
TERT OE
(200 ng)
hTRKO
#1 #2
Parental
hTR KO#1
LhTRmin
TERT OE
hTRmin
TERT OE
hTR KO#2
LhTRmin
TERT OE
hTRmin
TERT OE
200ng
40ng
10ng
Total protein
Amplified telomerase products
IC
C
Relative telomerase activity
2.0
1.5
1.0
0.5
0.0
hTRKO:
—
#1
#1
#2
#2
Parental
LhTRmin TERT OE
hTRmin TERT OE
LhTRmin TERT OE
hTRmin TERT OE
D
Parental
GFP
hTR
LhTRmin
LhTRmin
Lentiviral transgene:
AAVS1 TERT OE:
—
—
—
—
+
hTR
LhTRmin
LC
F-TERT
Tubulin
Amplified telomerase products
E
Parental
AAVS1: TERT OE
Lentiviral transgene:
GFP
hTRmin
Days post-targeting:
58 65 51 58 65 79 93 107
MW (kb)
23.1
9.4
6.6
4.4
2.3
2.0

Figure 3. Telomerase with hTRmin supports stable telomere length maintenance.
(A) Southern blot detection of telomere restriction fragment lengths (TRF) for HCT116 cell lines after release from selection. The telomerase-negative cell line TRFs were analyzed before cultures commenced cell death.
(B) Time course of TRF shortening in the telomerase-negative HCT116 cell lines. The 65 days post-targeting time point was the final cell collection before culture death. All lanes are from the same gel. Red dashed lines separate different genotypes.
(C) TRF analysis for multiple clonal cell lines expressing LhTRmin with TERT OE or hTRmin with TERT OE, all cultured in parallel and assayed at the same time point 111 days post-targeting.
(D) Time course of TRF in the clonal cell lines expressing LhTRmin with TERT OE or hTRmin with TERT OE. Days post-targeting refers to the hTR KO.
(E) Immunoblot and Northern blot analysis of telomerase subunit expression levels across the clonal cell lines expressing LhTRmin with TERT OE or hTRmin with TERT OE, performed using cells at 111 days post-targeting.
(F) Comparison of telomerase activity measured by QTRAP (purple bars) with telomerase subunit expression levels quantified from blots in (E). QTRAP (averaged, n=5) and RNA signals were normalized to parental HCT116 cell line activity and endogenous hTR. TERT OE signals were set relative to LhTRmin TERT OE clone #1.

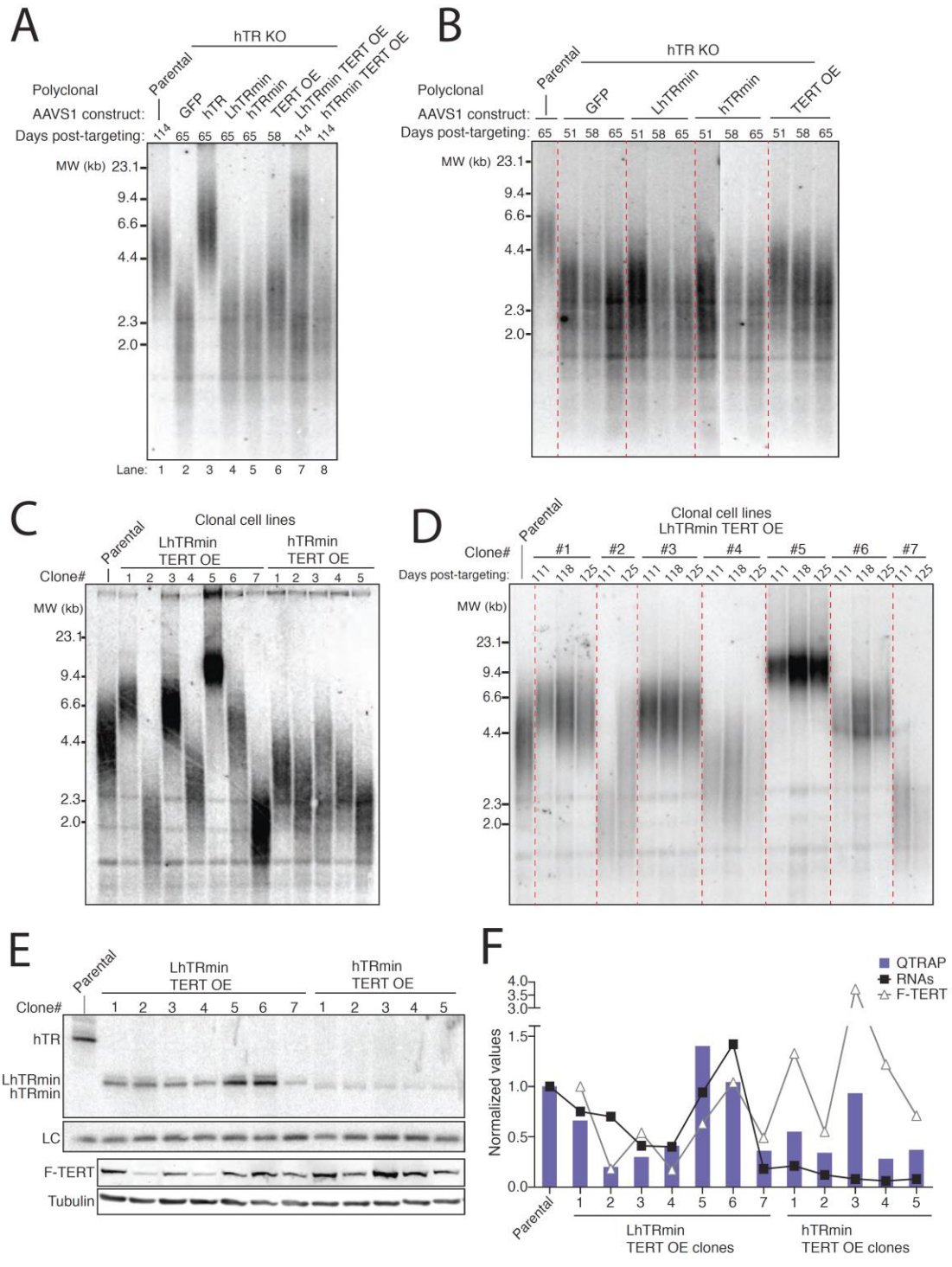
A
hTR KO
Parental
GFP
hTR
LhTRmin
hTRmin
TERT OE
LhTRmin TERT OE
hTRmin TERT OE
Polyclonal
AAVS1 construct:
Days post-targeting: 114 65 65 65 65 58 114 114
MW (kb) 23.1 9.4 6.6 4.4 2.3 2.0
Lane: 1 2 3 4 5 6 7 8
B
hTR KO
Parental
GFP
LhTRmin
hTRmin
TERT OE
Polyclonal
AAVS1 construct:
Days post-targeting: 65 51 58 65 51 58 65 51 58 65 51 58 65
MW (kb) 23.1 9.4 6.6 4.4 2.3 2.0
C
Clonal cell lines
Parental
LhTRmin TERT OE
hTRmin TERT OE
Clone# 1 2 3 4 5 6 7 1 2 3 4 5
MW (kb) 23.1 9.4 6.6 4.4 2.3 2.0
D
Clonal cell lines
LhTRmin TERT OE
Parental
Clone# #1 #2 #3 #4 #5 #6 #7
Days post-targeting: 111 118 125 111 125 111 118 125 111 118 125 111 118 125 111 118 125 111 125
MW (kb) 23.1 9.4 6.6 4.4 2.3 2.0
E
Parental
LhTRmin TERT OE
hTRmin TERT OE
Clone# 1 2 3 4 5 6 7 1 2 3 4 5
hTR
LhTRmin hTRmin
LC
F-TERT
Tubulin
F
QTRAP
RNAs
F-TERT
Normalized values
4.0 3.5 3.0 1.5 1.0 0.5 0.0
Parental 1 2 3 4 5 6 7 1 2 3 4 5
LhTRmin TERT OE clones
hTRmin TERT OE clones

Figure 3 – figure supplement 1. Characterization of telomere length maintenance and telomerase activity levels in hTRmin telomerase cell lines.
(A) Northern blot and TRF timecourse of HCT116 hTR KO#2 cell line rescue by transgene hTR.
(B) Time course of HCT116 TRF after introduction of transgene for TERT OE alone or with LhTRmin or hTRmin; cell cultures were polyclonal after transgene introduction. Cells with TERT OE alone died shortly after 65 days post-targeting, counted from the original hTR KO.
(C) Time course of TRF in clonal cell lines of HCT116 hTR KO with AAVS1 TERT OE and hTRmin. Days post-targeting refers to the original hTR KO.
(D) QTRAP data from Figure 3F with error bars from technical replicates (n=5).
(E) Telomerase activity measured by hotTRAP for the HCT116 clonal cell lines with TERT OE and LhTRmin or hTRmin. In each panel, all lanes are from the same gel.

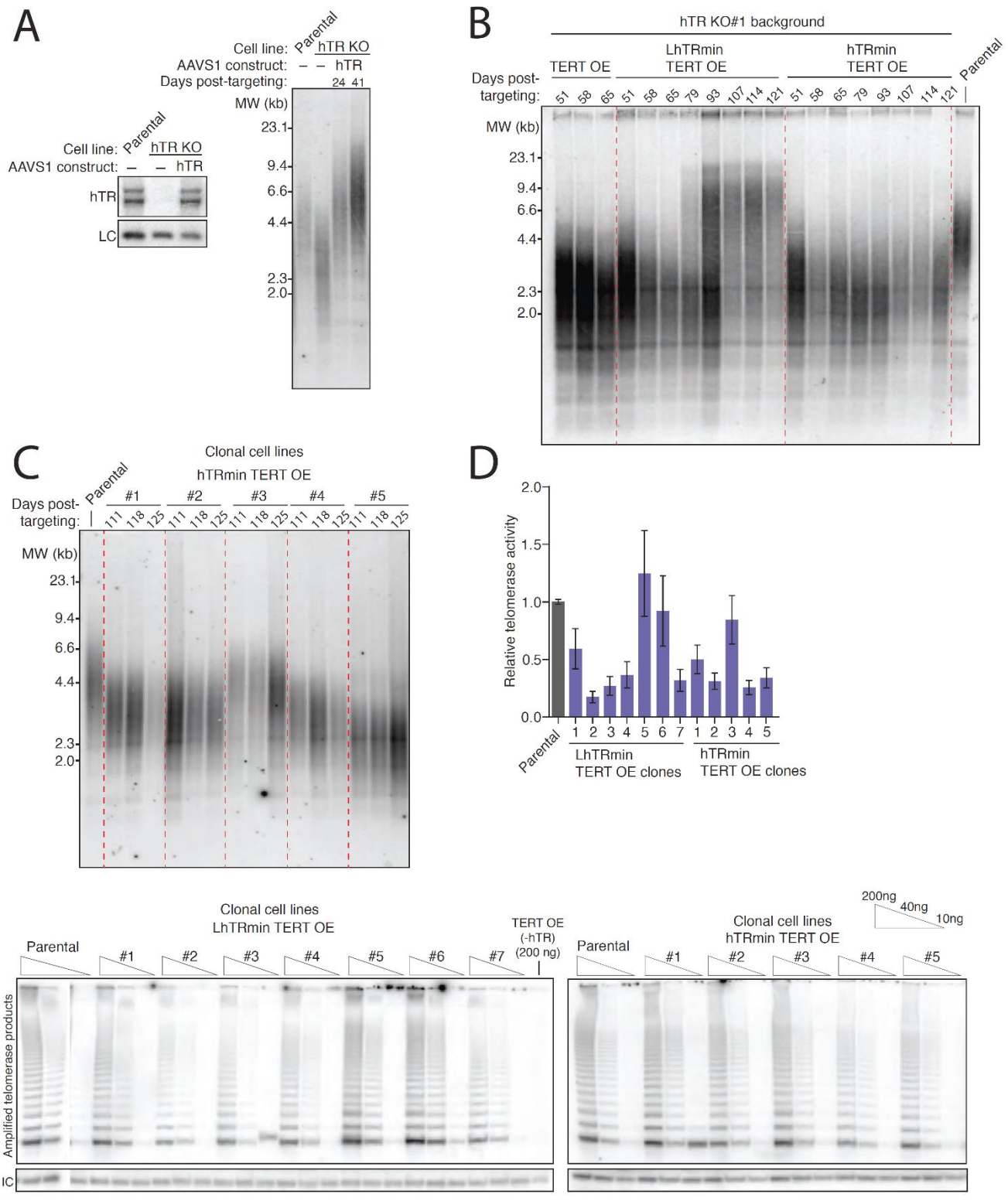
A
Cell line: Parental hTR KO
AAVS1 construct: – – hTR
Days post-targeting: 24 41
MW (kb)
23.1
9.4
6.6
4.4
2.3
2.0
Cell line: Parental hTR KO
AAVS1 construct: – – hTR
hTR
LC
B
hTR KO#1 background
TERT OE
LhTRmin TERT OE
hTRmin TERT OE
Parental
Days post-targeting:
51 58 65 51 58 65 79 93 107 114 121 51 58 65 79 93 107 114 121
MW (kb)
23.1
9.4
6.6
4.4
2.3
2.0
C
Clonal cell lines
hTRmin TERT OE
Parental
#1 #2 #3 #4 #5
Days post-targeting:
111 118 125 111 118 125 111 118 125 111 118 125 111 118 125
MW (kb)
23.1
9.4
6.6
4.4
2.3
2.0
D
Relative telomerase activity
2.0
1.5
1.0
0.5
0.0
Parental
1 2 3 4 5 6 7
LhTRmin TERT OE clones
1 2 3 4 5
hTRmin TERT OE clones
E
Clonal cell lines
LhTRmin TERT OE
Parental
#1 #2 #3 #4 #5 #6 #7
TERT OE (-hTR) (200 ng)
Clonal cell lines
hTRmin TERT OE
200ng 40ng 10ng
Parental
#1 #2 #3 #4 #5
Amplified telomerase products
IC

Figure 4. TCAB1 and Cajal bodies are not required for telomere maintenance by hTRmin telomerase.
(A) Schematic of Cas9-mediated disruption of TCAB1 and Coilin (COIL) loci with a HYGRO selection cassette.
(B) Immunoblot and QTRAP analysis of the polyclonal populations of LhTRmin or hTRmin TERT OE cells selected for disruption of TCAB1 or COIL loci. QTRAP values were normalized to the cell line before TCAB1 or COIL disruption (n=3).
(C) Immunofluorescence localization of TCAB1 and Coilin in HCT116 cells.
(D) Immunoblot analysis for TCAB1 and Coilin in clonal KO cell lines with LhTRmin + TERT OE or hTRmin + TERT OE.
(E) QTRAP assay of the clonal cell lines in (D). QTRAP values were normalized to the cell line before TCAB1 or COIL disruption (n=3).
(F) Stable TRF lengths in clonal cell lines lacking TCAB1 or Coilin. Days post-targeting refers to the TCAB1 or COIL KO.

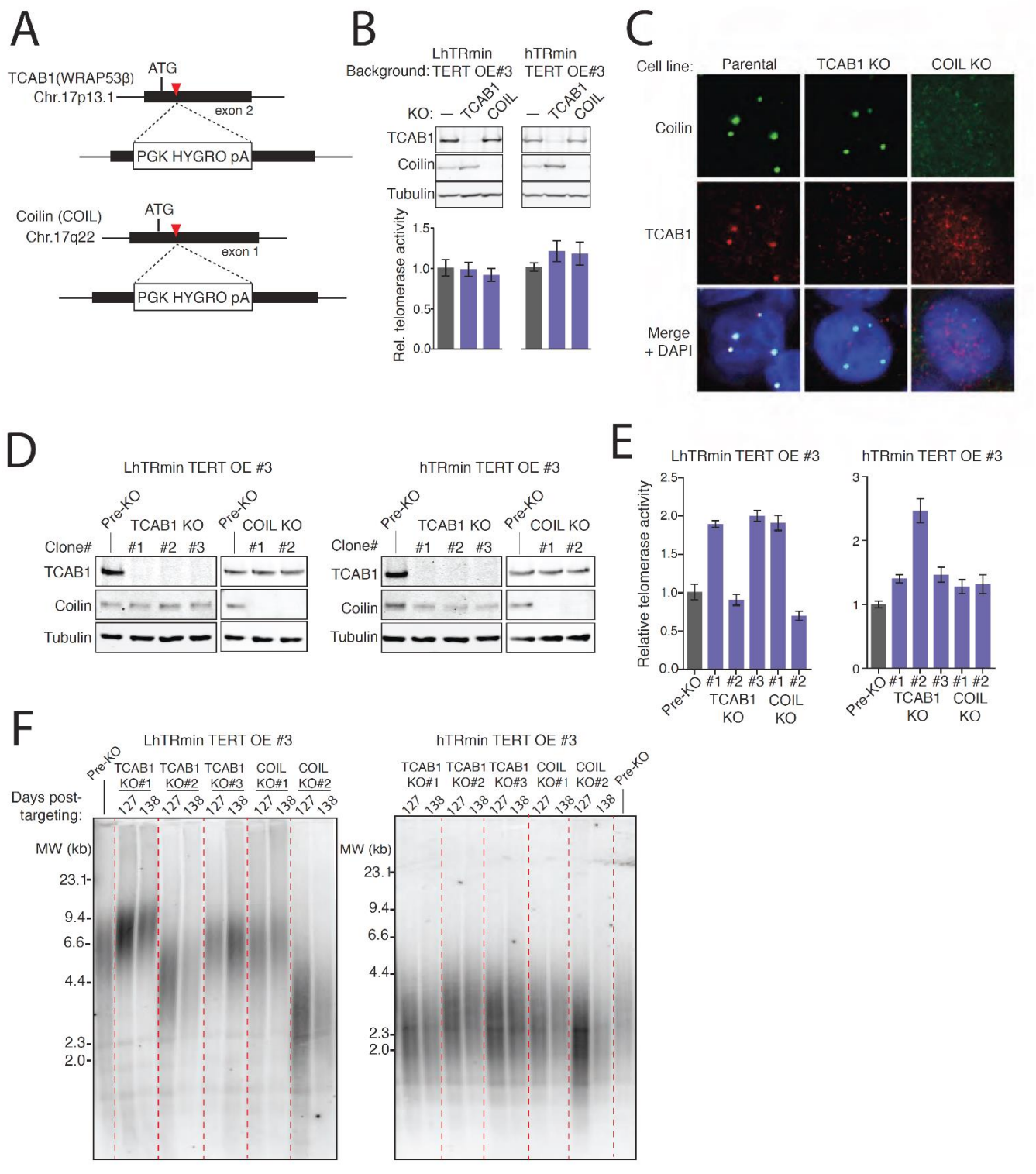
A
TCAB1(WRAP53β)
Chr.17p13.1
ATG
exon 2
PGK HYGRO pA
Coilin (COIL)
Chr.17q22
ATG
exon 1
PGK HYGRO pA
B
LhTRmin
TERT OE#3
hTRmin
TERT OE#3
Background:
KO: — TCAB1 COIL — TCAB1 COIL
TCAB1
Coilin
Tubulin
Rel. telomerase activity
1.5
1.0
0.5
0.0
C
Cell line:
Parental
TCAB1 KO
COIL KO
Coilin
TCAB1
Merge
+ DAPI
D
LhTRmin TERT OE #3
hTRmin TERT OE #3
Pre-KO
TCAB1 KO
COIL KO
Clone#
#1 #2 #3 #1 #2
TCAB1
Coilin
Tubulin
E
LhTRmin TERT OE #3
hTRmin TERT OE #3
Relative telomerase activity
2.5
2.0
1.5
1.0
0.5
0.0
3
2
1
0
Pre-KO #1 #2 #3 #1 #2
TCAB1 KO
COIL KO
F
LhTRmin TERT OE #3
hTRmin TERT OE #3
Pre-KO
TCAB1 KO#1
TCAB1 KO#2
TCAB1 KO#3
COIL KO#1
COIL KO#2
Days post-targeting:
127 138
MW (kb)
23.1
9.4
6.6
4.4
2.3
2.0

Figure 4 – figure supplement 1. Characterization of HCT116 hTRmin with TERT OE cell lines with TCAB1 KO or Coilin KO.
(A) Immunopurification from HCT116 hTR KO cell lines expressing LhTRmin with TERT OE or hTRmin with TERT OE. Protein A/G beads were coupled to anti-TCAB1 antibody and used to immunopurify TCAB1 complexes. Rabbit IgG and anti-FLAG antibody were used as negative and positive controls, respectively. Immunopurified samples were assayed by hotTRAP.
(B) Immunofluorescence localization of SMN in HCT116 TCAB1 KO and COIL KO cell lines.
(C,D) Immunoblot and PCR genotyping of HCT116 TCAB1 KO and COIL KO cell lines. The immunoblots are also shown in main figures. The TCAB1 KO clonal cell line #2 in LhTRmin TERT OE#3 background had one allele with target-site mutagenesis that produced an early translation stop codon.
(E) Extended culture TRF analysis of HCT116 TCAB1 KO and COIL KO clonal cell lines from the LTRmin and hTRmin telomerase backgrounds.

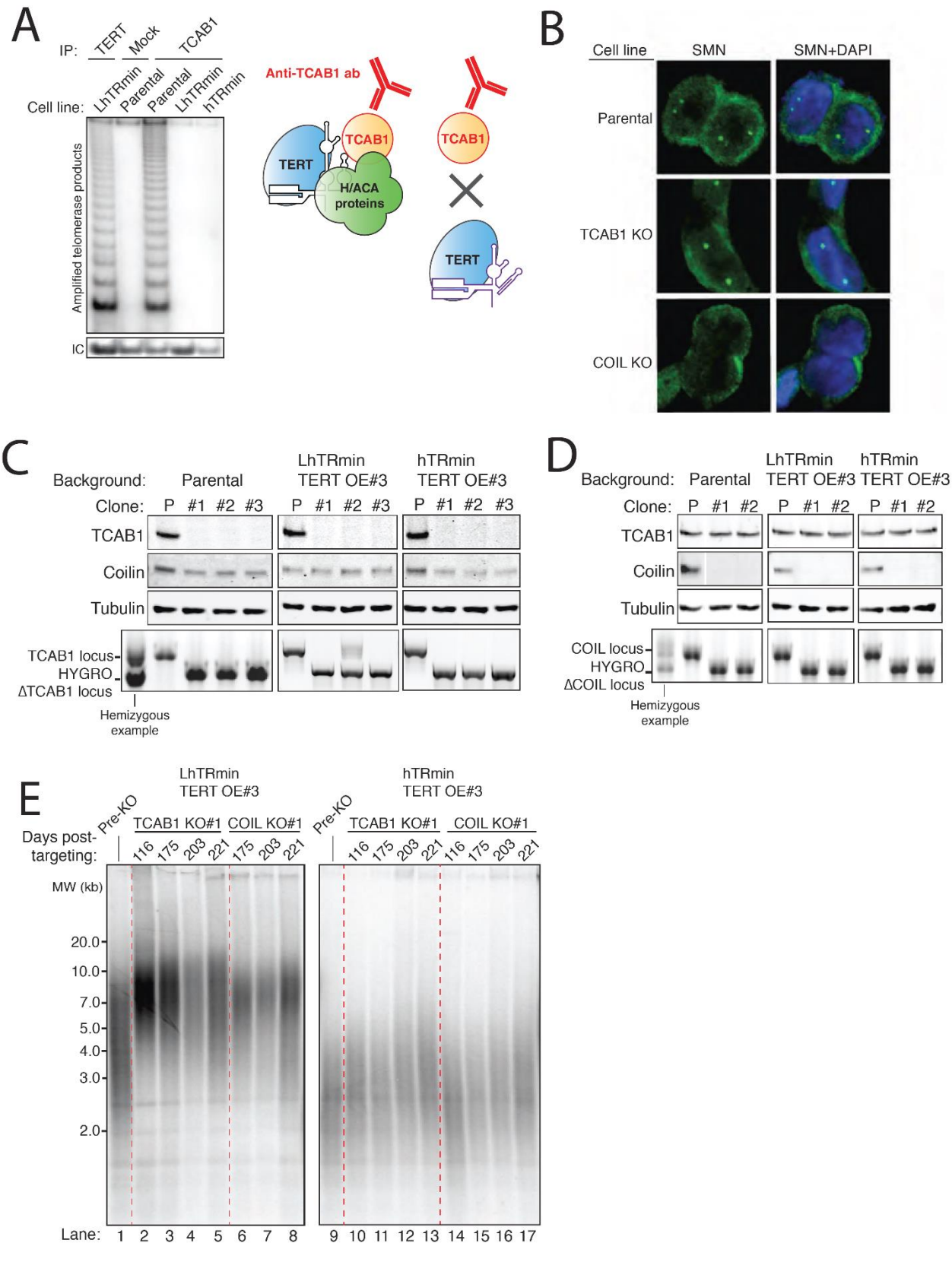
A
IP: TERT Mock TCAB1
Cell line: LhTRmin Parental Parental LhTRmin hTRmin
Amplified telomerase products
IC
Anti-TCAB1 ab
TCAB1
TERT
H/ACA proteins
B
Cell line
SMN
SMN+DAPI
Parental
TCAB1 KO
COIL KO
C
Background: Parental LhTRmin TERT OE#3 hTRmin TERT OE#3
Clone: P #1 #2 #3
TCAB1
Coilin
Tubulin
TCAB1 locus
HYGRO
ΔTCAB1 locus
Hemizygous example
D
Background: Parental LhTRmin TERT OE#3 hTRmin TERT OE#3
Clone: P #1 #2
TCAB1
Coilin
Tubulin
COIL locus
HYGRO
ΔCOIL locus
Hemizygous example
E
LhTRmin TERT OE#3
hTRmin TERT OE#3
Pre-KO
TCAB1 KO#1
COIL KO#1
Days post-targeting:
116 175 203 221 175 203 221
MW (kb)
20.0
10.0
7.0
5.0
4.0
3.0
2.0
Lane: 1 2 3 4 5 6 7 8 9 10 11 12 13 14 15 16 17

Figure 5. TCAB1 and Cajal bodies are not essential for telomere maintenance by endogenous telomerase.
(A) Immunoblot analysis of HCT116 TCAB1 KO and COIL KO clonal cell lines.
(B) Northern blot for hTR in HCT116 TCAB1 KO and COIL KO clonal cell lines.
(C) Lack of hotTRAP telomerase activity detection in the HCT116 TERT KO clonal cell lines.
(D) QTRAP analysis of telomerase activity in the HCT116 TCAB1 KO and COIL KO clonal cell lines. Values were normalized to the parental HCT116 cell line (n=3).
(E) Time course of TRF in the HCT116 TERT KO clonal cell lines.
(F,G) Time course of TRF in the HCT116 TCAB1 and COIL KO clonal cell lines.
(H) Immunoblot analysis of hESC TCAB1 KO and COIL KO clonal cell lines. Wild-type refers to an hESC clonal cell line subjected to Cas9 electroporation but retaining a wild-type genotype.
(I) QTRAP analysis of telomerase activity in the hESC TCAB1 KO and COIL KO clonal cell lines. Values were normalized to the parental hESC line (n=3).
(J,K) Time course of TRF in hESC TCAB1 KO and COIL KO clonal cell lines. Note that the long telomeres in mouse cells from the hESC feeder layer contribute some blot signal (indicated MEFs).

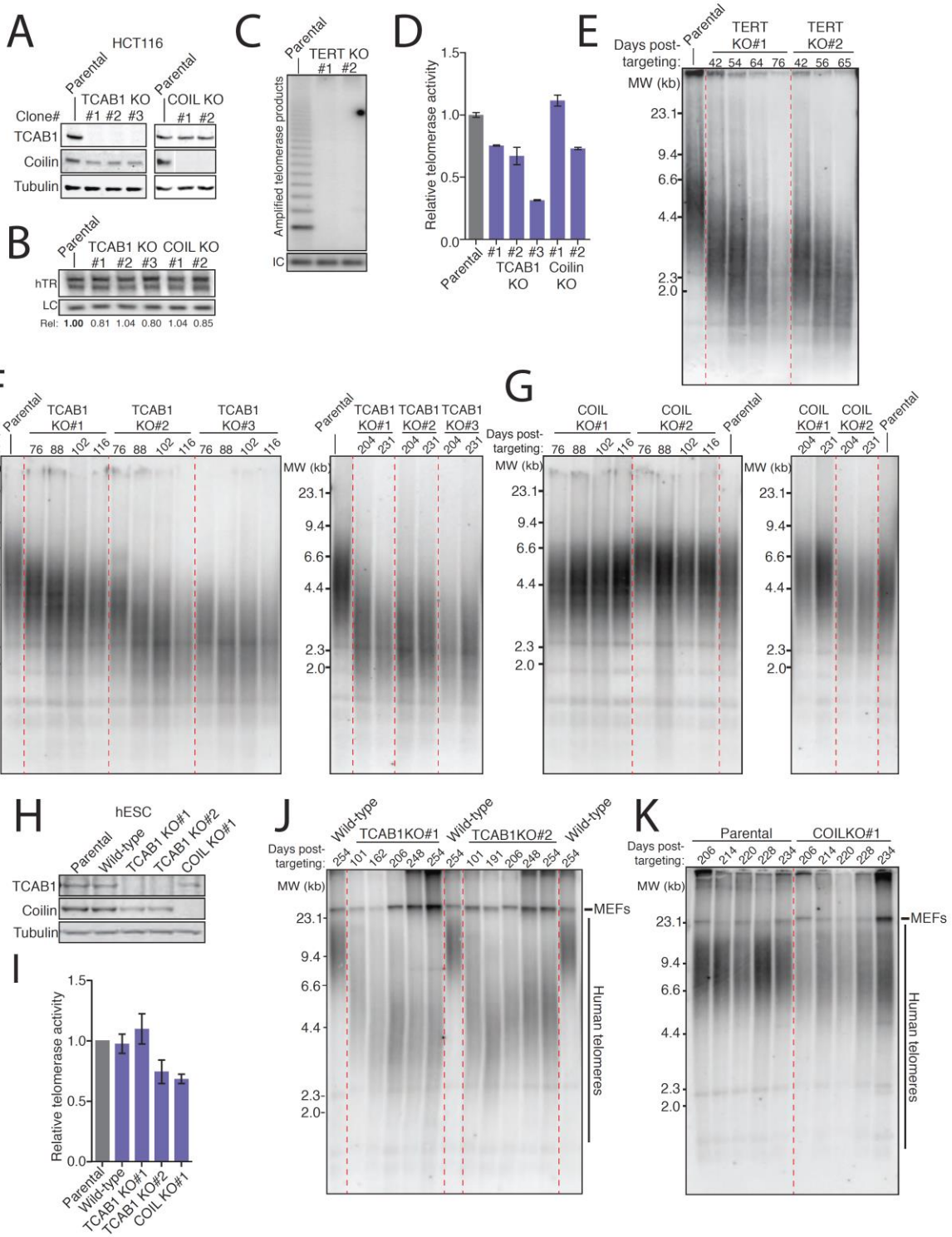
A
HCT116
Parental
TCAB1 KO
#1 #2 #3
Parental
COIL KO
#1 #2
Clone#
TCAB1
Coilin
Tubulin
B
Parental
TCAB1 KO #1 #2 #3
COIL KO #1 #2
hTR
LC
Rel: 1.00 0.81 1.04 0.80 1.04 0.85
C
Parental
TERT KO #1 #2
Amplified telomerase products
IC
D
Relative telomerase activity
1.5
1.0
0.5
0.0
Parental
#1 #2 #3 #1 #2
TCAB1 KO
Coilin KO
E
Days post-targeting:
Parental
TERT KO#1
TERT KO#2
42 54 64 76 42 56 65
MW (kb)
23.1
9.4
6.6
4.4
2.3
2.0
F
Days post-targeting:
Parental
TCAB1 KO#1
TCAB1 KO#2
TCAB1 KO#3
76 88 102 116 76 88 102 116 76 88 102 116
MW (kb)
23.1
9.4
6.6
4.4
2.3
2.0
Parental
TCAB1 KO#1
TCAB1 KO#2
TCAB1 KO#3
204 231 204 231 204 231
G
Days post-targeting:
COIL KO#1
COIL KO#2
Parental
76 88 102 116 76 88 102 116
COIL KO#1
COIL KO#2
Parental
204 231 204 231
H
hESC
Parental
Wild-type
TCAB1 KO#1
TCAB1 KO#2
COIL KO#1
TCAB1
Coilin
Tubulin
I
Relative telomerase activity
1.5
1.0
0.5
0.0
Parental
Wild-type
TCAB1 KO#1
TCAB1 KO#2
COIL KO#1
J
Wild-type
TCAB1KO#1
Wild-type
TCAB1KO#2
Wild-type
Days post-targeting:
254 101 162 206 248 254 254 101 191 206 248 254 254
MW (kb)
23.1
9.4
6.6
4.4
2.3
2.0
MEFs
Human telomeres
K
Parental
COILKO#1
Days post-targeting:
206 214 220 228 234 206 214 220 228 234
MW (kb)
23.1
9.4
6.6
4.4
2.3
2.0
MEFs
Human telomeres

Figure 5 – figure supplement 1. Characterization of HCT116 TERT KO, TCAB1 KO, and COIL KO cell lines with endogenous hTR.
(A) PCR genotyping of HCT116 TERT KO clonal cell lines.
(B) Immunopurification of TCAB1 complexes from parental, TCAB1 KO, and COIL KO HCT116 cell lines followed by hotTRAP.
(C) HotTRAP of HCT116 TCAB1 KO and COIL KO cell lines.

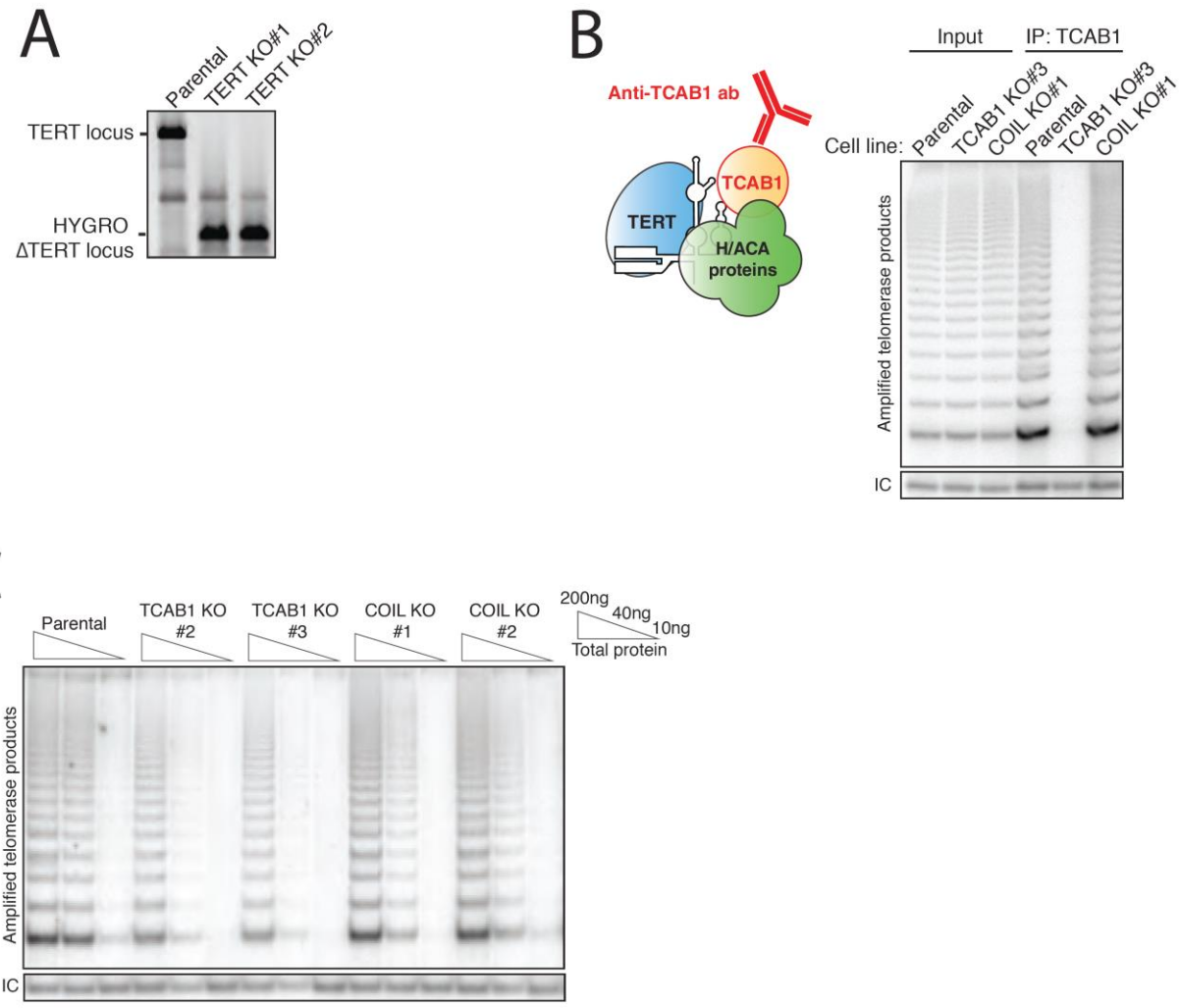

Figure 5 – figure supplement 2. Characterization of hESC TCAB1 KO and COIL KO lines with endogenous hTR.
(A) PCR genotyping of hESC TCAB1 KO and COIL KO clonal cell lines. Wild-type refers to an hESC clonal cell line subjected to Cas9 electroporation but retaining a wild-type genotype.
(B) HotTRAP of the TCAB1 KO hESC lines.
(C) Immunofluorescence localization of Coilin and TCAB1 in hESC lines.

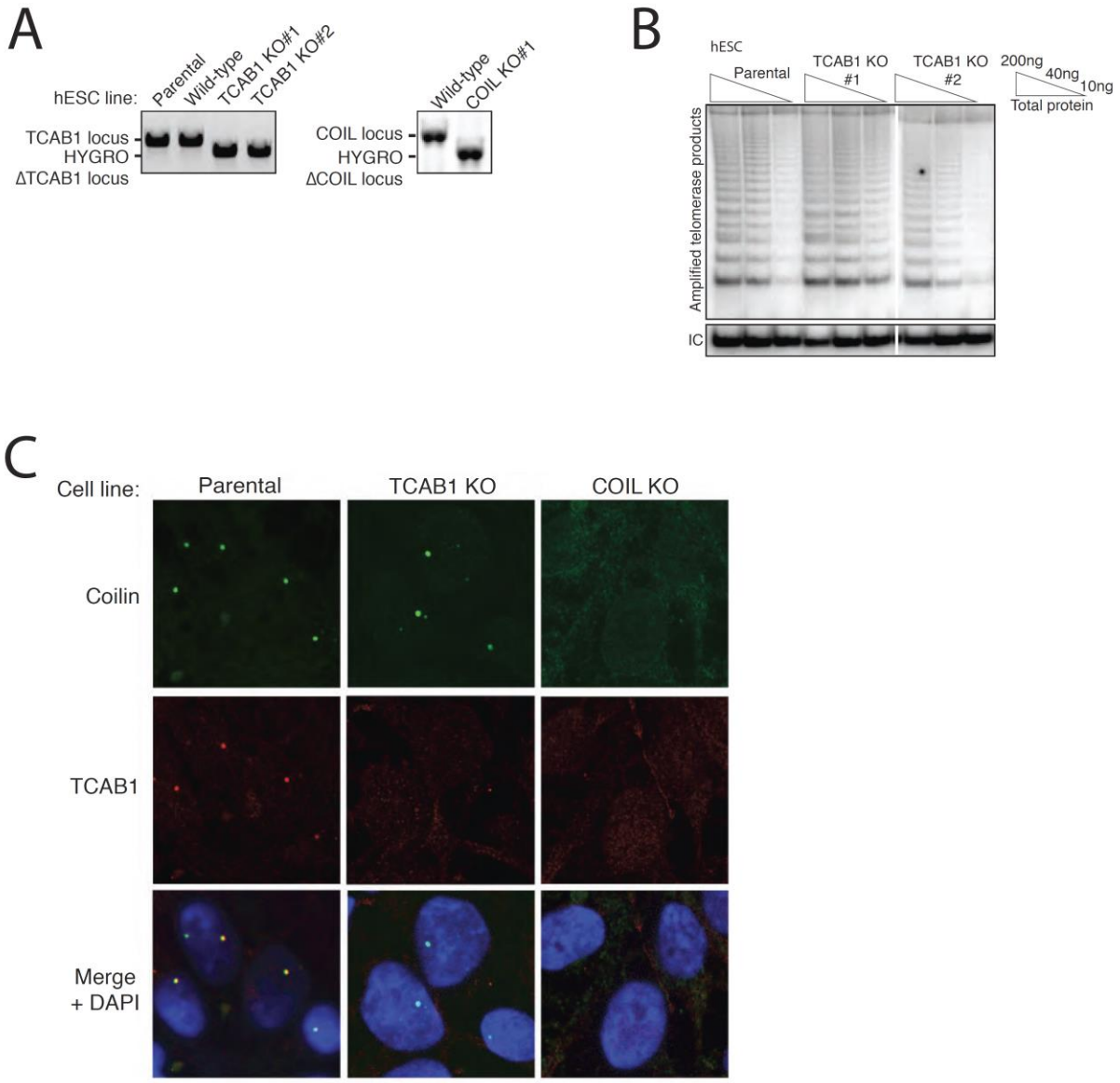

Figure 5 – figure supplement 3. Additional controls for TCAB1 loss-of-function in TCAB1 KO cell lines.
(A) Immunoblot and QTRAP analysis of HCT116 parental and TCAB1 KO cell lines expressing F-tagged TCAB1 or GFP from transgenes at AAVS1. QTRAP values were normalized to the GFP cell line signal (n=3). Days post-targeting refers to transgene integration.
(B) Time course of TRF in cell lines from (A).
(C) Immunoblot and QTRAP analysis of hESC parental and TCAB1 KO cell lines expressing F-tagged TCAB1 transgene at AAVS1. QTRAP values were normalized to the unrescued TCAB1 KO cell line signal (n=3). Days post-targeting refers to transgene integration.
(D) Time course of TRF in cell lines from (C).
(E) TCAB1 double-exon-disruption schematic with TCAB1 exon 2 and exon 8 KO genotyping by PCR. TCAB1 exon 8 targeting was performed in the HCT116 TCAB1 KO#2 background, which has a hygromycin resistance cassette inserted in TCAB1 exon 2.
(F) TRF of HCT116 parental, TCAB1 KO#2 background, and exon 8 disrupted TCAB1 KO#2 (double-exon-disruption) cell lines. DNA was purified from double-exon-disruption cells at 43 days post-targeting the second KO.
(G) Immunofluorescence staining for Coilin (green) and TCAB1 (red) in double-exon-disruption cells.

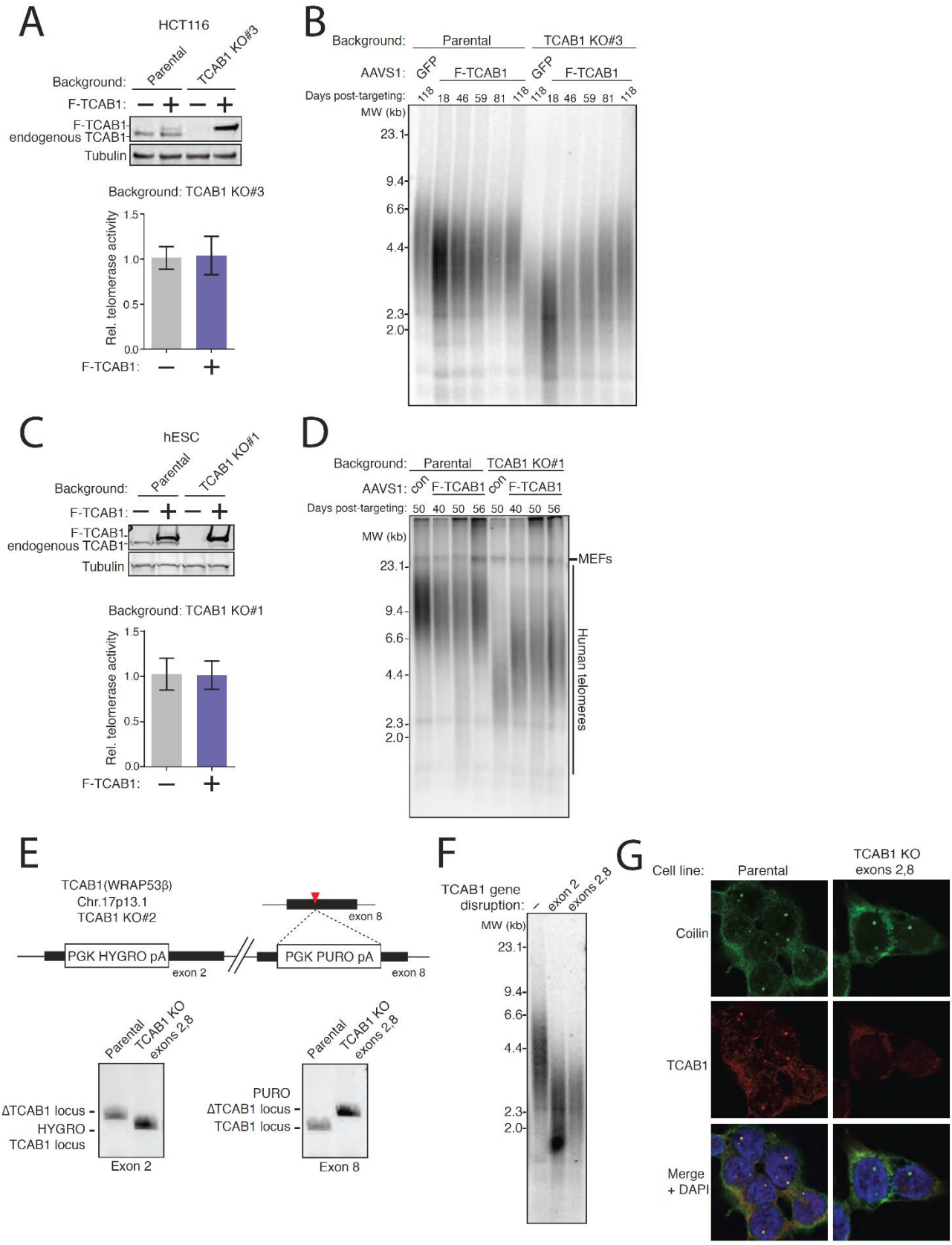
A
HCT116
Parental
TCAB1 KO#3
Background:
F-TCAB1:
F-TCAB1
endogenous TCAB1
Tubulin
Background: TCAB1 KO#3
Rel. telomerase activity
F-TCAB1:
B
Background:
Parental
TCAB1 KO#3
AAVS1:
GFP
F-TCAB1
Days post-targeting:
MW (kb)
23.1
9.4
6.6
4.4
2.3
2.0
C
hESC
Parental
TCAB1 KO#1
Background:
F-TCAB1:
F-TCAB1
endogenous TCAB1
Tubulin
Background: TCAB1 KO#1
Rel. telomerase activity
F-TCAB1:
D
Background:
Parental
TCAB1 KO#1
AAVS1:
con
F-TCAB1
Days post-targeting:
MW (kb)
23.1
9.4
6.6
4.4
2.3
2.0
MEFs
Human telomeres
E
TCAB1(WRAP53β)
Chr.17p13.1
TCAB1 KO#2
exon 8
PGK HYGRO pA
exon 2
PGK PURO pA
exon 8
Parental
TCAB1 KO
exons 2,8
ΔTCAB1 locus
HYGRO -
TCAB1 locus
Exon 2
PURO
ΔTCAB1 locus
TCAB1 locus
Exon 8
F
TCAB1 gene
disruption:
exon 2
exons 2,8
MW (kb)
23.1
9.4
6.6
4.4
2.3
2.0
G
Cell line:
Parental
TCAB1 KO
exons 2,8
Coilin
TCAB1
Merge
+ DAPI

Figure 6. Cajal bodies promote telomere elongation upon increased telomerase expression level.

(A) Immunoblot, northern blot, and QTRAP characterization of TCAB1 KO and COIL KO HCT116 cells overexpressing hTR and TERT at AAVS1 (HiT). QTRAP values were normalized to parental HCT116 (n=3).

(B) Time course of TRF in the HiT HCT116 TCAB1 KO and COIL KO cell cultures polyclonal following HiT transgene introduction. Days post-targeting refers to HiT transgene introduction. The lanes labeled "con" are the indicated cell line without HiT transgene introduction.

(C) FISH for hTR localization in HiT HCT116 cell lines.

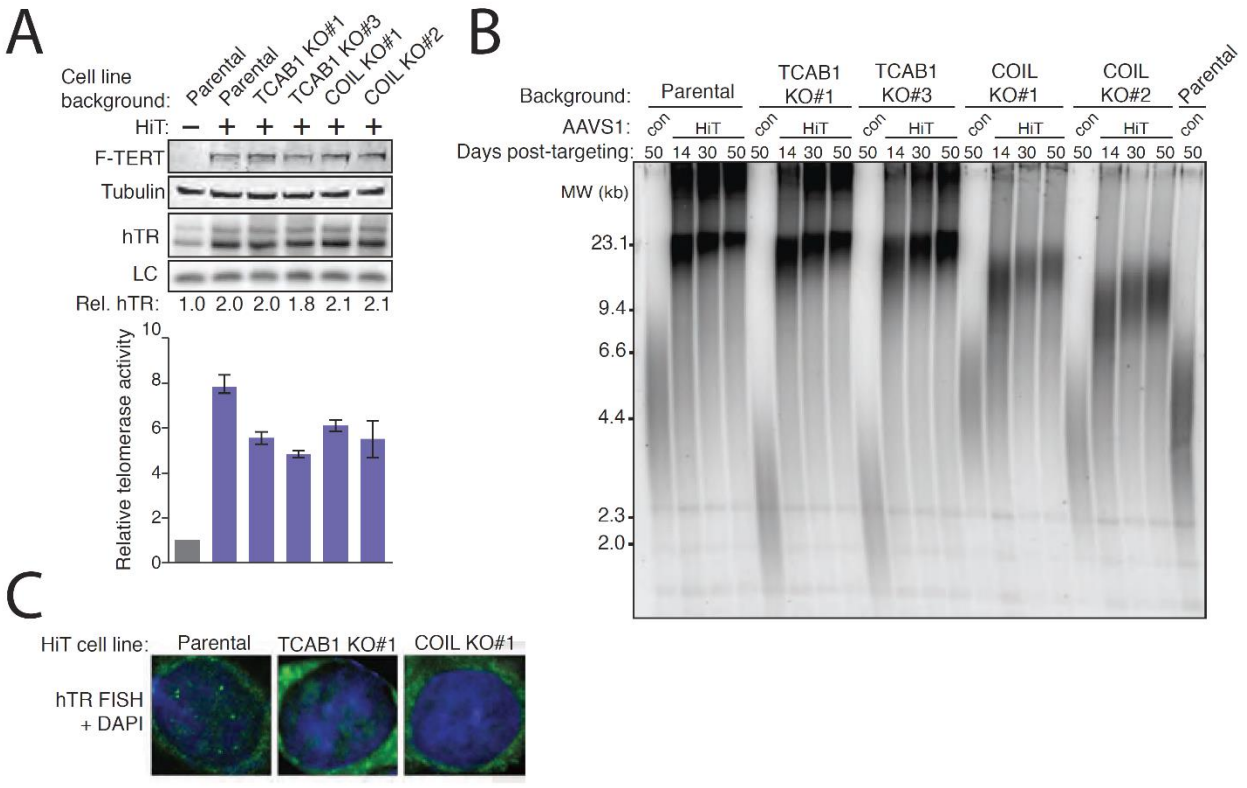

Figure 7. Multiple traffic pathways for human telomerase biogenesis and action at telomeres.
At left, hTRmin telomerase assembles and acts at telomeres without supplemental trafficking instructions. At right, endogenous hTR and TERT are trafficked for their assembly and for telomerase action at telomeres.

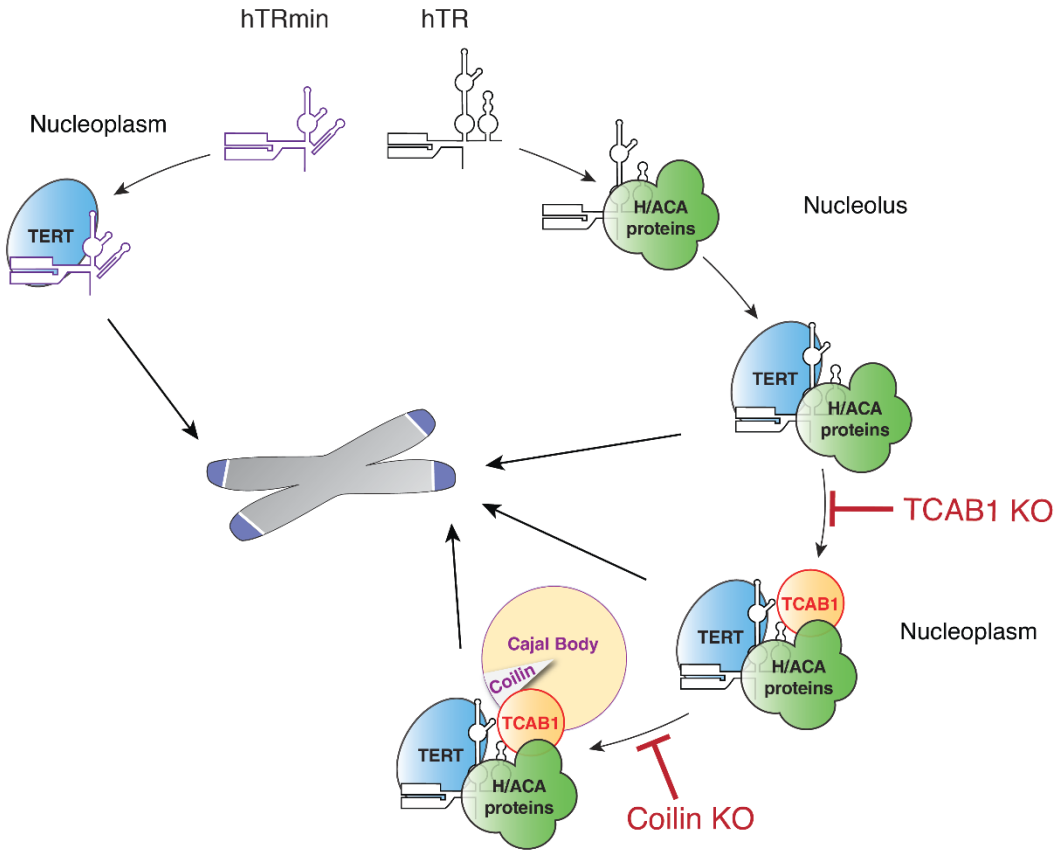

References

Andersen, C. L., J. L. Jensen, and T. F. Orntoft. 2004. 'Normalization of real-time quantitative reverse transcription-PCR data: a model-based variance estimation approach to identify genes suited for normalization, applied to bladder and colon cancer data sets', *Cancer Res*, 64: 5245-50.

Armanios, M., and E. H. Blackburn. 2012. 'The telomere syndromes', *Nat. Rev. Genet.*, 13: 693-704.

Arnoult, N., and J. Karlseder. 2015. 'Complex interactions between the DNA-damage response and mammalian telomeres', *Nat Struct Mol Biol*, 22: 859-66.

Aubert, G. 2014. 'Telomere dynamics and aging', *Prog Mol Biol Transl Sci*, 125: 89-111.

Batista, L. F., M. F. Pech, F. L. Zhong, H. N. Nguyen, K. T. Xie, A. J. Zaug, S. M. Crary, J. Choi, V. Sebastiano, A. Cherry, N. Giri, M. Wernig, B. P. Alter, T. R. Cech, S. A. Savage, R. A. Reijo Pera, and S. E. Artandi. 2011. 'Telomere shortening and loss of self-renewal in dyskeratosis congenita induced pluripotent stem cells', *Nature*, 474: 399-402.

Baumann, P., and C. Price. 2010. 'Pot1 and telomere maintenance', *FEBS Lett*, 584: 3779-84.

Biessmann, H., and J. M. Mason. 1997. 'Telomere maintenance without telomerase', *Chromosoma*, 106: 63-9.

Blackburn, E. H., and K. Collins. 2011. 'Telomerase: an RNP enzyme synthesizes DNA', *Cold Spring Harb. Perspect. Biol.*, 3: 205-13.

Blackburn, E. H., and J. G. Gall. 1978. 'A tandemly repeated sequence at the termini of the extrachromosomal ribosomal RNA genes in Tetrahymena', *J. Mol. Biol.*, 120: 33-53.

Blackburn, E.H., C.W. Greider, and J.W. Szostak. 2006. 'Telomeres and telomerase: the path from maize, *Tetrahymena* and yeast to human cancer and aging', *Nat. Med.*, 12: 1133-38.

Box, J. A., J. T. Bunch, W. Tang, and P. Baumann. 2008. 'Spliceosomal cleavage generates the 3' end of telomerase RNA', *Nature*, 456: 910-4.

Brown, J. A., M. L. Valenstein, T. A. Yario, K. T. Tycowski, and J. A. Steitz. 2012. 'Formation of triple-helical structures by the 3'-end sequences of MALAT1 and MENbeta noncoding RNAs', *Proc. Natl. Acad. Sci. USA*, 109: 19202-7.

Bryan, T. M., A. Englezou, M. A. Dunham, and R. R. Reddel. 1998. 'Telomere length dynamics in telomerase-positive immortal human cell populations', *Exp Cell Res*, 239: 370-8.

Cesare, A. J., and J. Karlseder. 2012. 'A three-state model of telomere control over human proliferative boundaries', *Curr Opin Cell Biol*, 24: 731-8.

Chen, L. Y., S. Redon, and J. Lingner. 2012. 'The human CST complex is a terminator of telomerase activity', *Nature*, 488: 540-4.

Chen, Y., Z. Deng, S. Jiang, Q. Hu, H. Liu, Z. Songyang, W. Ma, S. Chen, and Y. Zhao. 2015. 'Human cells lacking coilin and Cajal bodies are proficient in telomerase assembly, trafficking and telomere maintenance', *Nucleic Acids Res*, 43: 385-95.

Chiba, K., and D. Hockemeyer. 2015. 'Genome editing in human pluripotent stem cells using site-specific nucleases', *Methods Mol Biol*, 1239: 267-80.

Chow, T. T., Y. Zhao, S. S. Mak, J. W. Shay, and W. E. Wright. 2012. 'Early and late steps in telomere overhang processing in normal human cells: the position of the final RNA primer drives telomere shortening', *Genes Dev*, 26: 1167-78.

Collins, K. 2008. 'Physiological assembly and activity of human telomerase complexes', *Mech. Ageing Dev.*, 129: 91-98.

Cristofari, G., E. Adolf, P. Reichenbach, K. Sikora, R. M. Terns, M. P. Terns, and J. Lingner. 2007. 'Human telomerase RNA accumulation in Cajal bodies facilitates telomerase recruitment to telomeres and telomere elongation', *Mol. Cell*, 27: 882-9.

Dai, X., C. Huang, A. Bhusari, S. Sampathi, K. Schubert, and W. Chai. 2010. 'Molecular steps of G-overhang generation at human telomeres and its function in chromosome end protection', *EMBO J*, 29: 2788-801.
de Lange, T. 2010. 'How shelterin solves the telomere end-protection problem', *Cold Spring Harb. Symp. Quant. Biol.* , 75: 167-77.
———. 2015. 'A loopy view of telomere evolution', *Front Genet*, 6: 321.
Dionne, I., S. Larose, A. T. Dandjinou, S. Abou Elela, and R. J. Wellinger. 2013. 'Cell cycle-dependent transcription factors control the expression of yeast telomerase RNA', *RNA*, 19: 992-1002.
Donjerkovic, D., and D. W. Scott. 2000. 'Regulation of the G1 phase of the mammalian cell cycle', *Cell Res*, 10: 1-16.
Egan, E. D., and K. Collins. 2012a. 'An enhanced H/ACA RNP assembly mechanism for human telomerase RNA', *Mol. Cell. Biol.*, 32: 2428-39.
Egan, E.D., and K. Collins. 2012b. 'Biogenesis of telomerase ribonucleoproteins', *RNA*, 18: 1747-59.
Etheridge, K. T., S. S. Banik, B. N. Armbruster, Y. Zhu, R. M. Terns, M. P. Terns, and C. M. Counter. 2002. 'The nucleolar localization domain of the catalytic subunit of human telomerase', *J Biol Chem*, 277: 24764-70.
Forsyth, N. R., W. E. Wright, and J. W. Shay. 2002. 'Telomerase and differentiation in multicellular organisms: turn it off, turn it on, and turn it off again', *Differentiation*, 69: 188-97.
Fu, D., and K. Collins. 2003. 'Distinct biogenesis pathways for human telomerase RNA and H/ACA small nucleolar RNAs', *Mol. Cell*, 11: 1361-72.
———. 2006. 'Human telomerase and Cajal body ribonucleoproteins share a unique specificity of Sm protein association', *Genes Dev.*, 20: 531-36.
———. 2007. 'Purification of human telomerase complexes identifies factors involved in telomerase biogenesis and telomere length regulation', *Mol. Cell*, 28: 773-85.
Gallardo, F., and P. Chartrand. 2008. 'Telomerase biogenesis: The long road before getting to the end', *RNA Biol.*, 5: 212-15.
Gallardo, F., N. Laterreur, E. Cusanelli, F. Ouenzar, E. Querido, R. J. Wellinger, and P. Chartrand. 2011. 'Live cell imaging of telomerase RNA dynamics reveals cell cycle-dependent clustering of telomerase at elongating telomeres', *Mol. Cell*, 44: 819-27.
Gallardo, F., N. Laterreur, R. J. Wellinger, and P. Chartrand. 2012. 'Telomerase caught in the act: united we stand, divided we fall', *RNA Biol*, 9: 1139-43.
Gao, H., R.B. Cervantes, E.K. Mandell, J.H. Otero, and V. Lundblad. 2007. 'RPA-like proteins mediate yeast telomere function', *Nat. Struct. Mol. Biol.*, 14: 208-14.
Garg, M., R. L. Gurung, S. Mansoubi, J. O. Ahmed, A. Dave, F. Z. Watts, and A. Bianchi. 2014. 'Tpz1TPP1 SUMOylation reveals evolutionary conservation of SUMO-dependent Stn1 telomere association', *EMBO Rep*, 15: 871-7.
Giraud-Panis, M. J., M. T. Teixeira, V. Geli, and E. Gilson. 2010. 'CST meets shelterin to keep telomeres in check', *Mol Cell*, 39: 665-76.
Greider, C. W. , and E. H. Blackburn. 1989. 'A telomeric sequence in the RNA of *Tetrahymena* telomerase required for telomere repeat synthesis', *Nature*, 337: 331-37.
Greider, C. W., and E. H. Blackburn. 1985. 'Identification of a specific telomere terminal transferase activity in *Tetrahymena* extracts', *Cell*, 43: 405-13.
Griffith, J. D., L. Comeau, S. Rosenfield, R. M. Stansel, A. Bianchi, H. Moss, and T. de Lange. 1999. 'Mammalian telomeres end in a large duplex loop', *Cell*, 97: 503-14.
Henriksson, S., and M. Farnebo. 2015. 'On the road with WRAP53beta: guardian of Cajal bodies and genome integrity', *Front Genet*, 6: 91.
Hiyama, E., and K. Hiyama. 2007. 'Telomere and telomerase in stem cells', *Br J Cancer*, 96: 1020-4.
Hockemeyer, D., and K. Collins. 2015. 'Control of human telomerase action at telomeres', *Nat. Struct. Mol. Biol.*, in press.
Hockemeyer, D., and R. Jaenisch. 2016. 'Induced Pluripotent Stem Cells Meet Genome Editing', *Cell Stem Cell*, 18: 573-86.

Hockemeyer, D., F. Soldner, C. Beard, Q. Gao, M. Mitalipova, R. C. DeKelver, G. E. Katibah, R. Amora, E. A. Boydston, B. Zeitler, X. Meng, J. C. Miller, L. Zhang, E. J. Rebar, P. D. Gregory, F. D. Urnov, and R. Jaenisch. 2009. 'Efficient targeting of expressed and silent genes in human ESCs and iPSCs using zinc-finger nucleases', *Nat Biotechnol*, 27: 851-7.

Holohan, B., W. E. Wright, and J. W. Shay. 2014. 'Cell biology of disease: Telomeropathies: an emerging spectrum disorder', *J Cell Biol*, 205: 289-99.

Holt, S.E., D.L. Aisner, J.W. Shay, and W.E. Wright. 1997. 'Lack of cell cycle regulation of telomerase activity in human cells', *Proc. Natl. Acad. Sci. USA*, 94: 10687-92.

Hu, X., J. Liu, H. I. Jun, J. K. Kim, and F. Qiao. 2016. 'Multi-step coordination of telomerase recruitment in fission yeast through two coupled telomere-telomerase interfaces', *Elife*, 5.

Huang, J., A. F. Brown, J. Wu, J. Xue, C. J. Bley, D. P. Rand, L. Wu, R. Zhang, J. J. Chen, and M. Lei. 2014. 'Structural basis for protein-RNA recognition in telomerase', *Nat Struct Mol Biol*, 21: 507-12.

Hug, N., and J. Lingner. 2006. 'Telomere length homeostasis', *Chromosoma*, 115: 413-25.

Hwang, H., N. Buncher, P. L. Opresko, and S. Myong. 2012. 'POT1-TPP1 regulates telomeric overhang structural dynamics', *Structure*, 20: 1872-80.

Jády, B. E., E. Bertrand, and T. Kiss. 2004. 'Human telomerase RNA and box H/ACA scaRNAs share a common Cajal body-specific localization signal', *J. Cell Biol.*, 164: 647-52.

Jády, B.E., P. Richard, E. Bertrand, and T. Kiss. 2006. 'Cell cycle-dependent recruitment of telomerase RNA and Cajal bodies to human telomeres', *Mol. Biol. Cell.*, 17: 944-54.

Jiang, J., H. Chan, D. D. Cash, E. J. Miracco, R. R. Ogorzalek Loo, H. E. Upton, D. Cascio, R. O'Brien Johnson, K. Collins, J. A. Loo, Z. H. Zhou, and J. Feigon. 2015. 'Structure of Tetrahymena telomerase reveals previously unknown subunits, functions, and interactions', *Science*, 350: aab4070.

Jiang, J., E. J. Miracco, K. Hong, B. Eckert, H. Chan, D. D. Cash, B. Min, Z. H. Zhou, K. Collins, and J. Feigon. 2013. 'The architecture of *Tetrahymena* telomerase holoenzyme', *Nature*, 496: 187-92.

Kim, N.W., M.A. Piatyszek, K.R. Prowse, C.B. Harley, M.D. West, P.L.C. Ho, G.M. Coviello, W.E. Wright, S.L. Weinrich, and J.W. Shay. 1994. 'Specific association of human telomerase activity with immortal cells and cancer', *Science*, 266: 2011-15.

Kiss, T., E. Fayet-Lebaron, and B.E. Jády. 2010. 'Box H/ACA small ribonucleoproteins', *Mol Cell*, 37: 597-606.

Lee, J. H., Y. S. Lee, S. A. Jeong, P. Khadka, J. Roth, and I. K. Chung. 2014. 'Catalytically active telomerase holoenzyme is assembled in the dense fibrillar component of the nucleolus during S phase', *Histochem Cell Biol*, 141: 137-52.

Lemieux, B., N. Laterreur, A. Perederina, J. F. Noel, M. L. Dubois, A. S. Krasilnikov, and R. J. Wellinger. 2016. 'Active Yeast Telomerase Shares Subunits with Ribonucleoproteins RNase P and RNase MRP', *Cell*, 165: 1171-81.

Lewis, K. A., and D. S. Wuttke. 2012. 'Telomerase and telomere-associated proteins: structural insights into mechanism and evolution', *Structure*, 20: 28-39.

Li, S., S. Makovets, T. Matsuguchi, J. D. Blethrow, K. M. Shokat, and E. H. Blackburn. 2009. 'Cdk1-dependent phosphorylation of Cdc13 coordinates telomere elongation during cell-cycle progression', *Cell*, 136: 50-61.

Lingner, J., T. R. Hughes, A. Shevchenko, M. Mann, V. Lundblad, and T. R. Cech. 1997. 'Reverse transcriptase motifs in the catalytic subunit of telomerase', *Science*, 276: 561-67.

Liu, J., M. D. Hebert, Y. Ye, D. J. Templeton, H. Kung, and A. G. Matera. 2000. 'Cell cycle-dependent localization of the CDK2-cyclin E complex in Cajal (coiled) bodies', *J Cell Sci*, 113 (Pt 9): 1543-52.

Loayza, D., and T. De Lange. 2003. 'POT1 as a terminal transducer of TRF1 telomere length control', *Nature*, 423: 1013-8.

Londono-Vallejo, J. A., and R. J. Wellinger. 2012. 'Telomeres and telomerase dance to the rhythm of the cell cycle', *Trends Biochem Sci*, 37: 391-9.

Lue, N. F., J. Chan, W. E. Wright, and J. Hurwitz. 2014. 'The CDC13-STN1-TEN1 complex stimulates Pol alpha activity by promoting RNA priming and primase-to-polymerase switch', *Nat Commun*, 5: 5762.
Lue, N. F., Y. C. Lin, and I. S. Mian. 2003. 'A conserved telomerase motif within the catalytic domain of telomerase reverse transcriptase is specifically required for repeat addition processivity', *Mol Cell Biol*, 23: 8440-9.
Machyna, M., P. Heyn, and K. M. Neugebauer. 2013. 'Cajal bodies: where form meets function', *Wiley Interdiscip Rev RNA*, 4: 17-34.
Machyna, M., K. M. Neugebauer, and D. Stanek. 2015. 'Coilin: The first 25 years', *RNA Biol*, 12: 590-6.
Mahmoudi, S., S. Henriksson, I. Weibrecht, S. Smith, O. Soderberg, S. Stromblad, K. G. Wiman, and M. Farnebo. 2010. 'WRAP53 is essential for Cajal body formation and for targeting the survival of motor neuron complex to Cajal bodies', *PLoS Biol*, 8: e1000521.
Mao, Y. S., B. Zhang, and D. L. Spector. 2011. 'Biogenesis and function of nuclear bodies', *Trends Genet*, 27: 295-306.
Min, B., and K. Collins. 2009. 'An RPA-related sequence-specific DNA-binding subunit of telomerase holoenzyme is required for elongation processivity and telomere maintenance', *Mol. Cell*, 36: 609-19.
———. 2010. 'Multiple mechanisms for elongation processivity within the reconstituted *Tetrahymena* telomerase holoenzyme', *J. Biol. Chem.*, 285: 16434-43.
Mitchell, J. R., J. Cheng, and K. Collins. 1999. 'A box H/ACA small nucleolar RNA-like domain at the human telomerase RNA 3' end', *Mol. Cell. Biol.*, 19: 567-76.
Mitchell, J. R., and K. Collins. 2000. 'Human telomerase activation requires two independent interactions between telomerase RNA and telomerase reverse transcriptase in vivo and in vitro', *Mol. Cell*, 6: 361-71.
Mitchell, J. R., E. Wood, and K. Collins. 1999. 'A telomerase component is defective in the human disease dyskeratosis congenita', *Nature*, 402: 551-55.
Mitchell, M., A. Gillis, M. Futahashi, H. Fujiwara, and E. Skordalakes. 2010. 'Structural basis for telomerase catalytic subunit TERT binding to RNA template and telomeric DNA', *Nat. Struct. Mol. Biol.*, 17: 513-18.
Morin, G.B. 1989. 'The human telomere terminal transferase enzyme is a ribonucleoprotein that synthesizes TTAGGG repeats.', *Cell*, 59: 521-29.
Moser, B. A., and T. M. Nakamura. 2009. 'Protection and replication of telomeres in fission yeast', *Biochem. Cell Biol.*, 87: 747-58.
Moser, B. A., L. Subramanian, Y. T. Chang, C. Noguchi, E. Noguchi, and T. M. Nakamura. 2009. 'Differential arrival of leading and lagging strand DNA polymerases at fission yeast telomeres', *EMBO J*, 28: 810-20.
Müller, H. J. 1938. 'The remaking of chromosomes', *Collecting Net*, 13: 181-98.
Nandakumar, J., and T. R. Cech. 2013. 'Finding the end: recruitment of telomerase to telomeres', *Nat. Rev. Mol. Cell Biol.*, 14: 69-82.
Nguyen, D., V. Grenier St-Sauveur, D. Bergeron, F. Dupuis-Sandoval, M. S. Scott, and F. Bachand. 2015. 'A Polyadenylation-Dependent 3' End Maturation Pathway Is Required for the Synthesis of the Human Telomerase RNA', *Cell Rep*, 13: 2244-57.
Nizami, Z., S. Deryusheva, and J. G. Gall. 2010. 'The Cajal body and histone locus body', *Cold Spring Harb. Perspect. Biol.*, 2: a000653.
Noël, J. F., S. Larose, S. Abou Elela, and R. J. Wellinger. 2012. "Budding yeast telomerase RNA transcription termination is dictated by the Nrd1/Nab3 non-coding RNA termination pathway." In *Nucleic Acids Res*.
Podlevsky, J. D., C. J. Bley, R. V. Omana, X. Qi, and J. J. Chen. 2008. 'The telomerase database', *Nucleic Acids Res.*, 36: D339-43.
Podlevsky, J. D., and J. J. Chen. 2012. 'It all comes together at the ends: Telomerase structure, function, and biogenesis', *Mutat. Res.*, 730: 3-11.

———. 2016. 'Evolutionary perspectives of telomerase RNA structure and function', *RNA Biol*: 1-13.
Price, C. M., K. A. Boltz, M. F. Chaiken, J. A. Stewart, M. A. Beilstein, and D. E. Shippen. 2010. 'Evolution of CST function in telomere maintenance', *Cell Cycle*, 9: 3157-65.
Ramakers, C., J. M. Ruijter, R. H. Deprez, and A. F. Moorman. 2003. 'Assumption-free analysis of quantitative real-time polymerase chain reaction (PCR) data', *Neurosci Lett*, 339: 62-6.
Ray, S., Z. Karamysheva, L. Wang, D.E. Shippen, and C.M. Price. 2002. 'Interactions between telomerase and primase physically link the telomere and chromosome replication machinery', *Mol Cell Biol*, 22: 5859-68.
Ribeyre, C., and D. Shore. 2013. 'Regulation of telomere addition at DNA double-strand breaks', *Chromosoma*, 122: 159-73.
Rice, C., and E. Skordalakes. 2016. 'Structure and function of the telomeric CST complex', *Comput Struct Biotechnol J*, 14: 161-7.
Richard, P., A. M. Kiss, X. Darzacq, and T. Kiss. 2006. 'Cotranscriptional recognition of human intronic box H/ACA snoRNAs occurs in a splicing-independent manner', *Mol Cell Biol*, 26: 2540-9.
Sarek, G., P. Marzec, P. Margalef, and S. J. Boulton. 2015. 'Molecular basis of telomere dysfunction in human genetic diseases', *Nat Struct Mol Biol*, 22: 867-74.
Schmidt, J. C., and T. R. Cech. 2015. 'Human telomerase: biogenesis, trafficking, recruitment, and activation', *Genes Dev*, 29: 1095-105.
Schmidt, J. C., A. J. Zaug, and T. R. Cech. 2016. 'Live Cell Imaging Reveals the Dynamics of Telomerase Recruitment to Telomeres', *Cell*.
Schmutz, I., and T. de Lange. 2016. 'Shelterin', *Curr Biol*, 26: R397-9.
Seto, A. G., A. J. Zaug, S. G. Sobel, S. L. Wolin, and T. R. Cech. 1999. '*Saccharomyces cerevisiae* telomerase is an Sm small nuclear ribonucleoprotein particle', *Nature*, 401: 177-80.
Sexton, A. N., and K. Collins. 2011. 'The 5' guanosine tracts of human telomerase RNA are recognized by the G-quadruplex binding domain of the RNA helicase DHX36 and function to increase RNA accumulation', *Mol Cell. Biol.*, 31: 736-43.
Shay, J. W. 2016. 'Role of Telomeres and Telomerase in Aging and Cancer', *Cancer Discov*, 6: 584-93.
Shay, J. W., and W. E. Wright. 2011. 'Role of telomeres and telomerase in cancer', *Semin. Cancer Biol.*, 21: 349-53.
Shippen-Lentz, D., and E. H. Blackburn. 1989. 'Telomere terminal transferase activity from *Euplotes crassus* adds large numbers of TTTTGGGG repeats onto telomeric primers', *Mol. Cell. Biol.*, 9: 2761-64.
Stanley, S. E., D. L. Gable, C. L. Wagner, T. M. Carlile, V. S. Hanumanthu, J. D. Podlevsky, S. E. Khalil, A. E. DeZern, M. F. Rojas-Duran, C. D. Applegate, J. K. Alder, E. M. Parry, W. V. Gilbert, and M. Armanios. 2016. 'Loss-of-function mutations in the RNA biogenesis factor NAF1 predispose to pulmonary fibrosis-emphysema', *Sci Transl Med*, 8: 351ra107.
Stern, J.L., K.G. Zyner, H.A. Pickett, S.B. Cohen, and T.M. Bryan. 2012. 'Telomerase recruitment requires both TCAB1 and Cajal bodies independently', *Mol. Cell. Biol.*, 32: 2384-95.
Stone, M.S., M. Mihalusova, C.M. O'Connor, R. Prathapam, K. Collins, and X. Zhuang. 2007. 'Stepwise protein-mediated RNA folding directs assembly of telomerase ribonucleoprotein', *Nature*, 446: 458-61.
Stuart, B. D., J. Choi, S. Zaidi, C. Xing, B. Holohan, R. Chen, M. Choi, P. Dharwadkar, F. Torres, C. E. Girod, J. Weissler, J. Fitzgerald, C. Kershaw, J. Klesney-Tait, Y. Mageto, J. W. Shay, W. Ji, K. Bilguvar, S. Mane, R. P. Lifton, and C. K. Garcia. 2015. 'Exome sequencing links mutations in PARN and RTEL1 with familial pulmonary fibrosis and telomere shortening', *Nat Genet*, 47: 512-7.
Tang, W., R. Kannan, M. Blanchette, and P. Baumann. 2012. "Telomerase RNA biogenesis involves sequential binding by Sm and Lsm complexes." In *Nature*.
Teixeira, M. T., M. Arneric, P. Sperisen, and J. Lingner. 2004. 'Telomere length homeostasis is achieved via a switch between telomerase- extendible and -nonextendible states', *Cell*, 117: 323-35.

Theimer, C. A., B. E. Jády, N. Chim, P. Richard, K. E. Breece, T. Kiss, and J. Feigon. 2007. 'Structural and functional characterization of human telomerase RNA processing and cajal body localization signals', *Mol. Cell*, 27: 869-81.

Tomlinson, R. L., E. B. Abreu, T. Ziegler, H. Ly, C. M. Counter, R. M. Terns, and M. P. Terns. 2008. 'Telomerase reverse transcriptase is required for the localization of telomerase RNA to cajal bodies and telomeres in human cancer cells', *Mol. Biol. Cell*, 19: 3793-800.

Tomlinson, R. L., J. Li, B. R. Culp, R. M. Terns, and M. P. Terns. 2010a. 'A Cajal body-independent pathway for telomerase trafficking in mice', *Exp. Cell Res.*, 316: 2797-809.

———. 2010b. 'A Cajal body-independent pathway for telomerase trafficking in mice', *Exp Cell Res*, 316: 2797-809.

Tomlinson, R. L., T. D. Ziegler, T. Supakorndej, R. M. Terns, and M. P. Terns. 2006. 'Cell cycle-regulated trafficking of human telomerase to telomeres', *Mol. Biol. Cell*, 17: 955-65.

Tong, A. S., J. L. Stern, A. Sfeir, M. Kartawinata, T. de Lange, X. D. Zhu, and T. M. Bryan. 2015. 'ATM and ATR Signaling Regulate the Recruitment of Human Telomerase to Telomeres', *Cell Rep*, 13: 1633-46.

Tseng, C. K., H. F. Wang, A. M. Burns, M. R. Schroeder, M. Gaspari, and P. Baumann. 2015. 'Human Telomerase RNA Processing and Quality Control', *Cell Rep*, 13: 2232-43.

Tucey, T. M., and V. Lundblad. 2014. 'Regulated assembly and disassembly of the yeast telomerase quaternary complex', *Genes Dev*, 28: 2077-89.

Tycowski, K. T., M. D. Shu, A. Kukoyi, and J. A. Steitz. 2009. 'A conserved WD40 protein binds the Cajal body localization signal of scaRNP particles', *Mol. Cell*, 34: 47-57.

Upton, H. E., K. Hong, and K. Collins. 2014. 'Direct Single-Stranded DNA Binding by Teb1 Mediates the Recruitment of Tetrahymena thermophila Telomerase to Telomeres', *Mol Cell Biol*, 34: 4200-12.

Venteicher, A. S., E. B. Abreu, Z. Meng, K. E. McCann, R. M. Terns, T. D. Veenstra, M. P. Terns, and S. E. Artandi. 2009. 'A human telomerase holoenzyme protein required for Cajal body localization and telomere synthesis', *Science*, 323: 644-8.

Vogan, J. M., X. Zhang, D. T. Youmans, S. G. Regalado, J. Z. Johnson, D. Hockemeyer, and K. Collins. 2016. 'Minimized human telomerase maintains telomeres and resolves endogenous roles of H/ACA proteins, TCAB1, and Cajal bodies

', *eLife*.

Vogan, J.M., and K. Collins. 2015. 'Dynamics of human telomerase holoenzyme assembly and subunit exchange across the cell cycle', *J. Biol. Chem.*, 290: 21320-35.

Wan, B., T. Tang, H. Upton, J. Shuai, Y. Zhou, S. Li, J. Chen, J. S. Brunzelle, Z. Zeng, K. Collins, J. Wu, and M. Lei. 2015. 'The Tetrahymena telomerase p75-p45-p19 subcomplex is a unique CST complex', *Nat Struct Mol Biol*, 22: 1023-6.

Wang, F., E.R. Podell, A.J. Zaug, Y. Yang, P. Baciu, T.R. Cech, and M. Lei. 2007. 'The POT1-TPP1 telomere complex is a telomerase processivity factor', *Nature*, 445: 506-10.

Wang, Q., I. A. Sawyer, M. H. Sung, D. Sturgill, S. P. Shevtsov, G. Pegoraro, O. Hakim, S. Baek, G. L. Hager, and M. Dundr. 2016. 'Cajal bodies are linked to genome conformation', *Nat Commun*, 7: 10966.

Wege, H., M. S. Chui, H. T. Le, J. M. Tran, and M. A. Zern. 2003. 'SYBR Green real-time telomeric repeat amplification protocol for the rapid quantification of telomerase activity', *Nucleic Acids Res*, 31: E3-3.

Weinrich, S. L., R. Pruzan, L. Ma, M. Ouellette, V. M. Tesmer, S. E. Holt, A. G. Bodnar, S. Lichsteiner, N. W. Kim, J. B. Trager, R. D. Taylor, R. Carlos, W. H. Andrews, W. E. Wright, J. W. Shay, C. B. Harley, and G. B. Morin. 1997. 'Reconstitution of human telomerase with the template RNA component hTR and the catalytic protein subunit hTRT', *Nat. Genet.*, 17: 498-502.

Wellinger, R. J., and V. A. Zakian. 2012. 'Everything you ever wanted to know about *Saccharomyces cerevisiae* telomeres: beginning to end', *Genetics*, 191: 1073-105.

Weng, N-P., L. Granger, and R. J. Hodes. 1997. 'Telomere lengthening and telomerase activation during human B cell differentiation', *Proc. Natl. Acad. Sci. USA*, 94: 10827-32.
Wenz, C., B. Enenkel, M. Amacker, C. Kelleher, K. Damm, and J. Lingner. 2001. 'Human telomerase contains two cooperating telomerase RNA molecules', *EMBO J.*, 20: 3526-34.
Witkin, K. L., and K. Collins. 2004. 'Holoenzyme proteins required for the physiological assembly and activity of telomerase', *Genes Dev.*, 18: 1107-18.
Wong, J.M., L. Kusdra, and K. Collins. 2002. 'Subnuclear shuttling of human telomerase induced by transformation and DNA damage', *Nature Cell Biol*, 4: 731-36.
Wu, P., H. Takai, and T. de Lange. 2012. 'Telomeric 3' overhangs derive from resection by Exo1 and Apollo and fill-in by POT1b-associated CST', *Cell*, 150: 39-52.
Wu, R. A., and K. Collins. 2014. 'Human telomerase specialization for repeat synthesis by unique handling of primer-template duplex', *EMBO J*, 33: 921-35.
Wu, R. A., Y. S. Dagdas, S. T. Yilmaz, A. Yildiz, and K. Collins. 2015. 'Single-molecule imaging of telomerase reverse transcriptase in human telomerase holoenzyme and minimal RNP complexes', *eLife*, 4: 10.7554/eLife.08363.
Xi, L., and T. R. Cech. 2014. 'Inventory of telomerase components in human cells reveals multiple subpopulations of hTR and hTERT', *Nucleic Acids Res*, 42: 8565-77.
Yi, X., V.M. Tesmer, I. Savre-Train, J.W. Shay, and W.E. Wright. 1999. 'Both transcriptional and posttranscriptional mechanisms regulate human telomerase template RNA levels', *Mol. Cell. Biol.*, 19: 3989-97.
Zhang, Q., N. K. Kim, and J. Feigon. 2011. 'Architecture of human telomerase RNA', *Proc. Natl. Acad. Sci. USA*, 108: 20325-32.
Zhao, Y., E. Abreu, J. Kim, G. Stadler, U. Eskiocak, M.P. Terns, R.M. Terns, J.W. Shay, and W.E. Wright. 2011. 'Processive and distributive extension of human telomeres by telomerase under homeostatic and nonequilibrium conditions', *Mol. Cell*, 42: 297-307.
Zhao, Y., A. J. Sfeir, Y. Zou, C. M. Buseman, T. T. Chow, J. W. Shay, and W. E. Wright. 2009. 'Telomere extension occurs at most chromosome ends and is uncoupled from fill-in in human cancer cells', *Cell*, 138: 463-75.
Zhong, F. L., L. F. Batista, A. Freund, M. F. Pech, A. S. Venteicher, and S. E. Artandi. 2012. 'TPP1 OB-fold domain controls telomere maintenance by recruiting telomerase to chromosome ends', *Cell*, 150: 481-94.
Zhong, F., S. A. Savage, M. Shkreli, N. Giri, L. Jessop, T. Myers, R. Chen, B. P. Alter, and S. E. Artandi. 2011. 'Disruption of telomerase trafficking by TCAB1 mutation causes dyskeratosis congenita', *Genes Dev.*, 25: 11-6.
Zhu, X., R. Kumar, M. Mandal, N. Sharma, H.W. Sharma, U. Dhingra, J.A. Sokoloski, R. Hsiao, and R. Narayanan. 1996. 'Cell-cycle dependent modulation of telomerase activity in tumor cells', *Proc. Natl. Acad. Sci. USA*, 93: 5091-6095.